Befekadu Chalew GASHE

Numerical Analysis of Wrinkling of Sandwich Structure

FRP++
Advanced structural analysis and design using composite materials

Master Dissertation
European Master Advanced Structural Analysis and Design using Composite Materials

Work developed under the supervision of
Professor Bruno CASTANIÉ
Professor Samuel RIVALLANT

Funded by the European Union

August 2024

DECLARATION

Name: Befekadu Chalew GASHE

Email: befekaduchalew@gmail.com **Phone number:** +330751044623

Citizen Card Number: XXXXXXXXXXXXXXXXXXX

Title of the Thesis: Numerical Analysis of Wrinkling of Sandwich Structure

Supervisors:

Professor Bruno CASTANIÉ

Professor Samuel RIVALLANT

Year of Conclusion: 2024

Master Course in Advanced Structural Analysis and Design using Composite Materials

University of Toulouse III Paul Sabatier, 19/08/2024

Signature:

ACKNOWLEDGEMENTS

First and foremost, I want to express my heartfelt gratitude to Almighty God for His unwavering support throughout my research journey. I was able to accomplish all my objectives with the strength and guidance He provided.

I express profound gratitude for the help and financial resources granted by the Erasmus+ Program of the European Union. Financial support has been crucial in facilitating my pursuit of a master's degree. I would like to convey my profound gratitude to the consortium in charge of curating the European Master's in Advanced Structural Analysis and Design using Composite Materials [FRP++] curriculum. Being involved in this exceptional chance to contribute to an innovative and forward-thinking project has not only expanded my academic knowledge but also equipped me with advanced understanding in the field of structural composites.

I would like to convey my truthful gratitude to my advisors Professor Samuel RIVALLANT and Professor Bruno CASTANIÉ for their invaluable guidance and motivation throughout this research. I am truly lucky to have them as my advisors and I thank them for inspiring me in my research I had never dreamt of, which afterwards became part of my life.

I would like to express my gratitude to Professor Bruno CASTANIÉ, the head of our [FRP++] master's dissertation at Institute Clement Ader (ICA), for his invaluable support and assistance in resolving the challenging professional and research difficulties I encountered. I would like to express my deep gratitude to the professors, PhD students, post-doctoral researchers, and other staff members of the ICA for their invaluable assistance in facilitating my dissertation research within the facility.

Finally, I express my sincere gratitude to GOD for His limitless compassion and favor during this journey. I would like to express my profound gratitude to my families for their steadfast affection, prayers, consistent motivation, and unwavering backing, which have been the fundamental basis of my accomplishments throughout the years.

Etude numérique du flambement local des structures sandwich

RESUME

Les structures sandwich, couramment utilisées dans l'aérospatiale, la marine et le génie civil pour leur excellent rapport résistance/poids, sont sujettes à un type spécifique de défaillance appelé flambement. Le flambement est un phénomène de flambage localisé qui compromet considérablement l'intégrité structurelle. Cet article examine en profondeur le comportement de flambement des panneaux sandwich sous des charges combinées de cisaillement et de flexion, en utilisant à la fois des modèles numériques et des tests expérimentaux. La recherche vise à combler une lacune importante dans la littérature en examinant la corrélation entre les prévisions numériques, les observations expérimentales et les modèles analytiques existants. L'expérience consistait à effectuer des essais de flexion en trois points sur des échantillons de sandwich constitués de peaux en fibre de verre-époxy avec des noyaux en mousse PMI Rohacell. L'objectif était d'observer l'initiation du flambement, qui est associée à la compression et à la rupture par cisaillement. Les expérience tests ont été réalisés et surveillés à l'aide de techniques de corrélation d'images numériques (DIC), en conjonction avec des capteurs de déplacement et de force. Les simulations numériques de rupture par compression, réalisées à l'aide de l'analyse par éléments finis (FEA) dans ABAQUS, ont été comparées aux résultats des tests expérimentaux et aux prévisions analytiques. Les simulations ont montré une bonne corrélation avec les données expérimentales et les modèles analytiques. Cependant, dans le cas de la rupture par cisaillement, l'analyse numérique a eu tendance à surestimer la charge de flambement par rapport aux résultats expérimentaux. De plus, l'étude a intégré les imperfections géométriques initiales pour étudier plus en détail les spécimens de rupture par cisaillement. La recherche a révélé que la taille du maillage utilisé dans les modèles numériques est essentielle pour prédire avec précision les charges de flambage et les modèles de plissement pour l'évolution de la longueur d'onde qui se produit pendant l'analyse de simulation de rupture par compression et par cisaillement.

MOTS-CLES : Flambement ; Structures sandwich ; Composite ; Analyse par éléments finis ; Expérience.

Numerical Analysis of Wrinkling of Sandwich Structure

ABSTRACT

Sandwich structures, commonly employed in aerospace, marine, and civil engineering for their excellent strength-to-weight ratio, are prone to a specific type of failure called wrinkling. Wrinkling is a localized buckling phenomenon that significantly compromises structural integrity. This paper conducts a thorough examination of the wrinkling behavior of sandwich panels under combined shear and bending loads, utilizing both numerical models and experimental tests. The research aims to address a significant gap in the literature by examining the correlation between numerical predictions, experimental observations, and existing analytical models. The experiment involved conducting three-point bending tests on sandwich specimens consisting of glass fiber-epoxy skins with PMI Rohacell foam cores. The objective was to observe the initiation of wrinkling, which is associated with compression and shear failure. The experimental tests were conducted and monitored by using Digital Image Correlation (DIC) techniques, in conjunction with displacement and force sensors. The numerical simulations for compression failure, performed using Finite Element Analysis (FEA) in ABAQUS, were compared with both experimental test results and analytical predictions. The simulations showed a good correlation with both the experimental data and analytical models. However, in the case of shear failure, the numerical analysis tended to overestimate the wrinkling load when compared to the experimental results. Additionally, the study incorporated initial geometric imperfections to further investigate shear failure specimens. The research also found that the size of the mesh used in numerical models is essential in accurately predicting the buckling loads and wrinkling patterns for wavelength evolution that occurs during compression and shear failure simulation analysis.

KEYWORDS: Wrinkling; Sandwich structures; Composite; Finite Element Analysis; Experiment.

TABLE OF CONTENTS

CONTENTS

LIST OF FIGURES

LIST OF TABLES

LIST OF ABBREVIATIONS AND SYMBOLS

Abbreviations

EASA	European Union Aviation Safety Agency
ISAE SUPAERO	Institut Supérieur de l'Aéronautique et de l'Espace SUPAERO
FRP	Fiber-Reinforced Polymer
FEM	Finite Element Modelling
LVDT	Linear variable differential transformer
LDS	Laser Displacement Sensor
DIC	Digital Image Correlation
PVC	Polyvinyl Chloride
GFRP	Glass Fiber Reinforced Polymer

Symbols

E_f	Elastic modulus of the skin
G_c	Core transverse shear modulus
E_c	Core normal Elastic modulus
t_f	Thickness of the facesheet
t_c	Thickness of the core
D_f	Bending Stiffness
vc	Poisson's ratio of the core

Notes: The terms skin, face and facesheet are used interchangeably.

1. CHAPTER 1: INTRODUCTION

1.1. Sandwich Structure

Sandwich structure is a type of lightweight panel consisting of a core material sandwiched between two strong and stiff outer layers, known as skins, on the top and bottom [1]. The primary function of the core is to significantly enhance the sandwich's bending stiffness and strength by being inserted between the face sheets. These cores can be made from materials such as aluminum honeycomb or solid cores [2]. Composite laminates and metals are frequently utilized for skins. The core materials are essential for stabilizing and determining the flexural stiffness of a structure, as well as managing shear and compressive stresses that occur in directions perpendicular to the plane. Conversely, the skins have the role of carrying and withstanding all bending and in-plane loads [3]. Most of the literature describes sandwich structures as having a core that can be orthotropic, anisotropic, or isotropic, sandwiched between two thin skins with high mechanical properties. Typically, these skins are made of materials that have significantly better mechanical qualities than the core, while being thin [4], [5]. Figure 1.1 shows that the sandwich structures behaves similarly to an I-beam, with the skin surfaces positioned away from the neutral axis on the core material. The design significantly enhances the sandwich structure's resistance to bending, while concurrently decreasing its overall weight [6].

Typically, face sheets in sandwich structures consist of composite laminates of glass and carbon fibers, as well as metals. These materials are accountable for bearing the flexural and plane loads. Conversely, the cores are composed of honeycombs, cellular foams, balsa wood, and lattice structures, which serve to stabilize the face sheets. An adhesive film is typically used to attach the face sheets to the core material, as shown in Figure 1.2 highlighting its important role in preserving the structural integrity and functionality of the sandwich panel [3].

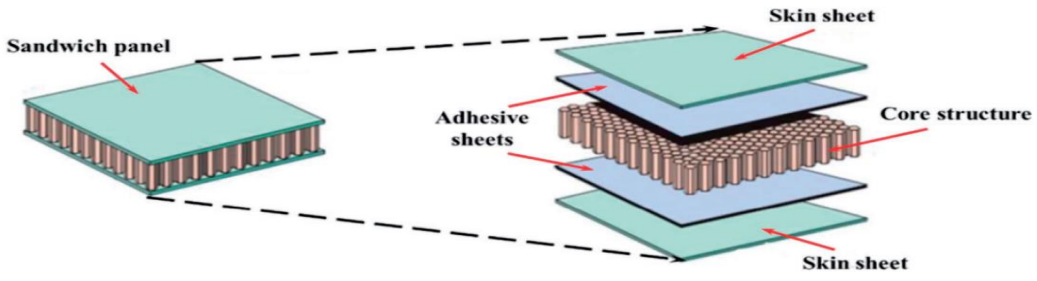

. Figure 1.1 : Typical Sandwich composite panel [7].

Figure 1.2 : Commonly used for core materials: (a) foam core (b) balsa wood (c) honeycomb core (d) trussed core [8].

Sandwich structures are used in various sectors, including aerospace, automotive, shipbuilding, civil infrastructure, and wind power generation, where extensive research has been conducted on their applications [9]. In these applications, reducing weight helps improve speed and reduce energy consumption while maintaining loading capacity [10]. They are particularly prominent in light aircraft structures, such as the recently certified "Elixir" by Elixir Aircraft, shown in Figure 1.3. Additionally, grid-scored sandwich structures are used in the aero foils of wind turbine blades, highlighting their versatility and effectiveness in various applications as shown in Figure 1.4 [11].

Figure 1.3 : The Elixir-light aircraft certified by the EASA 2006.

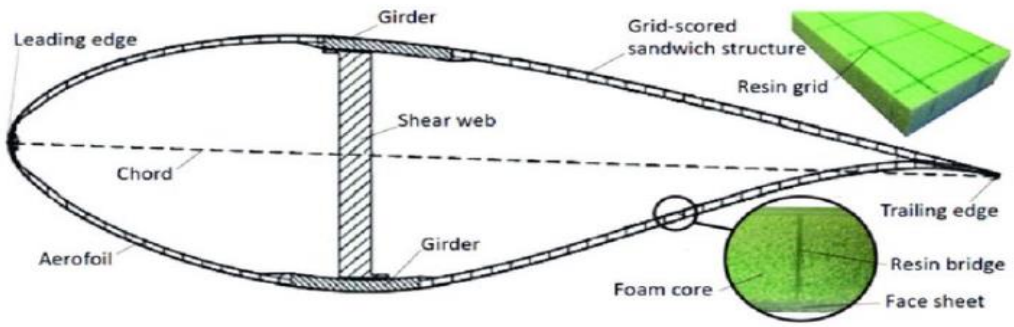

Figure 1.4 : Sandwich structure with grid scores that are utilized in wind turbine blade airfoils [11].

1.2. Motivation

The performance of sandwich structure is affected by various elements, including as the geometrical dimensions, adhesive bonding between the skins and the core, and qualities of facings. Sandwich structure beams can display different failure modes when exposed to bending, shear, and in-plane loads. The initiation, propagation, and interaction of these failure modes are determined by the qualities of the constituent materials, the geometry, and the nature of the loading [2], [3]. These failure modes are interrelated, meaning that the worsening of an initial failure can trigger the development of other modes. To ensure that sandwich constructions are reliable and structurally sound, it is crucial to understand how these different failure modes interact [12], [13].

Several articles by different authors and researchers have detailed the deformation and failure behavior of composite sandwich beams [1], [12]. Possible failure modes under quasi-static loading circumstances are global buckling, wrinkling of the compression face sheet, indentation failure under localized loading, debonding at the core/face sheet interface, tensile or compressive failure of the face sheets, and core failure [3].

Two different scales of buckling modes can be seen in sandwich structures: global buckling, which is like Euler's buckling for columns and, wrinkling, which are localized forms of skin buckling [14]. Facesheet wrinkling is one of several potential buckling modes that sandwich structures may display, and it has historically been understood as a local, short wavelength buckling phenomenon. Wrinkles can be understood as the deformation of small columns, known as faces, that are held up by a continuous elastic material termed the core [2]. The stiffness properties of the face sheets, the type of core material used, and the specific shape of the area where an impact indentation may occur all have an impact on the stress level at which wrinkling of the face sheets occurs. The loading conditions and adhesion properties at the interface between the core and face layers also have an impact on the stress that causes wrinkling [15]. In the past, researchers have used several techniques to study wrinkling and create basic formulation that designers might use in a creative way [16]. Research has confirmed that the core is essential in the enhanced method of calculating wrinkling loads [20].

Examining the failure modes in sandwich structures is crucial, especially when considering the core's features, since they directly affect the structural integrity and performance of the structures.

1.2.1. Failure modes in sandwich structures

Although sandwich structures are highly useful and have a wide range of applications, they can suffer from substantial decreases in effectiveness as a result of certain failure processes. The intrinsic complexity of their diverse components results in numerous potential failure scenarios. Composite designers have the responsibility of ensuring that any failure that occurs during service remains within acceptable limits under the prescribed loading conditions [17]. To get the best possible performance in real-world applications, it is important to carefully evaluate many elements. These considerations include manufacturing procedures, design philosophy (including provisions for post-buckling), geometric size, applied stresses, and the mechanical properties of the materials utilized. The possession of necessary qualities by both the face and core, as well as the successful transfer of stresses through the adhesive link between the skin and core, are of utmost importance. Otherwise, the structure's overall stiffness and strength will fall below expected levels [3].

In tested composite sandwich beams, several failure modes were noted and examined, including wrinkles in the compression facing, face sheet debonding, indentation of the loaded face, compressive facing failure, and other failures [12].

a. Wrinkling in compression failure

The compression or bending of sandwich beams results in the localized buckling of the compression facesheet, which is characterized by short wavelength wrinkling. This phenomena can be observed as the compression facesheet curving outward while being upheld by a flexible or deformable core. Wrinkling, a prevalent kind of failure in sandwich beams, results in a decrease in the beam's stiffness. The predominant factor contributing to the formation of wrinkles in the sandwich panel is mostly the result of the interaction between the facesheet and the core. The critical wrinkling load is dictated by the structure's form, the applied stress magnitude, and the stiffness of both the facesheet and core materials [3].

b. Face sheet debonding

Face sheet debonding in sandwich panels can arise either during the manufacturing process or due to external influences. Debonding weakens the rigidity of the panel and enhances its vulnerability to buckling under in-plane compression. In addition, the ability of the structure to withstand external forces is weakened by the separation of the skin and core, known as skin-core debonding. This separation can occur during the manufacturing process or due to external stresses. This can lead to buckling when subjected to in-plane compression, a decrease in stiffness, and a reduction in impact resistance. In order

to tackle these problems, engineers meticulously analyze the mechanical characteristics of the matrix or adhesive layer while designing sandwich structures. This guarantees that fracture loads remain within acceptable thresholds and that the structure maintains its strength and tolerance, even when debonding is present [12].

c. Indentation of loaded face

Indentation failure is the primary form of failure of sandwich structures when they are exposed to highly concentrated external loads, such as point or line loads. The process initiates with the local yielding and deformation of the core material in the substantially loaded region, which is then followed by substantial local deformation of the loaded facesheet into the core [18]. Composite sandwich beams, especially those with soft cores, exhibit a complicated elastic-plastic multiaxial stress state around the confined load, resulting in significant local stress concentrations [19].

d. Compressive facing failure

Sandwich structure skins can experience failure when subjected to uniaxial tension and compression forces. Composite skins are more prone to compressive failure because to their greater ability to resist tensile forces compared to compressive forces. This tendency is particularly evident in circumstances involving pure bending, when the qualities related to movement in a direction perpendicular to the plane are frequently disregarded, since it is assumed that the core can withstand failure in that direction [7]. When beams experience pure bending or a combination of bending and low shear, the composite facesheet is more susceptible to compressive failure rather than tensile failure due to its significantly lower strength in compression. The occurrence of this type of failure is minimized when the core exhibits a sufficiently high level of stiffness in the direction perpendicular to its thickness.

e. Core failure

The core is primarily chosen to carry shear loads [3]. Sandwich structure commonly fails due to core failure caused by shear. Short beams under three-point bending experience shear, which leads to failure when the greatest shear stress exceeds the core material's critical value (shear strength) [20].

f. Other failure

As summarized in the there are other failures on sandwich structures, which are mainly dependent on the core. For instance, facesheet dimpling, core crushing, core shear failure, facesheet-to-core debonding and global buckling. Accounting for all probable failure modes in the post-buckling phase is a big difficulty

when constructing sandwich structures. As a result, failures such as global buckling are frequently seen as the ultimate failure, as it becomes difficult to anticipate and combat all probable failure scenarios.

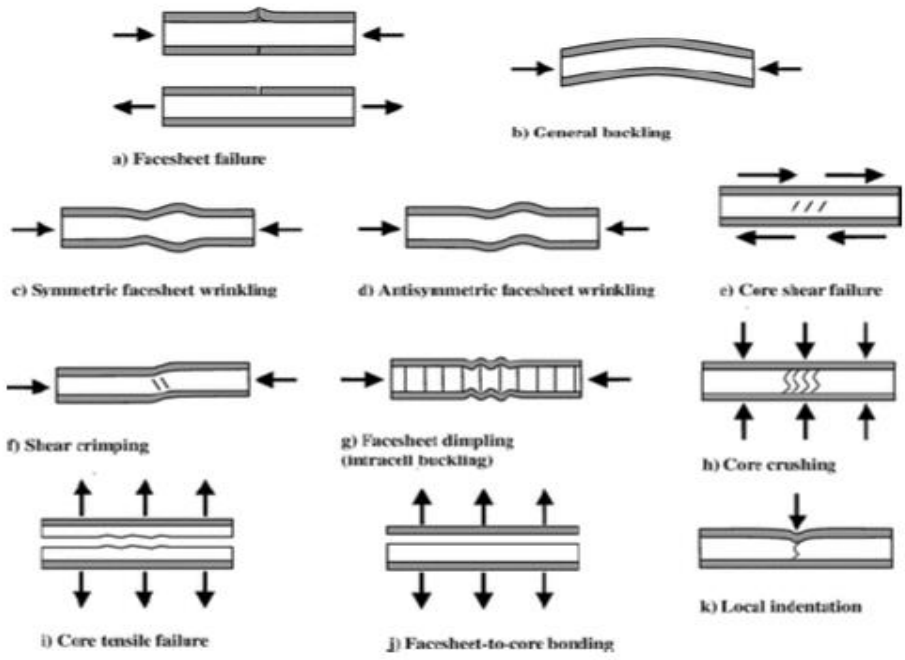

Figure1.5 : Summary for sandwich structure failure [21].

1.2.2. Classical Analytical Wrinkling Theory

Several writers have developed closed-form techniques for sandwich structure design and analysis that address the key wrinkling stress. For different wrinkling types of undamaged panels, expressions by Hoff and Mautner [6], Gough and De Bruyne [22], and Yusuff [23] provide the necessary wrinkling stress formulation. The essential wrinkling stress was described by Hoff and Mautner's result [2] as a function of simply the facesheet and core's material parameters. This result, which has been indicated in Equation (1-1) is typically regarded as suitable for an isotropic core [15]:

$$\sigma_{cr} = C \sqrt[3]{E_c E_f G_c} \quad (1\text{-}1)$$

Where E_f is the longitudinal Young's modulus of the face, E_c is the through-thickness of Young's modulus of the core, G_c is the transverse shear modulus of the core, and C is the constant usually taken as 0.5 to 0.9 [13].

Hoff and Mautner determined the constant C to be 0.91 based on strain energy. The factor of 0.91 was shown to be non-conservative when compared to experimental data, although a factor of 0.5 seemed to be consistent as a knockdown factor with a variety of Hoff and Mautner test results [6].

Su et al. [24] investigated how the size of the foam core cell influences the wrinkling stress of sandwich panels using the higher-order continuum theory. To take cell size effects into account, this sophisticated model integrates the couple-stress continuum theory and introduces a characteristic length as a special intrinsic scale parameter in the bending constitutive matrix of the core. The projected wrinkling stress obtained from the proposed method closely matched the actual data reported in the literature and exhibited behavior that varied with size. Their research uncovers a positive pattern, highlighting the potential importance of cell size in the development of wrinkling stress. In order to properly understand the consequences for the performance and design of sandwich panels, further research is required to expand upon these findings.

Syed Yusuff's [23] concept of wrinkling in sandwich structure is divided into two components. The first segment is believed to have a finite thickness of the core. The wrinkling stress can be determined by a simple square root calculation that incorporates the Young's moduli of the materials and the ratio of face to core thickness. In the second phase of the theory, the same method is applied, but with the additional consideration of shearing stresses in the core. Furthermore, the analysis is extended to encompass the scenario where the face is supported by a medium that is either sufficiently thick or semi-infinite. In the second scenario, the wrinkle stress is determined by a cubic root formula that is derived from the material moduli but indirectly depends on the structure's geometry. This formula is only applicable if the ratio of the core to the face thickness is greater than or equal to the width of the core's marginal zone of distortions to the ratio of the face.

According to Birman et.al [25] investigate two potential mechanisms of wrinkling in symmetrically laminated facings. Fagerberg [26] identified a long wave that is perpendicular to the load direction in sandwich panels with substantial anisotropy under biaxial loading. This wave can be used as a tool to forecast the wrinkling behavior of the panels. The technique relies on the premise that wrinkling takes place at a certain angle, which is determined by computing the disparity between the applied tension and the maximum load that the panel can endure without wrinkling. The second mode comprises rectangular creases oriented parallel to the direction of the stress. Three models was being examined: facing supported by elastic basis, faces supported by Hoff's core, and faces supported by plantema’s cores [25]. According to this paper, the elastic foundation model is applicable when dealing with large wrinkles, where core shear stress was not considered.

1.3. Objective of the study

As explained in section 1.2, there aren't many experimental and numerical investigations on sandwich structure on shear wrinkling in the literature. Furthermore, in practical it is very difficult to correlate between the analytical formulations, numerical results and the experimental tests. This emphasizes how urgently more thorough experimental and numerical studies on the behavior of wrinkling in sandwich structures are needed.

This study aims to examine how sandwich structures behave when subjected to combined shear and bending loads. This is based on Alawode A [16] experimental work on shear wrinkling failure and the ISAE SUPAERO students' study of compression wrinkling failure using various sandwich panel specimens. The study also aims to understand the onset and propagation of wrinkles and to correlate the experimental results with numerical predictions. Additionally this research create a short bibliographical study on wrinkling failure viewpoint on analytical, numerical and experimental testing.

In order to gain a deeper understanding of the physics and characteristics of this phenomena, the study aims to observe and measure the failure stress and wavelength of wrinkling. This research attempts to close the knowledge gap between numerical results, analytical predictions, and expermental behaviour by using a systematic approach, providing valuable data to enhance the understanding and design of sandwich structures.

1.4. Dissertation Structure

As an introduction to the study, Chapter 1 explains the purpose, motivation, and goals of the study. The literature study is covered in detail in Chapter 2, provides a comprehensive analysis of the current body of literature on the topic, emphasizing important research articles and their corresponding discoveries. This text explores the intricacies of wrinkling theory, offering a fundamental comprehension of the concepts and equations that dictate the wrinkling behavior in sandwich structures. Chapter 3 describes the numerical methodology used by Abaqus software, the test methodologies used throughout the study, and the experimental procedures and setups used to investigate the behaviour of sandwich structures under combined shear and bending loads, as conducted by Alawode A [16] experimental work on shear failure wrinkling and ISAE SUPAERO students' experimental work on compression failure wrinkling. Chapter 4 provides a detailed explanation of the numerical results particularly on the mesh size effect on buckling load and wrinkling pattern and experimental investigations, as well as a thorough discussion on the analysis and comparison of the gathered data. Chapter 5 highlights the research findings and provides

significant recommendations for future research, which will contribute to continued progress in the subject.

THIS PAGE WAS INTENTIONALLY LEFT BLANK

2. CHAPTER 2 LITERATURE REVIEW

In this chapter, the sandwich structures world will be discussed with a special focus on understanding the phenomena related to wrinkling. By following the historical overview of the sandwich structure, its various applications, and mechanics behind wrinkling—finally, we would like to obtain a picture of the interplay between these elements in affecting the performance and reliability of aerospace structures. The comprehensive account built from reviewing the empirical studies and embracing the latest of technological advancements is done side by side by examining the strides made through computational modeling so as to explain the current state of knowledge but also highlight the potential pathways for future innovations.

2.1. Historical overview and significance of the Sandwich structure

According to Hoff and Mautner in 1944 [6], "The sandwich panel is a panel with two thin, flat, stiff outer layers and a thick, lightweight, inner layer. This configuration provides the structure of the panel, which also constitutes the skins of sandwich-type monocoque wings or fuselages. In this regard, the inner layer is most often referred to as the core, while the outer layers are called the faces". Another definition by, Ley R et.al [2], from their Journal of Face Sheet Wrinkling in Sandwich Structure published by NASA in 1999," A sandwich structure consists of two slender, load-bearing face sheets attached to each side of a relatively thick, lightweight core. This structure is an aid to stopping the face sheets from buckling independently." Most academic literature refers to sandwich structures as consisting of two thin skins, both upper and lower, that have high mechanical strength. These skins are separated by a core, which will be a lighter material and usually with lower mechanical properties joined by the skins through an adhesive medium [9], [16]. This pattern is similar to an I-beam sandwich where materials are put as far away as possible from the center of bending or the neutral axis; thus, the structure becomes efficient in providing resistance against bending forces.

2.1.1. Significance in Aerospace

The sandwich structures have evolved from the date of invention to play a crucial role in contemporary aerospace technology, attesting to the advances in material science and engineering ingenuity [27]. The

lightweight core material sandwiched between two stiffer and stronger skins characterizes a sandwich structure that found utilitarian use in aircraft for the first time during World War II. The Mosquito, a British-made bomber, had seen service in Europe, the Middle and Far East, and the Russian front during World War II. Although it was originally designed as a bomber, it also performed well as a fighter, minelayer, and pathfinder for military transport and photo reconnaissance. It was constructed during the Battle of Britain, and less than a year after design work was commenced, in November 1940, as the prototype shown in Figure 2.1 took to the air for the first time. From the engineering point of view, it has one really outstanding feature: the fuselage is made from a molded plywood-balsa sandwich material that is light and strong—important in times of war [28].

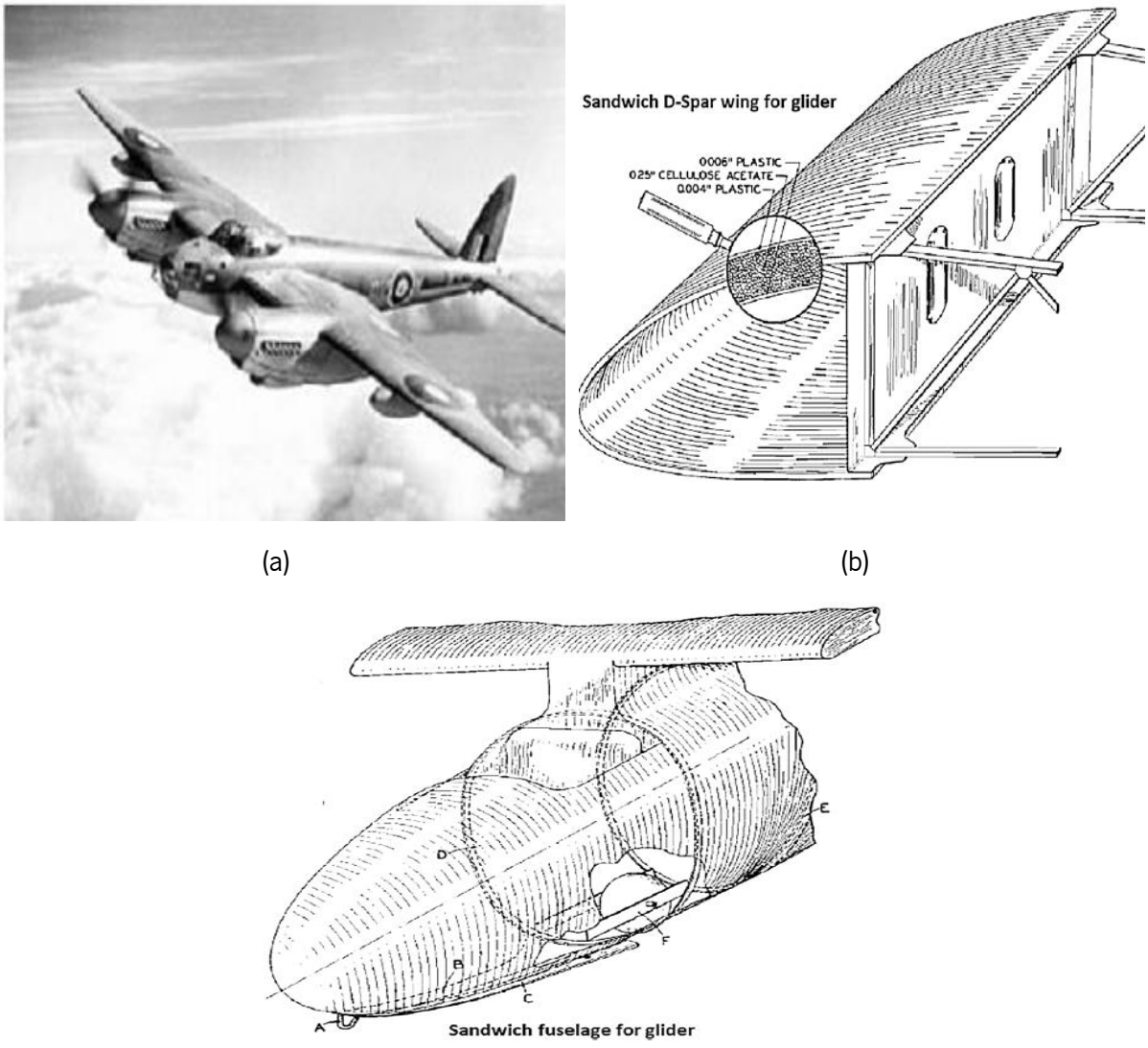

(a) (b)

(c)

Figure 2.1 : Picture of aircraft Sandwich structure (a) Mosquito (b) Sandwich D-Spar wing for glider (C) Sandwich fuselage for Gliders [29].

According to Castanie B et. al's [29] Review of Composite Sandwich Structure in Aeronautic Application gliders were perhaps the first flying structures to have a complete sandwich design. The requirements were aerodynamic refinement, lightweight construction, low production costs, toughness, ease of maintenance, and the ability to build double-curved structures." Figure 2.1(b) illustrates a D-Spar sandwich structure including a glider fuselage that was commonly used during that time. The D-Spar's elegant shape is notable for its ability to emphasize the benefits of sandwich or composite constructions, particularly its capability to optimize designs and reduce the number of components.

The evolution was characterized by some major turning points. Originally, these structures were built using basic materials, like balsa wood cores, but to realize better ways of performance and durability, there was the introduction of synthetic foams and honeycomb materials that had much higher strength-to-weight ratios and, in addition, superb fatigue resistance. By significantly increasing their load-bearing capability and resistance to environmental conditions, the introduction of sophisticated composites, such as carbon fiber and fiberglass, in the face sheets further revolutionized their application [30].

The adoption of composite skins in sandwich structures for civil aircraft has been a careful and step-by-step process, mainly because safety is the industry's top concern. Initially, they were employed in non-structural elements, such as interior panels, side walls, overhead bins, and floors. That remains the case to this day. As growing confidence in the technology started surfacing, sandwich composites started being used in more critical parts like spoilers, rudders, ailerons, and flaps [31].

With the Boeing 747, first flown in 1969, sandwich structures were used extensively for large civil aircraft: half the area of the wing and other items like the belly fairing were in glass fiber/Nomex honeycomb. But all the major structural components, such as the wing and tail boxes and the fuselage, were still the usual stiffened aluminum panels as shown in the Figure 2.2. The march toward composite materials pressed on with aircraft such as the ATR 72, which, in 1988, had its maiden flight, becoming the first civil aircraft in which a primary structure—the wing box—was certified in carbon fiber. This airplane and newer models, such as the Airbus A320, A330, and A340, also used a variety of sandwich structures for secondary structural parts based on skins constructed from glass, Kevlar, and carbon. Although sandwich composites have been used widely in the past, the modern design of aircraft has depicted a general shift to monolithic structures, which offer economic benefit. For instance, in the new models such as Airbus A380, Boeing 787, and Airbus A350, as indicated on Figure 2.3, the use of sandwich materials is only limited to critical parts, among them being the belly fairing and the nacelles; other parts go for self-stiffened monolithic structures. This evolution reflects ongoing advances and economic considerations in aerospace material technologies [29].

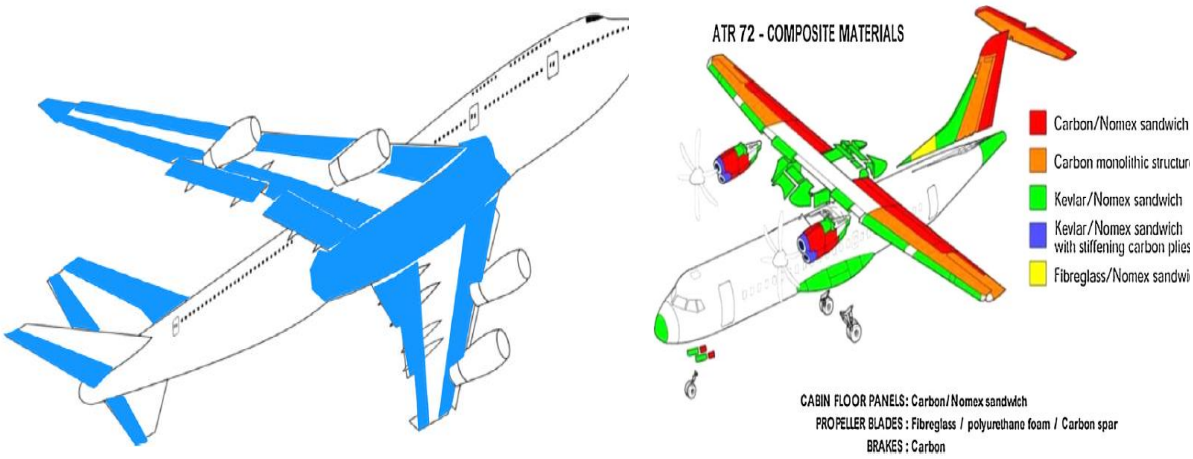

Figure 2.2 : (a) Boing B747 overview of sandwich structure (b) ATR 72-Composite Material [29].

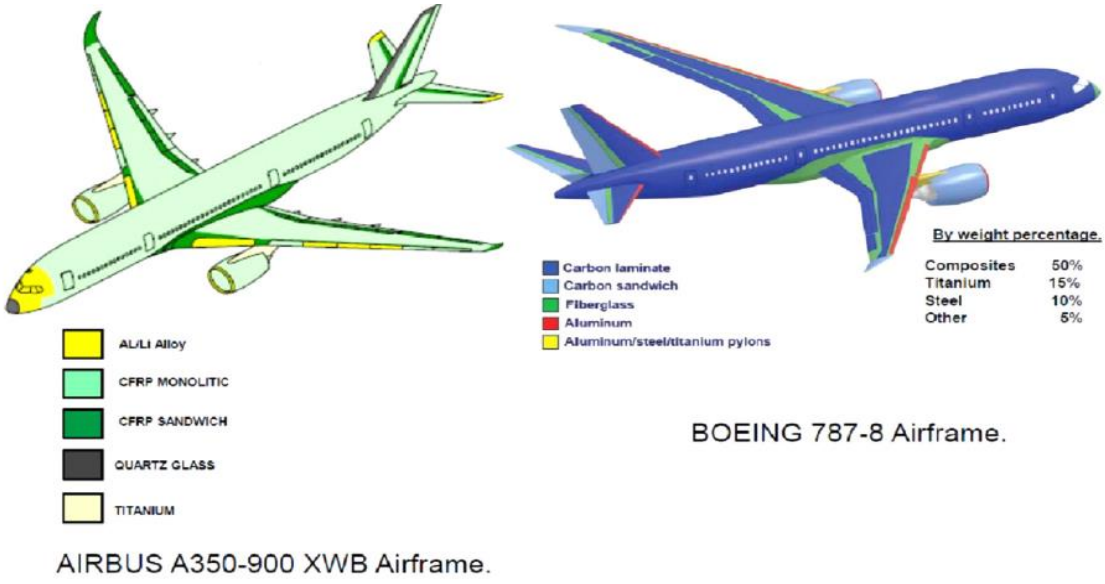

Figure 2.3 : Sandwich and composite structures A350 and B787 composite Aircrafts [29].

2.1.2. Sandwich Structures on Marine Transportation

The marine sector has shown increasing interest in composite sandwich materials and their use to primary structural parts in recent years. These materials' success in the aerospace industry has led to study and development in the marine field [32]. Conventional fiberglass composites have dominated the recreational boating market for more than 30 years due to their many benefits over other building materials with their low start-up cost [33], [34]. The marine sector makes extensive use of these materials because of their high specific strength and stiffness, ability to realize complex geometries, and good resistance to the environment [34].

The research on composite materials has tremendously been bettered in the selection of components and the techniques for manufacturing them. An essential move was the one done by the marine industry, one of the most important industrials, from its usual monolithic steel to sandwich structures: a light core material with either foam or wood and laminated skins. Such changes have allowed manual processes, more sophisticated procedures, and, in recent years, many shipyards all over the world to quick development [34] [32].

Following this, the use of sandwich structures has gained immense popularity in the race for faster and larger ships. This design direction, in turn, helps to build lighter yet stronger vessels, offering numerous advantages such as increased acceleration, lower fuel consumption, and a lower environmental footprint when we compared to ordinary ships which are made from steel as shown on Figure 2.4. That will also enable light ships to run with less engine power and hold more cargoes, which are heavy in weight. Consequently, a sandwich structure may well be considered a very attractive alternative concept for boat building with respect to modern trends in optimization of material use and structural efficiency in shipbuilding [34].

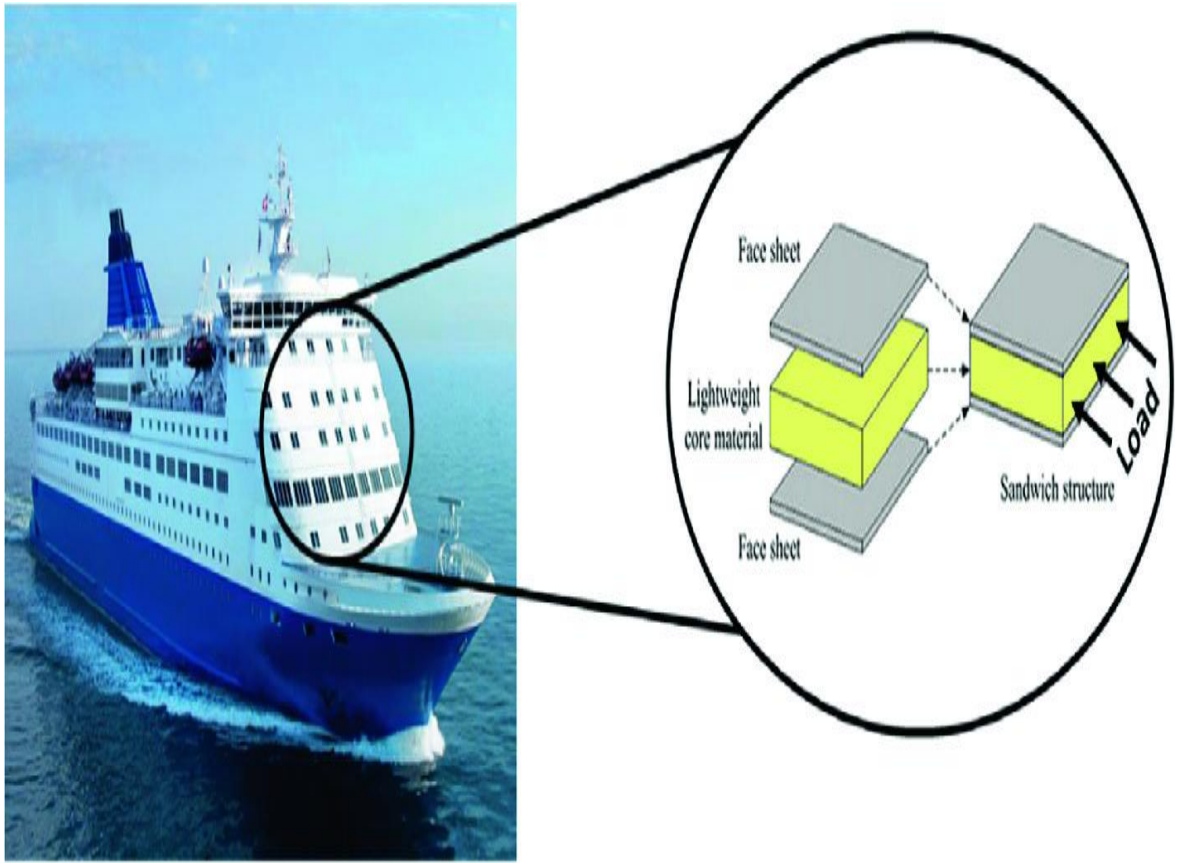

Figure 2.4 : Potential substitution of steel with composite sandwich structure for boat construction [35].

2.1.3. Sandwich structure on Civil construction and Architecture

Fiber-reinforced polymer (FRP) sandwich systems are special types of laminated composite built by attaching two thin layers to a substantial but light core. Such systems have found great application in those situations where high bending stiffness and strength are demanded, while the material itself needs to be lightweight. As mentioned previously, FRP sandwich systems are very widely used in industries for aerospace, aircraft, and marine applications due to optimization in vehicle performance. More recently, interest in these materials has arisen within the construction industry because of the successful alternative being offered by these systems for special application in civil infrastructure [36]. The last decade has witnessed an increasing utilization of composite materials in bridge applications. Applications have found wide acceptance in the area of reinforcement and repair. A considerable number of newer constructed bridges are either hybrid (using conventional materials with reinforced polymer) or all-FRP constructions. This increase has mainly been due to the useful properties of FRP composites, such as high resistance to corrosion and fatigue, low self-weight, high strength, and a high degree of free formability. The first hybrid FRP-concrete road traffic bridge was the Miyun bridge in China in 1982. The simply supported two-lane bridge comprises six honeycomb sandwich FRP box girders and a 10 cm thick reinforced concrete deck stiffened to the girders with shear bolts. A composite bridge was built in Australia in 2002. This is a ten-meter design spanning bridge. The structure is designed with the use of side-by-side-aligned FRP beams that are joined together using epoxy adhesive. The beams are further connected at the bottom through a transverse laminate to provide plate behavior and enhance stiffness in the transverse direction. A layer of concrete in the compression zone, bounded by epoxy to the FRP, allows for composite action [37].

In addition to this, sandwich panels of novel designs, again using bonded FRP mostly in combination with other materials, are developed for use with railway sleeper technologies [38]. This technology specifically aims at replacing deteriorating timber sleepers in mainline tracks, turnouts, and transoms among others for uses in the railway as illustrated on Figure 2.5. The sandwich panel sleeper of FRP is an important design where it is utilized edgewise with top and bottom GFRP plates and a polymer coating based on epoxy [8]. This sleeper arrangement takes care of the special loading requirements for mainline railways where the sleeper is mainly laden at the points where it hits the rails. Its practical use is further expanded by the ability that, like common timber sleepers, this design allows on-site drilling. Fifty of this sleeper type were cast for use on the Queensland Rail Line in Australia in 2014 and have been in operation ever since [36].

Figure 2.5 : FRP sandwich panels for Railway sleepers (a) timber replacement sleepers (b) Turnout sleepers [36].

2.2. Mechanics of Wrinkling of Sandwich Structure

Wrinkling of sandwich beams during compression or bending refers to a specific type of buckling when the compression facing develops localized, short wavelength wrinkles as illustrated in Figure 2.6. Wrinkling can be understood as the buckling of the compressed surface that is supported by a flexible or partially flexible material, known as the core. It is a common failure mode of sandwich beams, leading to a loss in beam stiffness. The wrinkling phenomenon is characterized by the interaction between the core and the facing of the sandwich structure. Thus, the critical wrinkling load is a function of the stiffnesses of the core and facing, the geometry of the structure and the applied load [13].

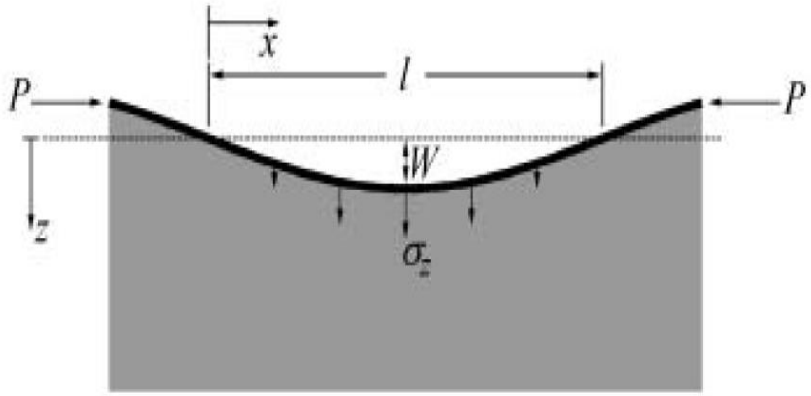

Figure 2.6 : Basic wrinkling wave.

Several authors had earlier studied all three modes of wrinkling [6][23], [39]. Niu and Talreja et.al [40] had provided a coherent theoretical foundation for understanding and solving these three modes as illustrated in Figure 2.7. The modes are based on the elasticity and thickness of the core, whether isotropic or anisotropic. The first failure mode is One-sided wrinkling or "Rigid base," which occurs in pure compression if the sandwich consists of asymmetric face sheets with different wrinkle loads, or occurs in bending where only one face sheet gets compressed. An example of one-sided face wrinkling, such as in the axially compressed sandwich panel with thick, unsymmetrical face layers or a cylindrically bent sandwich panel in which just the face under compression is wrinkled and the other face is left flat.

The second mode, known as antisymmetric wrinkling (in-phase) or the 'Snake' mode, isn't strictly a localized phenomenon and shouldn't be addressed using traditional wrinkling formulas. Unlike other forms, in this mode, the core's middle plane is not left undeformed, and the core's thickness plays a crucial role in determining both the natural wavelength and the critical load. This instability is more accurately described by global buckling formulas, which consider the overall dimensions of the sandwich structure [41]. This mode typically becomes relevant only in very narrow plate scenarios. For beam-type structures (those without supported unloaded edges), this kind of thin sandwich is more prone to global buckling [2]. Moreover, sandwiches that have honeycomb or other anisotropic cores with a high ratio of out-of-plane Young's modulus to shear modulus are more susceptible to this 'Case II' wrinkling but generally face even lower loads before failing due to global stability issues [40].

The third mode, referred to as symmetric (out-phase) or the "hourglass" mode, is essentially a distinct form of one-sided wrinkling that is impossible to observe in reality. If the sandwich is thin enough for one face sheet to affect the stability of the other, it will result in symmetric wrinkling. This situation has a shorter natural wavelength and a higher stability failure load compared to the other two possibilities [41].

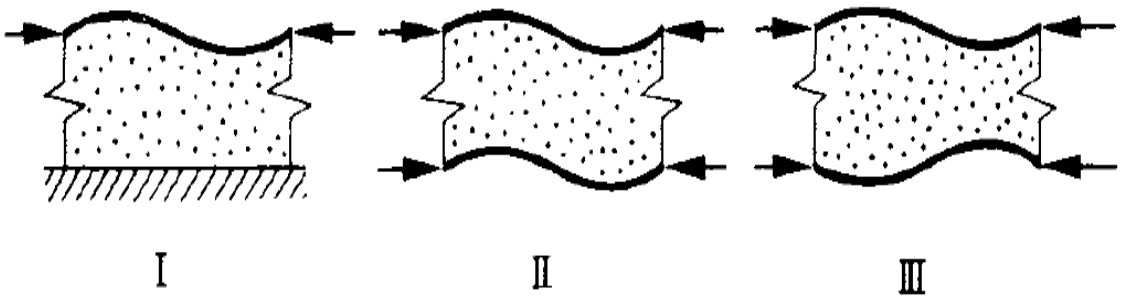

Figure 2.7 : Wrinkling Mode Case I-III [39].

2.2.1. Analytical Wrinkling of sandwich structure with soft cores and Isotropic face sheets

The earliest studies on the wrinkling of sandwich struts focused strictly on designs with isotropic face sheets and a solid, isotropic core. This pioneering research was done by Gough et al [22]. which developed classical theories of beam buckling and elasticity while accounting for the consequences of the support provided by a continuous elastic medium. Starting with basic beam theory equations, the analysis focuses on how lateral support affects the critical buckling load. The core assumptions include the isotropic and homogeneous nature of both the skin and the supporting medium [39]. They operated under three key assumptions: first, that the face sheets could not extend; second, that the core was firmly attached right at the middle surface of the face sheets; and third, that the effect of compressive stresses in the core, aligned with the direction of the applied load, could be overlooked when considering the stability of the face sheets [2]. Gough, Elam, and de Bruyne [22] explored the wrinkling behaviour of sandwich struts under these conditions, the first class focuses on a sandwich beam likely to experience wrinkling only in the compression face, while the tensile face remains flat, and the second case, when both faces bear equal axial thrusts, and the third, deal with symmetrical wrinkling by using the specific boundary conditions for the core shown in Figure 2.8 [39]. Theoretical analysis explores the stability of composite structures through a range of support scenarios and boundary conditions. The assumptions about the mechanical and physical interactions between the skin and supporting medium—both in adhesion-free and adhesion-filled cases—are described in great depth.

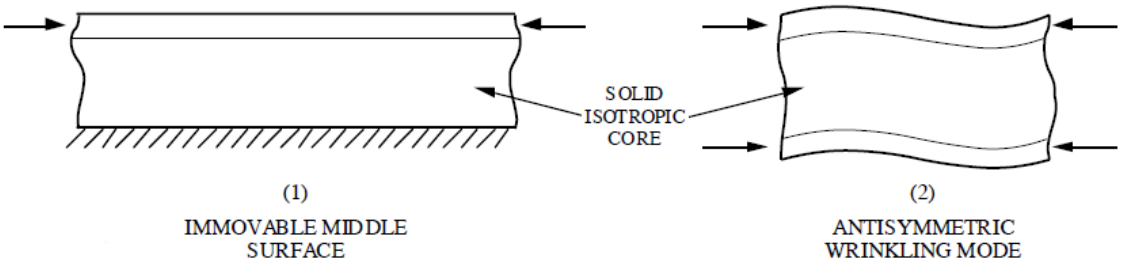

Figure 2.8 : wrinkling model by Gouge, Elam and de Bruyne [2].

According to Gough, Elam, and de Bruyne[22], for the sandwich structure with a sufficiently thick core, the stress at which wrinkling would theoretically occur σ_{wr}, is given by:

$$\sigma_{wr} = 0.794^{*}\sqrt[3]{E_f E_c G_c} \tag{2-1}$$

where E_f is the longitudinal Young's modulus of the face, E_c is the through-thickness of Young's modulus of the core, G_c is the transverse shear modulus of the core. Since the thickness of the core is infinite thickness it should satisfy the following :

$$\left(\frac{t_f}{t_c}\right)\left(\frac{E_f}{E_c}\right)^{1/3} < 0.2 \quad (2\text{-}2)$$

Where t_f is the thickness of the facesheet, t_c is the thickness of the core, and by assuming that the Poisson ratio, V_c is taken as zero [2].

For a sandwich structure with a thinner core, the stress of wrinkling load will be:

$$\sigma_{wr} = 0.630 * \sqrt[3]{E_f E_c G_c} \quad (2\text{-}3)$$

The thickness of the core should satisfy the following,

$$\left(\frac{t_f}{t_c}\right)\left(\frac{E_f}{E_c}\right)^{1/3} > 0.2 \quad (2\text{-}4)$$

The analysis revealed that the critical wrinkling conditions depend heavily on the material properties and the thickness of both the core and the facesheet. Particularly, when the core is sufficiently thick relative to the facesheet and the modulus of the core is substantially less than the modulus of the facesheet, the assembly can be treated as a plate on an elastic foundation [39].

Syed Yusuff [23] studied a comprehensive theory of wrinkling in sandwich structures which was investigated in two distinct parts. The first part of the analysis considers the core to be of definite thickness where the stress leading to wrinkling is determined by a straightforward formula. This formula incorporates Young's moduli of the materials involved and the thickness ratio between the face sheet and the core. The overall methodology remains basically the same as that detailed in the second segment of the study, though it is further developed to account for the influences brought by shearing stresses within the core. The analysis also provides for cases wherein the face sheet is supported on a very thick or possibly semi-infinite medium. When the core of a sandwich structure is relatively thin, it may fail under compressive end loads by causing the entire structure to bow, similar to how Euler buckling affects slender columns [42]. On the other hand, if the thickness of the sandwich structure is sufficient to prevent this type of global failure, the face of the sandwich is more likely to experience buckling in short waves. For a sandwich struture with a finite core thickness, where ripples symmetric to the central plane of the core exist in both skins, buckling is expected to occur as depicted in Figure 2.9. This kind of failure includes the skin bending and the core fibers compressing or elongating perpendicular to the central plane [23].

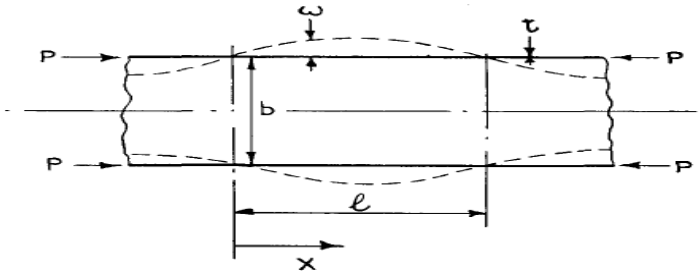

Figure 2.9 : Sandwich wrinkling with a thinner core [23].

As a type of buckling, wrinkles can be explained using the differential of the fourth-order bending theory, which is elastically supported and subjected to the axial force p.

$$\frac{d^4w}{dx^4} - \frac{P}{EI}\frac{d^2w}{dx^2} + \frac{k}{EI}w = 0 \tag{2-5}$$

Where P is the axial load per unit width, E is the modulus of elasticity in the face sheet, I is the moment of inertia, K is the Modulus of the foundation provided by the core which is expressed by mass per unit area per a deflection, which is given by one-half of the core, and dependent on Young's modulus of the core, and the thickness of the core.

$$\mathrm{K} = \frac{2E_c}{b} \tag{2-6}$$

and w is the deflection of the beam, since this analysis is a periodic solution of equations, the beam (skin) may be assumed to buckle in a sine wave of deflection, which is dependent on the amplitude of the wave (A) and angular frequency of the wave which is described by half wavelength across in the X-direction.

$$w = A * sin\left(\frac{\pi x}{L}\right) \tag{2-7}$$

By using the above equations, Yusuff [23], develops the critical wrinkling stress for a thinner core sandwich structure provided by a straightforward square root formula that consists of the material's Young's moduli and the face-to-core thickness ratio as follows:

$$\sigma_{cr} = \left(\sqrt[2]{2/3\, E_f E_c\, t/b}\right) \tag{2-8}$$

Where $\mathrm{E_f}$ is Young's modulus of the face, $\mathrm{E_c}$ is Young's modulus of the core, t is the thickness of the core, and b is the thickness of the core.

The second part of the study, developed by Syed Yusuff [23], was a buckling of a sandwich panel with a face supported by a thick enough core. To make it a bit more complete, this part of the study also considers the shearing stresses in the core. The faces are analyzed as if they were beams supported by an elastic foundation. Shearing stresses are present in this section, however, and it is difficult to make a direct determination of the modulus of the foundation as was previously done. As shown in Figure 2.10,

the buckling pattern is assumed as symmetrical, and only in the narrow or marginal zone of width W adjacent to the faces can displacements occur within the core. The width of the zone where displacements occur is limited to at most half the thickness of the core. These displacements are most stated at the interface between the core and the face, diminishing linearly to zero by the time they reach the full depth of W.

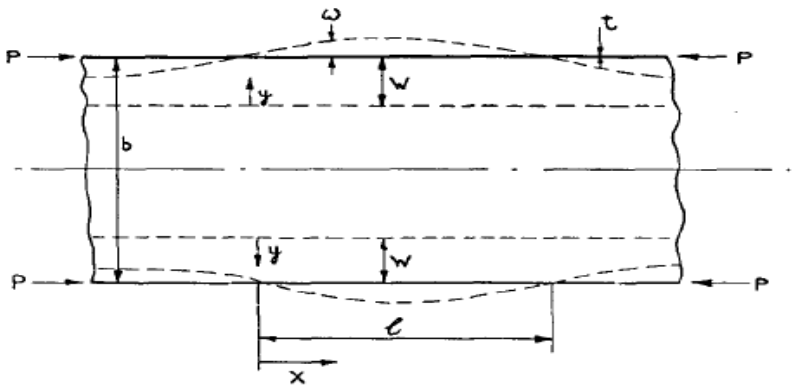

Figure 2.10 : Sandwich wrinkling of construction when the thickness of the core is large [23].

According to Yusuff [23] the principle of maximum strain energy accumulated in the springs can be employed to derive the critical wavelength and the critical stress from the sum of strain energies, extensional and shear, which arise from compression or tension and shear stress, respectively, that are stored in the core material. This principle ensures the conservation of mechanical energy within the system. It balances the energy discharge from the springs to the energy input to the core by deformation. Consequently, Yusuf has formulated the following equation for finding the critical stress:

$$\sigma_{wr} = 0.961 * \sqrt[3]{E_f E_c G_c} \tag{2-9}$$

Where $\mathrm{E_f}$ is the longitudinal Young's modulus of the face, $\mathrm{E_c}$ is the through-thickness of Young's modulus of the core, $\mathrm{G_c}$ is the transverse shear modulus of the core. The analythical formulation for Yusuff wrinkling stress illustrates on part 2 of Annex I.

Hoff and Mautner [6] outlined more straightforward symmetric models for sandwich struts with isotropic face sheets and solid cores, as illustrated in Figure 2.11. The assumption was made that deformations in the core would linearly decrease to zero across a narrow zone with a width (w) which is called a marginal zone. The width is chosen by the smaller of two values: half the thickness of the core or a number that minimizes the stress on the facesheet, calculated using a total potential energy technique. The buckling load is determined by verifying that the work done by the compressive force, which causes a vertical displacement at the site of application due to the bending of the face layer, is equal to the total strain energy accumulated. This total includes the strain energy stored in the face material from bending,

along with the strain energy in the core from shear and extension. The Hoff and Mautner [6] equations for critical stress often rely on the sandwich structure width-to-thickness ratio. Nonetheless, the expression for symmetric wrinkling of a sandwich structure with a thick core (where w < b/2) gives a fair estimate of critical stress in all circumstances, this critical stress can be expressed by:

$$\sigma_{wr} = 0.910 * \sqrt[3]{E_f E_c G_c} \quad \text{(without Knockdown factor)} \tag{2-10}$$

$$\sigma_{wr} = 0.5 * \sqrt[3]{E_f E_c G_c} \quad \text{(with Knockdown factor)} \tag{2-11}$$

Where E_f is the longitudinal isotropic Young's modulus of the face, E_c is the through-thickness of Young's modulus of the core, G_c is the transverse shear modulus of the core. The analythical formulation for Hoff and Mautner wrinkling stress without Knockdown factor presents on part 1 of Annex I.

If the width of the marginal width zone (w) is greater than half of the core thickness (w > t_c /2), the critical wrinkling stress can be expressed as:

$$\sigma_{wr} = \sqrt{E_f E_c}\sqrt{t/b} + 0.1667 G_c (b/t) \tag{2-12}$$

Where E_f is the longitudinal isotropic Young's modulus of the face, E_c is the through-thickness of Young's modulus of the core, G_c is the transverse shear modulus of the core, t is the thickness of the face sheet, and b is the thickness of the core.

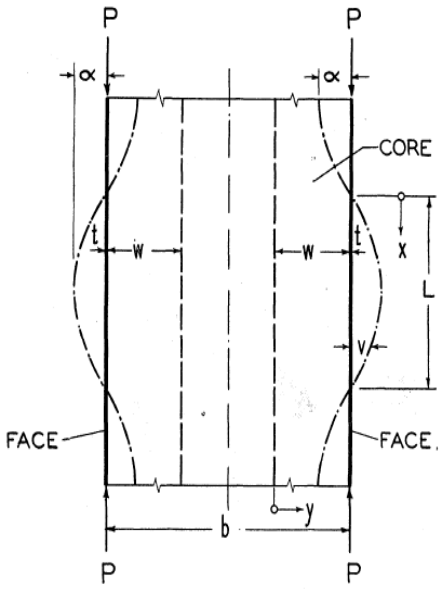

Figure 2.11 : Symmetric shape of sandwich structure proposed by Hoff and Mautner [6].

Subsequently, to align with experimental results, the factor of 0.91 in these formulas was knockdown to 0.5. This adjustment is still used in the industry today, where the factor 0.5 precedes the cube root expression. This modification was suitable at a time when sandwich panels were constructed with quasi-isotropic face sheets reinforced by fiber or isotropic metal face sheets [15].

Plantema introduced an improved theory for examining sandwich strucures. He departed from the conventional belief that face sheet materials are isotropic and homogeneous, and instead proposed a description that relies on local bending stiffness. In addition, he substituted the linear stress decay model across the material's thickness with an exponential decay function. This function exhibits a fast decrease in stress at the loading source, followed by a plateau or gradual decrease as it approaches other regions [43]. This technique recognizes the intricacies of material behavior, specifically in composite materials and constructions where the stress distribution is non-uniform. Plantema's theory incorporates the fluctuations in bending stiffness and utilizes a more exact stress decay model. This theory offers a more realistic and accurate framework for forecasting the performance of sandwich panels under different loads. As a result, it improves the design and safety of engineering applications. The formula proposed by Plantema is provided as follows [41] :

$$\mathrm{P_{cr}} = \frac{2}{3}\sqrt[3]{D_f E_c G_c} \tag{2-13}$$

Where $\mathrm{P_{cr}}$ is a critical load, $\mathrm{E_c}$ is Young's modulus of the face, $\mathrm{G_c}$ shear modulus of the face, and $\mathrm{D_f}$ is a bending stiffness. The bending stiffness for isotropic face sheet material can be calculated as follows:

$$\mathrm{D_f} = \frac{E_f t_f^3}{12} \text{ for a narrow beam} \tag{2-14}$$

$$\mathrm{D_f} = \frac{E_f t_f^3}{12(1-v_f^2)} \text{ for a plate in cylindrical bending} \tag{2-15}$$

By substituting the bending stiffness equations (2-14) and (2-15) on equation (2-13) we can get the wrinkling critical stress for a narrow beam and for a plate:

$$\sigma_{\mathrm{wr}} = 0.825 * \sqrt[3]{E_f E_c G_c} \text{ for a narrow beam} \tag{2-16}$$

$$\sigma_{\mathrm{wr}} = 0.85 * \sqrt[3]{E_f E_c G_c} \text{ for a plate (with poisson ratio = 0.3)} \tag{2-17}$$

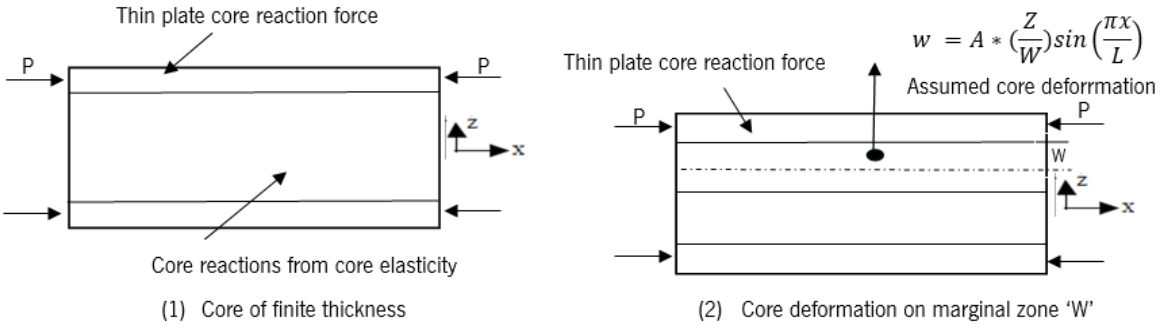

Figure 2.12 : Sandwich model for finite core thickness (1) and infinite thickness (2).

Table 2.1 : Summary for analytical wrinkling formulation.

Reference	Model	Parameter	σ_{cr}	Half-wavelength	Hypothesis and Assumption
Hoff and Mutiner (W<tc/2) [6]	(2)	Ef,Ec,Gc	$0.961*\sqrt[3]{E_f E_c G_c}$	$1.648 t_f \sqrt[6]{\frac{E_f^2}{E_c G_c}}$	Strain Energy theory. Work done by compressive force is equal to the summation of the strain energy of bending stored and strain energy of Extensional and shear stored energy.
Hoff and Mutiner (W>tc/2) [6]	(2)	Ef,Ec,Gc,t,b	$\sqrt{E_f E_c}\sqrt{t/b} + 0.1667 G_c(b/t)$		
Gouge, Elam and Debruyen[22] $(tf/tc)(Ef/Ec)^{1/3} < 0.2$	(1)	Ef,Ec,Gc	$0.794*\sqrt[3]{E_f E_c G_c}$	-	The solution to this is by solving Biharmonic equation of elasticity for the core stress function by ensuring the core is in a state of plane stress and by enforcing the core boundary condition. The face sheet is inextensible. The core has different boundary conditions.
Gouge, Elam and Debruyen[22] $(tf/tc)(Ef/Ec)^{1/3} > 0.2$	(1)	Ef,Ec,Gc	$0.630*\sqrt[3]{E_f E_c G_c}$	-	
Plantema (For narrow beam) [41]	(1)	Ef,Ec,Gc	$0.825*\sqrt[3]{E_f E_c G_c}$	$1.9 t_f \sqrt[6]{\frac{E_f^2}{E_c G_c}}$	Strain energy theory. By assuming the total potential energy is the sum of the bending energy of the face and strain energy of the core.
Plantema (For plate with poisson ratio=0.3) [41]	(1)	Ef,Ec,Gc	$0.85*\sqrt[3]{E_f E_c G_c}$		
Yusuff [23] (W<tc/2)	(2)	Ef,Ec,Gc	$0.960*\sqrt[3]{E_f E_c G_c}$	$1.307 t_f \sqrt[6]{\frac{E_f^2}{E_c G_c}}$	Strain energy theory, Strain energy stored in the core is equivalent to the sum of extensional and shear strain energies stored in the core
Yusuff [23] (W=tc/2)	(2)	Ef,Ec,Gc	$0.820*\sqrt[3]{E_f E_c G_c}$		
Yusuf [23] (W>tc/2)	(1)	Ef,Ec,t,b	$\sqrt[2]{2/3\, E_f E_c\, (t/b)}$		Assumes when the outer face layers bend and the core fibers either compress or elongate in directions that are perpendicular to the central plane.

Allen [16]	-	$\frac{3}{\sqrt[3]{12(3-vc)^2(1+vc)^2}}\sqrt[3]{E_f E_c^2}$	$2.09 t_f \sqrt[6]{\frac{E_f}{E_c}}$	

where the core normal modulus, the core transverse shear modulus, the skin Young's modulus, skin thickness, Poisson's ratio of the core and wrinkling stress are represented as $\mathrm{E_c}$, $\mathrm{G_c}$, $\mathrm{E_f}$, $\mathrm{t_f}$, v_c and σ_{cr} respectively.

2.2.2. Experimental viewpoints of sandwich wrinkling

In 2004, Vinod Vadakke and his colleagues conducted an experimental study on a sandwich sample consisting of glass/vinyl ester face sheets and PVC foams. The objective of the investigation was to examine the compression failure of the sample by employing an end-loading test fixture [44]. The primary aim of the study was to examine the roles of the faces and core in the failure process under extreme stress circumstances. The compression failure mechanism test involved the examination of several foam cores sandwich specimens with composite face sheets by using sandwich compression end-loading test fixture as shown in Figure 2.13. Various failure modes were identified in the specimens, including face sheet compression and global buckling, based on factors such as core stiffness, core thickness, and gage length. It was found that the failure mechanism of a specific sandwich changed from compressing the face sheet to wrinkling as the length of the measurement varied from short to long [12]. Additionally, it was seen that even longer specimens failed due to global buckling. The transition from face compression to wrinkling was found to be controlled by the thickness and density of the core. Specifically, a sandwich with a thick, low-density core is more prone to wrinkling.

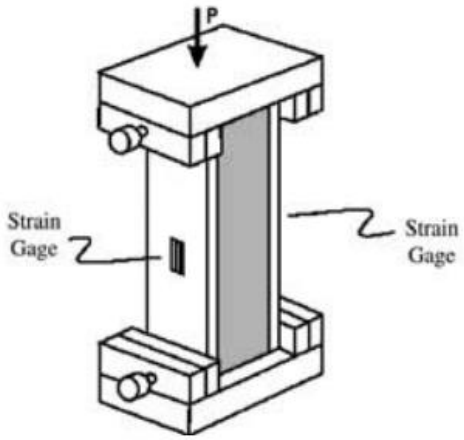

Figure 2.13 : Sandwich compression end-loading test fixture [44].

Daniel et al. [12] employed three different loading configurations, namely three-point, four-point, and end-loaded cantilever beams as illustrated on Figure 2.14, to investigate alternate failure processes in

sandwich structures. The specimens were subjected to shear and bending moments due to various loading arrangements. Fluctuations were detected in the wrinkling load recorded for each load condition. The specimens utilized to measure the wrinkling failure loads were sandwich columns subjected to end compression, beams subjected to three- and four-point bending, and cantilever beams subjected to end loading. Wrinkling can occur when the core material is still within the plastic range or the linear elastic range, depending on the elastic properties of the core material (Young's modulus and shear modulus) and the length of the beam. In order to compensate for the decrease in core stiffness during the three-point bending scenario, a factor for reducing core stiffness was selected. The investigation results revealed that wrinkling is predominantly influenced by the core moduli. Specimens with foam cores exhibited wrinkling, while those with honeycomb cores did not.

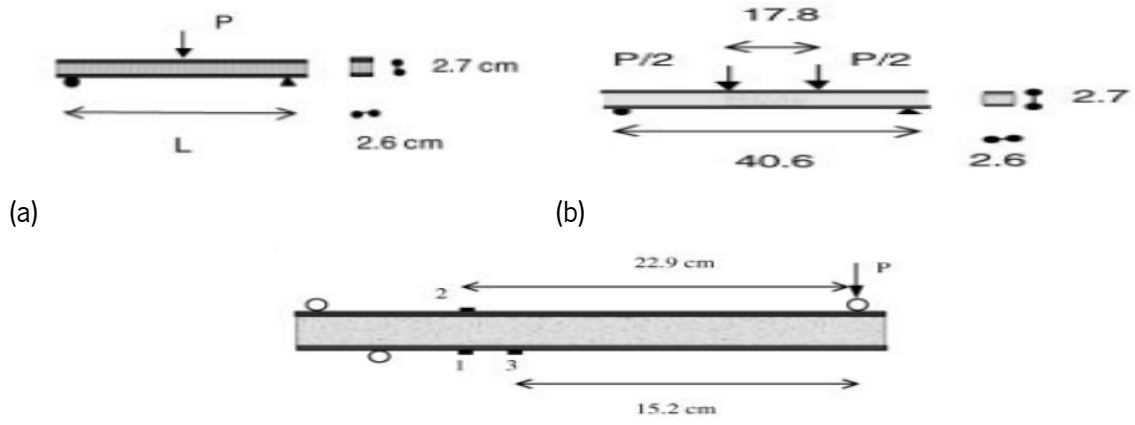

Figure 2.14 : Three-point bending (a), four-point bending (b), and End-loaded cantilever beam (c) [12]

Manshadi B. et.al. conducted an experimental investigation [45]. A sandwich panel consisting of a glass fibre-reinforced polymer face sheet and a stabilized polyurethane core was subjected to an in-plane biaxial compression-tension wrinkling experiment by using Instron planar biaxial cruciform testing machine as shown in the Figure 2.15. Shear wrinkling is a critical failure mechanism that occurs in the sandwich webs due to the application of shear pressure, leading to local buckling. A square sandwich panel was made using hand lay-up technique. The panel consists of two unidirectional E-glass fiber face sheets and one thin face sheet, which is stabilized by a thick PU foam. During the in-plane biaxial compression-tension test, two typical forms of wrinkling failures were observed: a wrinkled wave on the face sheet that either penetrated the foam or appeared on its surface. with lower tension loads, the wrinkling loads demonstrate a noticeable declining pattern that decelerates with higher tension loads.

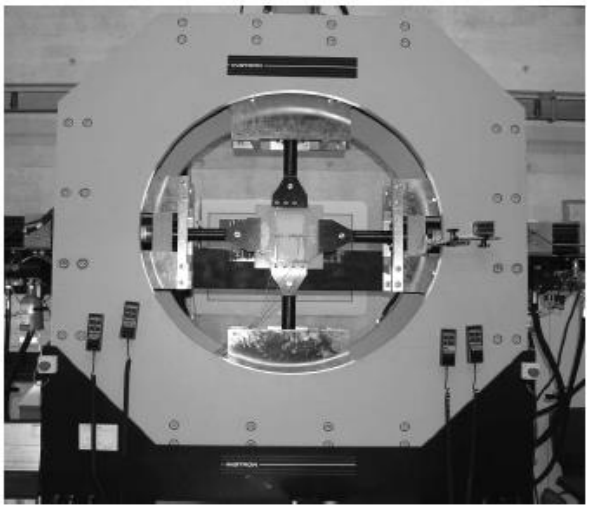

Figure 2.15 : Instron planar biaxial cruciform testing machine [45].

2.2.3. Numerical Analysis of Wrinkling Theory

Fagerberg et.al. [26] performed a study on the stability of wrinkling issues using linear elastic Finite Element (FE) simulations with the FE-code ABAQUS. The simulation investigation involved the application of both a uniaxial force and a biaxial load to the specimen. The central model utilized 20 node-brick elements for the uniaxial loading condition, while the face sheets employed eight node-shell elements. The simulation utilized linear elastic material behavior and characteristics for the core and face sheet parts. In this finite element analysis, the two opposing loading edges were modeled as parallel and coplanar. The face sheets' edges, which were subjected to a load, were immobilized in rotation along their axis to prevent localized buckling at the point where the stress was applied. The buckling load was determined using the eigenvalue buckling method implemented in the finite element program. The Finite Element (FE) model utilized a sufficiently refined mesh density to accurately approximate the buckling load. The selection of mesh density for the model is additionally determined by the computational capacity at hand. The finite element (FE) computations as shown in Figure 2.16 showed excellent agreement with both experimental tests and analytical solutions under uniaxial loading conditions. The results of the wrinkling angle likewise demonstrate a strong concurrence between the numerical method and the test results. The angle was calculated by assessing the ratio between the applied stress and the load capacity of the panel, namely the point at which wrinkling occurs. Fagerberg et al.[26] conducted a biaxial loading test to evaluate the results of the finite element analysis with the analytical results. The finite element (FE) model utilized for the biaxial loading situation was analogous to the model used for the uniaxial loading scenario. However, in this case, additional forces known as multi-point constraint forces were placed at

the borders of the structure to maintain its flatness. This finite element (FE) model roughly replicates the test configuration, but it deviates significantly from the assumptions established in the analytical approach. In addition, the wrinkling pattern does not accurately represent the purely cylindrical bending of the face sheets and cannot be adequately characterized by a basic sinusoidal wave pattern.

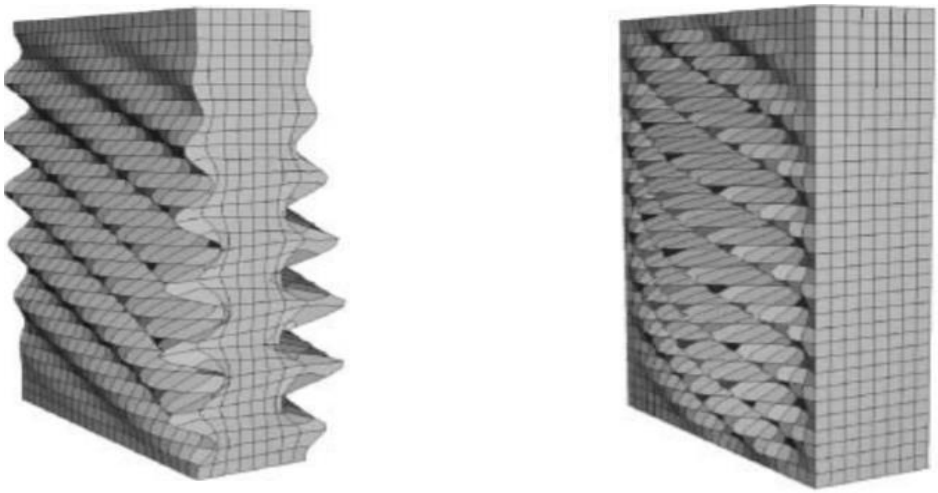

(a) (b)

Figure 2.16 : Uniaxial FE wrinkling result (a), Biaxial FE wrinkling result (b) [26].

Manshadi B. et.al [45] conducted a study on the shear wrinkling of a sandwich panel made of glass fiber-reinforced (GFRP) with a cell-core structure. The panel was subjected to biaxial compression-tension stress. This study conducted in-plane biaxial compression-tension wrinkling experiments on GFRP sandwich laminates with polyurethane foam cores. The experimental findings were then validated by finite element analysis with the first buckling mode value as shown in the Figure 2.17. The wrinkling stability was analyzed using ANSYS software through a linear elastic finite element (FE) analysis. The foam in the face sheets of the specimens was simulated using 8-node layered shell elements (Shell-91) and 20-node structural solid elements (Solid-95). A mesh consisting of 5432 components was utilized. The provided sample investigates the experimental findings on the wrinkling properties of sandwich panels subjected to different levels of transverse tension strains. The phenomena exhibits a significant decrease in the frequency of wrinkles as the applied strain intensifies. However, when the level of stress increases, the rate at which it decreases slows down and eventually stops. Despite its tendency to amplify experimental data and its inability to accurately reflect the plateau, finite element (FE) analysis nevertheless confirms these conclusions. This continuing experiment aims to evaluate the effects of varying foam core densities and face sheet fiber patterns. To improve comprehension and forecasting abilities in this field, researchers also strive to create an analytical framework that predicts wrinkling loads using transverse tension stresses.

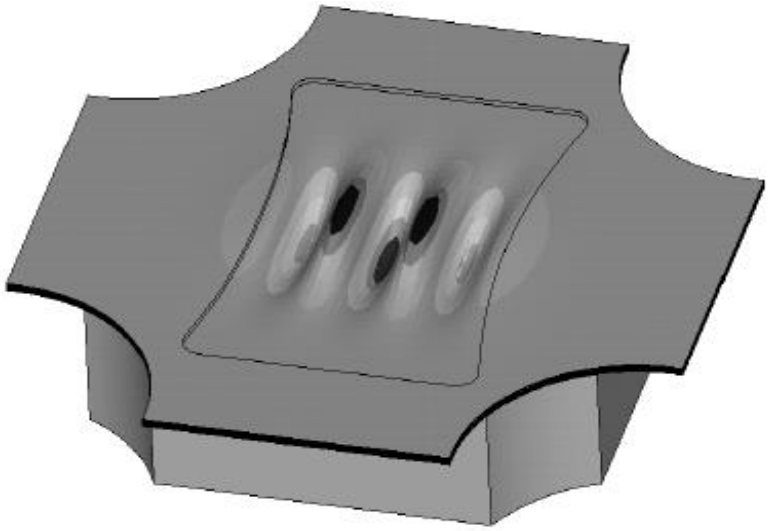

Figure 2.17 : First mode buckling solution [45].

THIS PAGE WAS INTENTIONALLY LEFT BLANK

3. CHAPTER 3. RESEARCH METHODOLOGY

This part of the dissertation explores the materials and numerical simulations employed, along with details on the numerical finite element analysis conducted to meet the objectives of the study.

3.1. Experimental test for shear and compression failure approach

The specimens used for shear failure and compressive failure samples in this study are similar with those used in the experimental tests done by Alawode A. [16] and ISAE SUPAERO students. Moreover, this specimen functions as a reference sample for the aeronautical engineers in the industrial sector at ISAE SUPAERO. Moreover, this specimen functions as a standard reference sample for the aeronautical engineers in the industrial sector at ISAE SUPAERO. The design depicted in Figure 3.1 illustrates the precise dimensions of the shape, which are 50 mm wide, 50 mm height, and 500 mm long.

The sandwich specimen was positioned onto the foundation of the manually operated three-point bending machine, and it was lightly secured to avoid any initial stress in the form of tension or compression on the specimen. In Figure 3.2, the two outer arms functioned as supports, while the central arm was used for applying the load. During three-point bending, the partitions indicate the positions of the wooden structures that are strategically placed to prevent the sandwich foam core from being crushed due to the concentration of force, thereby avoiding localized failure.

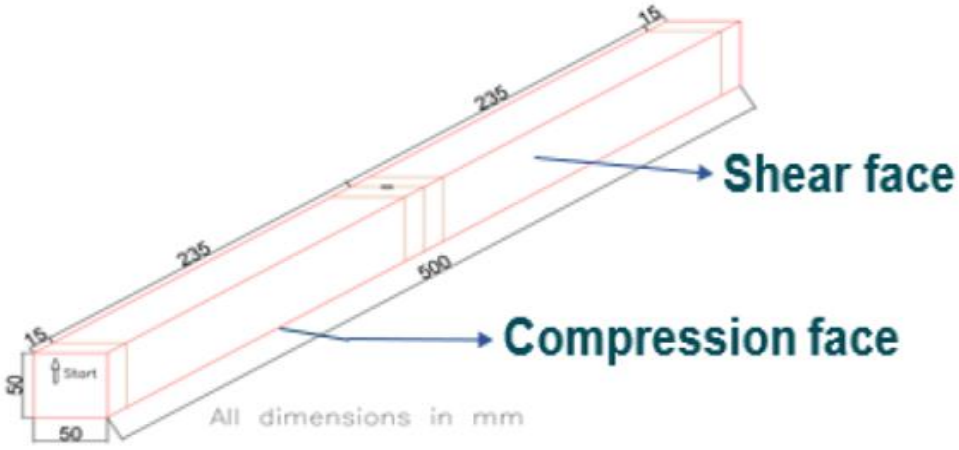

Figure 3.1 : Specimen dimension.

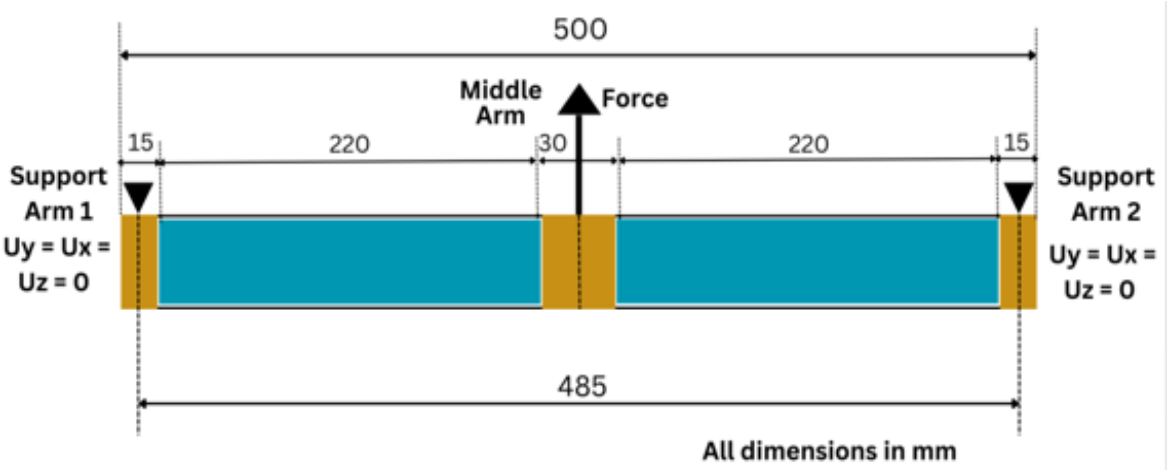

Figure 3.2 : Classical three-point bending test loading scheme [16].

A 25mm LVDT displacement sensor was mounted on the middle arm to measure the vertical displacement during loading for shear failure specimen and a 20mm LVDT displacement sensor for compression failure specimen as illustrated on Figure 3.3. In addition, for both shear and compression failure specimen, a 2mVN HBM S9M/10kN force sensor was attached on the middle arm to accurately measure the force being exerted. The LVDT displacement sensor and the force sensor were linked to an acquisition system for the purpose of storing data. For this study, two DIC cameras with a resolution of 5 Megapixels [picture size of 2462 (H) x 2052 (V)] were used to observe the deformation of the specimen and examine wrinkling. Two cameras were positioned on the sides of the specimen to watch shear failure, while on the other test setup, two cameras were placed at the bottom to monitor the compression failure of the specimen.

(a) (b)

Figure 3.3 : Experimental set-up for classical three-point bending test (a) shear failure, (b) Compression failure.

3.2. Materials and description of sandwich specimen's samples

The sandwich specimen for the skin, which is prone to shear and compression wrinkling failure, consists of a combination of unidirectional [UD] glass fiber-epoxy layers and bi-directional [EC68] fabrics. The core of the specimen is made of isotropic PMI Rohacell 51 WF foam core. Table 3.1 presents the mechanical properties of the skins, Table 3.2 describes the mechanical properties of isotropic foam cores, and Table 3.3 displays the mechanical characteristics of plywood material used at the loading and support locations in the sandwich structure to prevent local failure. The materials used in the Finite Element Analysis simulation were chosen to precisely match their actual counterparts. The model utilized E-glass fibers, PMI ROHACELL 51 WF foam, and wood material, with each component thoroughly characterized to achieve an accurate representation of their individual mechanical properties. The materials used for both the shear and compression test specimens are the same. This setting meant that the simulation precisely matched the material interactions and responses that are expected in the actual production and testing methods.

Table 3.1 : Mechanical properties of skin material [16].

Skin Material	E1 [MPa]	E2 [MPa]	Nu12	G12 [MPa]	G13 [MPa]	G23 [MPa]	Thickness, ts [mm]
Unidirectional	38000	10000	0.25	4000	4000	4000	0.30
Bidirectional [fabrics]	23000	23000	0.098	2900	2900	2900	0.16

Table 3.2 : Mechanical properties of Isotropic core material [16].

Core Material	E [MPa]	G [MPa]	Density [Kg/m3]	Shear Strength [MPa]	Thickness, tc [mm]
Rohacell 51 WF	75	24	52	0.8	50

Table 3.3 : Mechanical characteristics of plywood material [46].

Plywood Material	E11 [MPa]	E22 [MPa]	E33 [MPa]	G12 [MPa]	G13 [MPa]	G23 [MPa]	Nu12 [MPa]	Nu13 [MPa]	Nu23 [MPa]	Density [Kg/m3]
Poplar	10,900	1,003	469	818	752	120	0.392	0.318	0.329	480
Okoume	9000	828	387	675	621	99	0.392	0.312	0.329	430

The stacking pattern for the shear failure has been carefully investigated to capture the localized failure mode on its side of sandwich specimens. To get such kind of wrinkling failure mode, the stacking sequences are for the two sides were stacked with one 45^0 bidirectional plies, and for the top and bottom

laminates composed of five unidirectional plies stacked at 0^0 with an additional two extra 45^0 bidirectional pies at the top, and one extra 45^0 bidirectional pies at the bottom as illustrated on Figure 3.5. The stacking on the top $[0_5/\pm45]$, bottom $[0_5/\pm45_2]$ and on the two sides [±45]. By this configuration, as illustrated by Figure 3.4 the Finite Element Analysis simulations are expected to develop wrinkling on the shear face sides induced by the three-point bending test [16].

For the second type of specimen, which is the compression failure test done by ISAE SUPAERO students, the localized failure was seen on the bottom compression part of the sandwich specimen. The stacking sequences for two sides stacked with one 45^0 bidirectional plies, and for the top and bottom laminates composed of one unidirectional ply stacked at 0^0 with an additional two extra 45^0 bidirectional pies at the top, and one extra 45^0 bidirectional pies at the bottom. The stacking is arranged on the top $[O/\pm45_2]$, bottom $[O/\pm45]$ and the two sides [±45] as shown in Figure 3.6. By this configuration, the Finite Element Analysis simulations are expected to develop wrinkling on the bottom compression side induced by the three-point bending test.

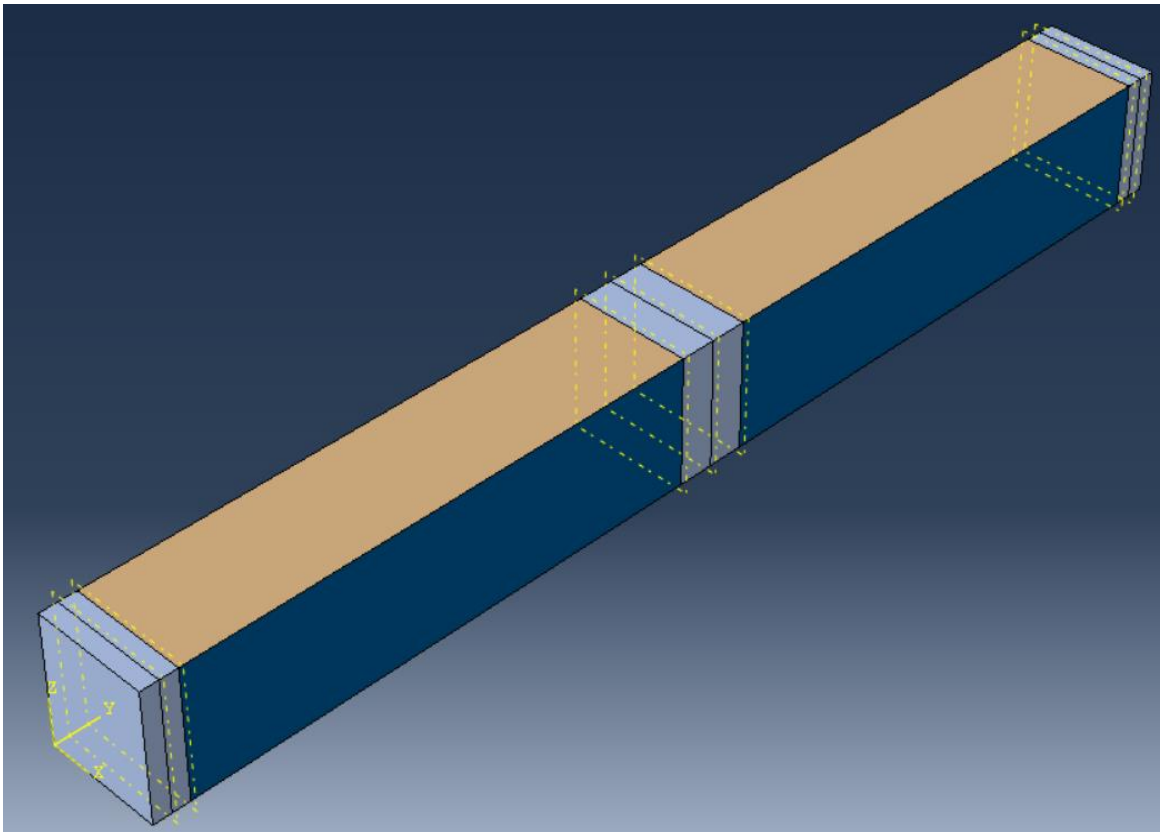

Figure 3.4 : Typical specimen geometrical scheme for sandwich structure on FEA.

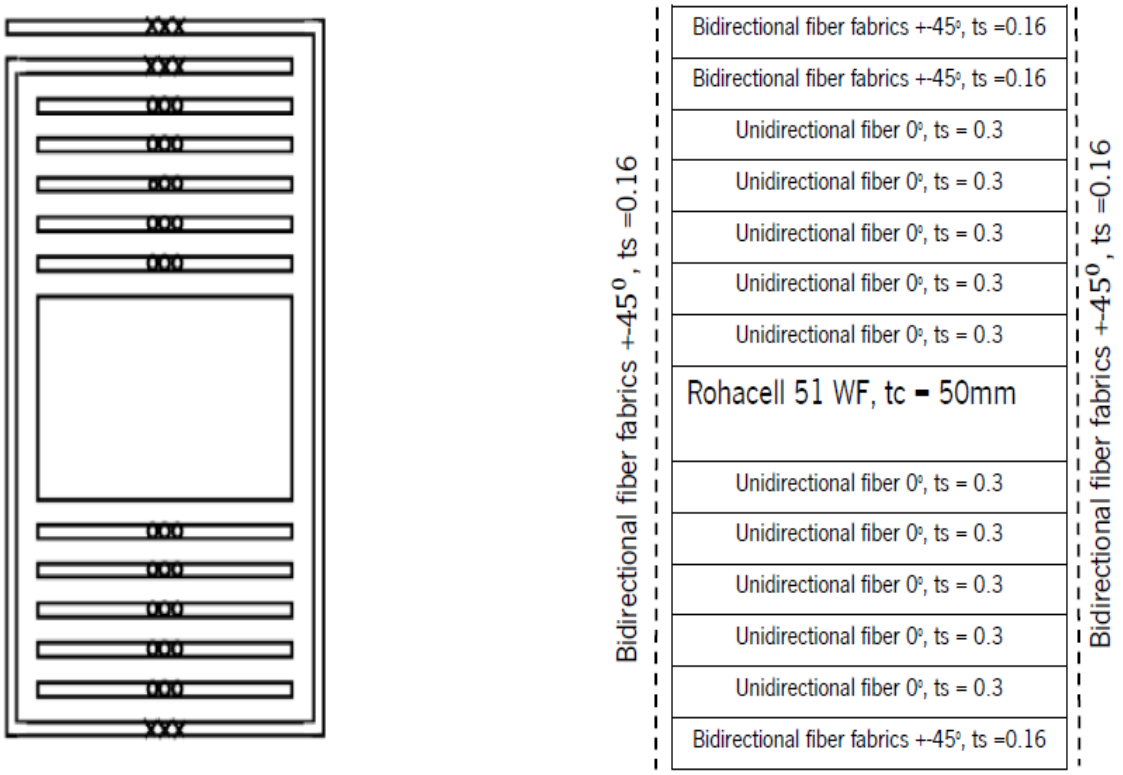

Figure 3.5 : Shear wrinkling failure stacking sequence

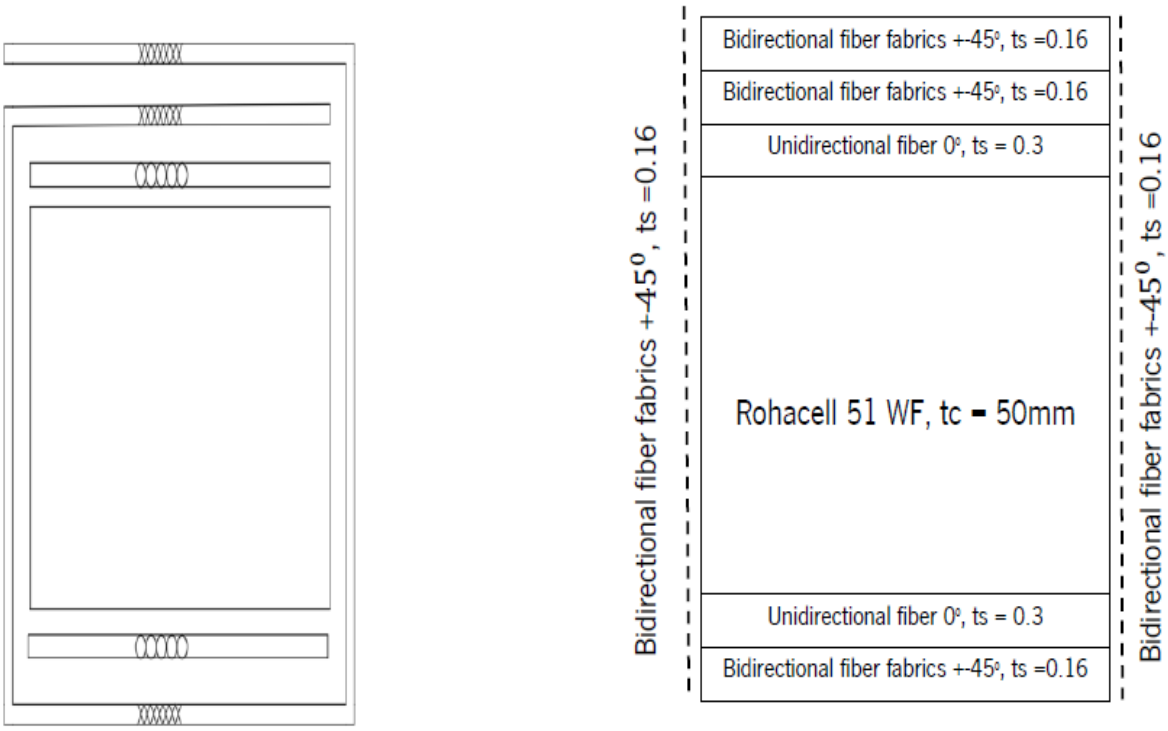

Figure 3.6 : Compression wrinkling failure stacking sequence.

3.3. Simulation of Numerical Analysis

This research effort focused on doing a thorough investigation into the behaviors of shear and compression wrinkling failures in sandwich composite panels. The panels, consisting of Rohacell 51 WF and glass fiber skins, underwent three-point bending tests to investigate the occurrence of local buckling phenomena. There are many advanced finite element programs that can be used for structural analysis and design. These programs are capable of effectively dealing with extremely complicated situations. Notable software programs in this category include ABAQUS, ANSYS, NASTRAN, NISA, and SAP. We selected ABAQUS for our investigation because of its extensive capabilities and ease of use. This tool facilitated our accurate modeling and thorough analysis of the wrinkling effects encountered by the sandwich panels in our investigation.

In our numerical investigation, we utilized the finite element software offered by Simulia, notably the Dassault Systèmes Abaqus Standard Version 2022. The numerical computation was performed on an Intel Core i9 computer with licensed access to the full professional package of Abaqus, provided by the INSA institute. This computer is equipped with a 13th Generation Intel Core i9 processor, which has a clock speed of 2.20 GHz and includes Intel Graphics. Additionally, it is equipped with 32 gigabytes of RAM and operates on a 64-bit operating system.

This section provides a thorough examination of the finite element analysis performed on glass fiber skins and Rohacell 51 WF core. The study involves conducting three-point bending experimental tests to investigate the properties of materials in relation to their maximum strength, post-buckling phenomena, and the impacts of wrinkling in shear and compression wrinkling situations. The method begins by offering a thorough explanation of the models, including precise details on the utilized components, the type of element mesh, boundary conditions, and the analytical techniques applied.

3.4. Finite Element Analysis

3.4.1. Types of Models

Various types of numerical models can be utilized and analyzed in a finite element study to develop a precise and reliable finite element model that accurately reproduces the actual behavior of sandwich panels [47]. The research utilized a full-scale model to accurately represent the dimensions of the structure, removing the need for any parametric studies to reduce the model's size. In order to replicate

the experimental test arrangement, we utilized circular discrete rigid body for both the support condition and the loading condition, as depicted in Figure 3.7.

The shear wrinkling failure specimen consists of a seven-ply laminate on the top side of the sandwich panel, a six-ply laminate on the bottom side, and one bidirectional ply for the side of the panels, as illustrated in Figure 3.7.

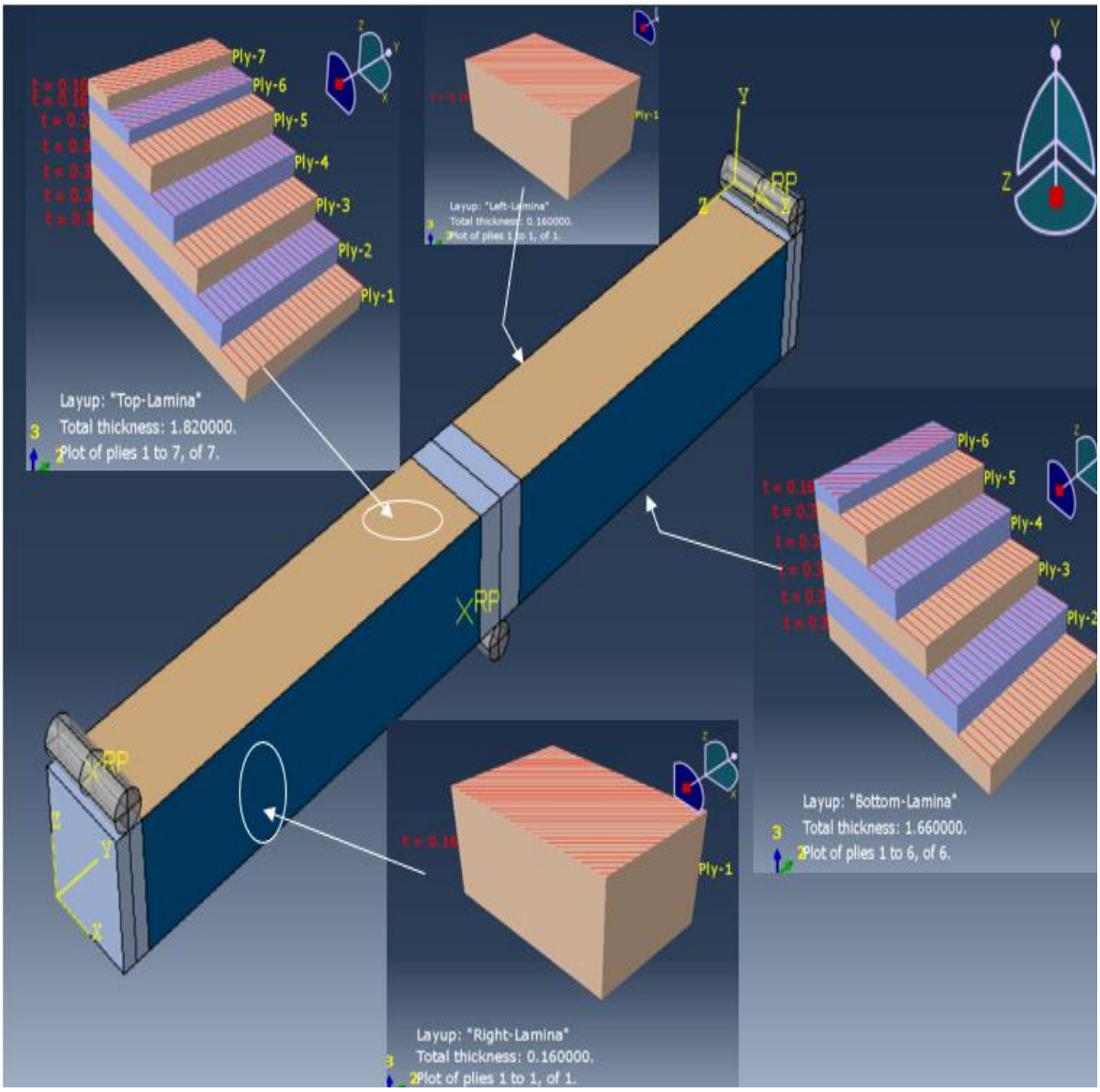

Figure 3.7 : Shear wrinkling failure Finite element model lamina arrangement.

The compression wrinkling failure specimen consists of a three-ply laminate on the top side of the sandwich panel, a two-ply laminate on the bottom side, and a single bidirectional ply on the side of the panels, as depicted in Figure 3.8.

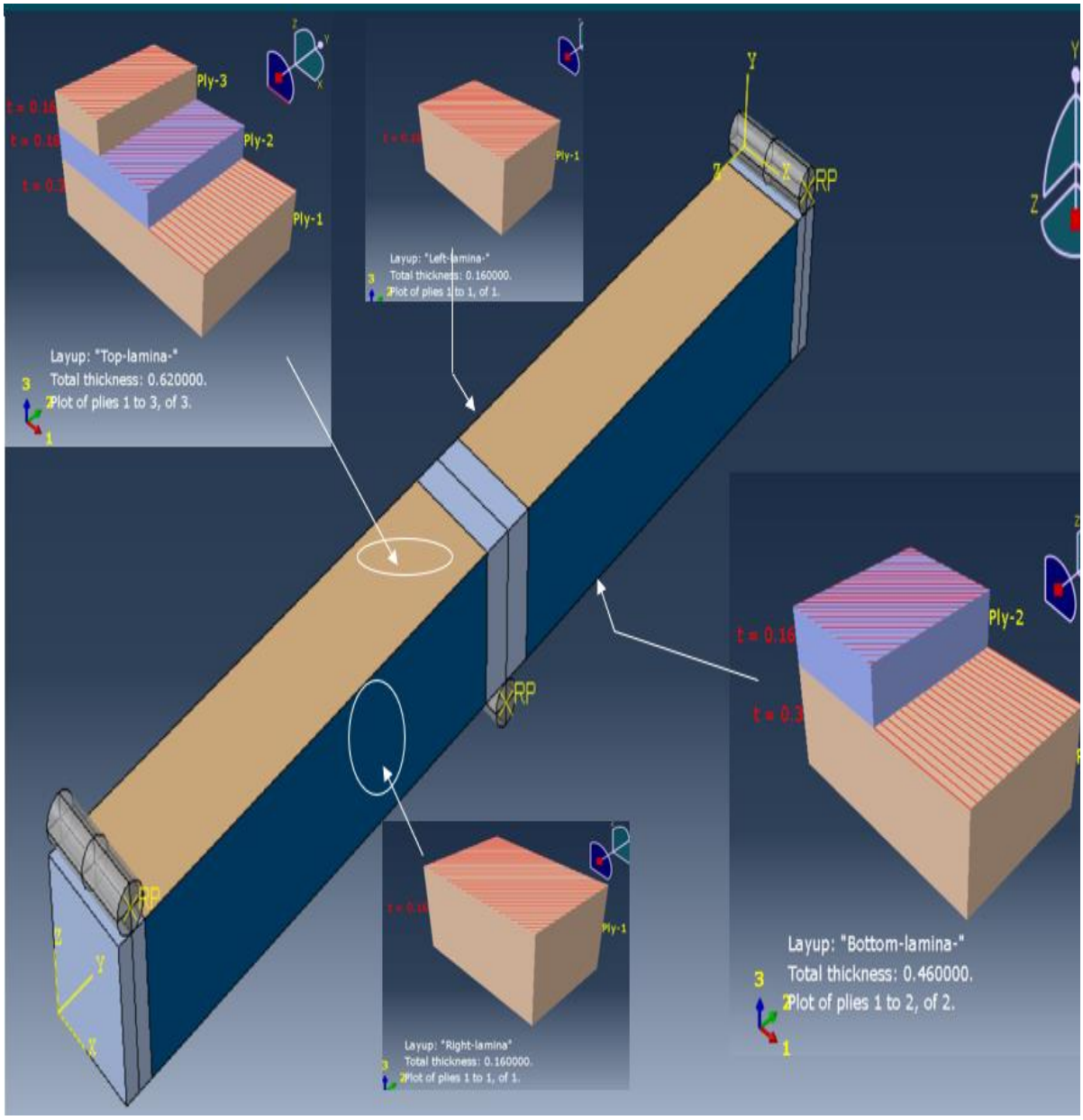

Figure 3.8 : Compression wrinkling failure Finite element model lamina arrangement.

To prevent local failure in the sandwich structure during both shear and compression wrinkling tests, plywood was utilized at the points of support and loading. At the end of the specimen where support is required, we used plywood that is 15 cm thick. For the loading areas, the plywood thickness was increased to 30 cm. This plywood is made from two types of wood, Okoume and Poplar, which exhibit orthotropic material behavior, we applied engineering constants in our Finite Element Analysis to accurately represent their material properties.

3.4.2. Mechanical Material Property

There are many constitutive models that can be used to describe the material behavior of various types of materials found in structural analysis problems. The constitutive library in ABAQUS provides comprehensive coverage of linear and non-linear, isotropic and anisotropic material models for most engineering materials [48]. Various modeling strategies are available for commonly encountered materials, such as metals, with each technique suitable for specific types of analysis applications. Customers have the freedom to select any constitutive model that is required for the modeling process[49]. By associating section properties with specific material names, it is possible to connect different sections in a model to unique material definitions [47].

The research work aimed to develop models of both unidirectional and bidirectional laminates using the unique elastic material properties of the lamina stated in Table 3.1. Afterwards, these laminates were examined utilizing geometric non-linear analysis. The core material exhibited isotropic material behavior, as described in Table 3.2, and was also studied using geometric non-linear approaches. The plywood, which is used to strengthen and control high levels of stress, was represented in the model using anisotropic engineering constants, as shown in Table 3.3. The buckling analysis was based on the assumption that all materials had linear elastic behavior.

3.4.3. Boundary Conditions

For the three-point bending test, the load was applied as a concentrated load on a discrete rigid body, and this discrete rigid body has general contact interaction with the sandwich structure specifically with plywood section area. This concentrated load was distributed along the sandwich structure by the means of discrete rigid object.

The proper choice of boundary conditions has a significant impact on how accurate of the results produced by the finite element modeling [50]. In this research analysis, we uses the following notations for the constraints of displecment and rotation conditions to be used in numerical analysis.

1. U1 = X axis translation
2. U2 = Y axis translation
3. U3 = Z axis translation
4. UR1 = X axis rotation
5. UR2 = Y axis rotation

6. UR3 = Z axis rotation

At the end of the two supports for the discrete rigid bodies, we use all the displacement and rotations are fixed, to restrict any movement and rotation when we apply the load. At the center of the discrete rigid body for load application, we restrict all axis of rotation and X and Z axis of translation and allow free translation on the Y-axis in the direction of load application. For the sandwich panel, at the center of the panel, we restrict all axis of rotation and X and Z axis of translation and allow free translation on the Y-axis in the direction of the load application.

3.4.4. Elements

In the Finite Element Analysis of the sandwich panel, unidirectional and bidirectional fabrics were laminated with a foam core, employing specific skin properties. For the outer face skin material, conventional shell elements were used, while the core material and plywood were modeled using solid homogeneous elements.

The sandwich panel structure was modeled using C3D8R three-dimensional solid (continuum) elements. These elements, referred to as 8-node linear bricks, consist of eight nodes and provide three degrees of freedom per node, excluding rotational degrees of freedom. To enhance computational efficiency, these elements were subjected to reduced integration. This method employs a reduced number of integration points in contrast to fully integrated components, resulting in more efficient computations, lower computational costs, and enhanced convergence rates [47].

In order to precisely depict the intricate patterns of wrinkling in shear and compression testing, we employed a fine mesh element with a size of 0.7mm, as depicted in Figure 3.9. The skin faces and foam core were designed as a unified entity, guaranteeing that there would be no relative displacement between them, hence maintaining the integrity of the simulation.

We employed rigid discrete bodies of the R3D4 type in a linear geometric order for the support and loading portions. These elements are rigid bodies in three dimensions, with four nodes each. These inflexible components have a four-sided geometry, which enables the approximation of more intricate structures when combined in several pieces. This approach guarantees the creation of strong and precise models of the support and loading zones within the structure.

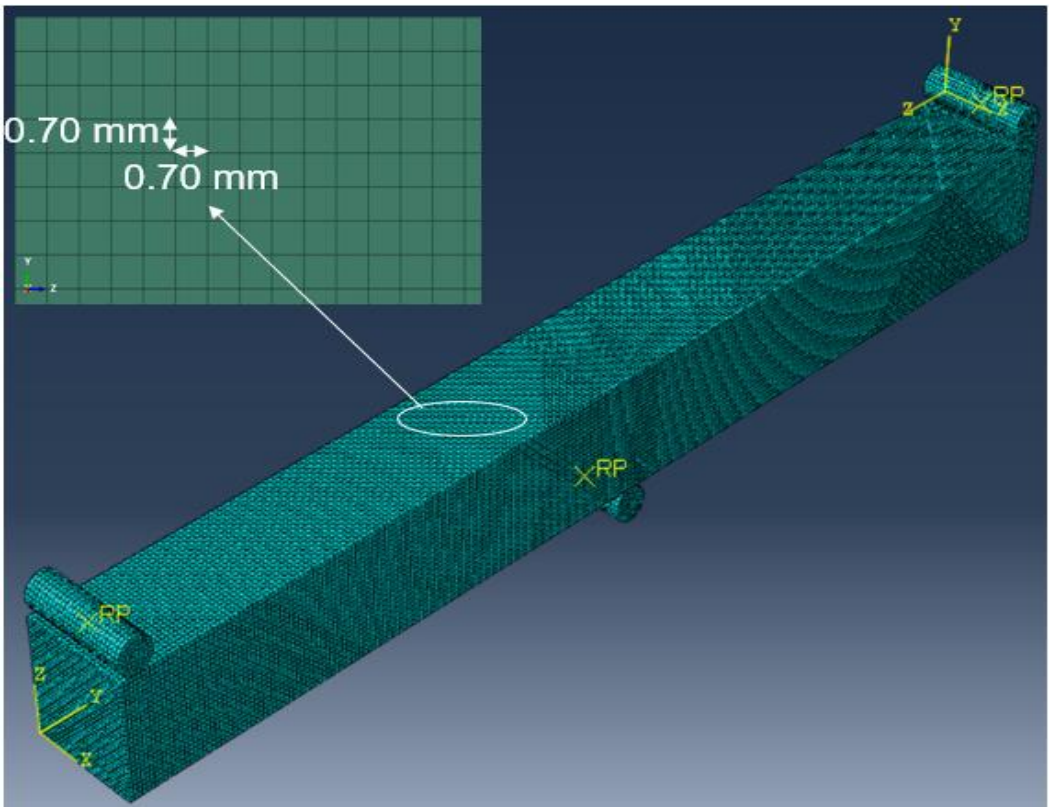

Figure 3.9 : Mesh element size for shear and compression failure specimen.

3.4.5. Methods of Analysis

The three-point bending test for glass fiber laminate face sheets with Rohacell 51 WF foam core elements was investigated for local buckling wrinkling behavior by using elastic linear buckling analysis and geometric non-linear analysis. To estimate of eigen buckling value, we used a linear perturbation analysis in the elastic buckling study. This approach helped determine the critical buckling stress, buckling shape, and half-wave buckle length necessary to fully develop the sandwich model.

To fit the curve with the experiment values, evaluate the stiffness and to check the value of force at wrinkling occurs we perform non-linear geometrical analysis. For this analysis, general static step analysis with default convergence tolerance were used in the geometrical non-linear analysis.

Furthermore, the eigenmodes were also obtained through elastic linear buckling analysis to examine in the study of initial geometric imperfection for shear failure tests necessary for the gemetrical non-linear analysis to fit the curve with the expermental data and to check the stiffness.

THIS PAGE WAS INTENTINALY LEFT BLANK

4. CHAPTER 4. RESULT AND DISCUSSION

This chapter of the dissertation provides a detailed explanation of the results gained from the numerical analysis conducted on shear and compression wrinkling failure. Furthermore, it includes a discussion on the comparison of the numerical analysis results with the experimental and analytical data. This section presents the results of the numerical analysis and derives significant conclusions from them.

4.1. Mesh size effect for compression and shear numerical analysis

The mesh size in numerical simulations of local buckling in sandwich structures has a considerable impact on the shape of wrinkling, particularly the wavelength of the wrinkling pattern. Furthermore, the buckling load is influenced by the size of the mesh, which is calculated as the eigenvalue obtained from the buckling analysis.

4.1.1. Impact of mesh size on buckling load for compression failure numerical analysis

For the compression wrinkling failure test, we conducted a numerical simulation to examine the impact of mesh size on the eigenvalue of the buckling load. In this research, we used seven different mesh sizes, ranging from a minimum of 0.7 mm to a maximum of 5 mm, including 0.75 mm, 1 mm, 2 mm, 3 mm, and 4 mm. We employed the C3D8R element type, which is an 8-node linear brick with reduced integration and hourglass control, for the isotropic foam and wood material. We utilized conventional shell elements for the laminates and deployed the R3D4 element type, a 4-node 3D bilinear quadrilateral, for the support load conditions at the center and ends. In this analysis, a structured hexagonal element form was employed for the foam, wood material, laminates, and support load circumstances.

The eigenvalue of the buckling load in the compression numerical simulation was determined to be 3.94 KN for the smallest mesh size of 0.7 mm and 4.20 KN for the largest mesh size of 5 mm, as illustrated in Figure 4.1. By examining the figure, it is evident that there is a steady and proportional rise in the buckling load with the increase in mesh size. It is worth mentioning that there is a convergence in the buckling load values when the mesh sizes range from 1 mm to the smallest size of 0.7 mm. This suggests that once the mesh size is reduced to 1 mm, the buckling load values remain constant, regardless of any additional reduction in mesh size. The convergence of buckling load values indicates that utilizing the

lowest mesh size is appropriate when comparing with experimental load values. This approach offers a precise and dependable depiction of the buckling behavior, eliminating the requirement for excessively thin mesh sizes.

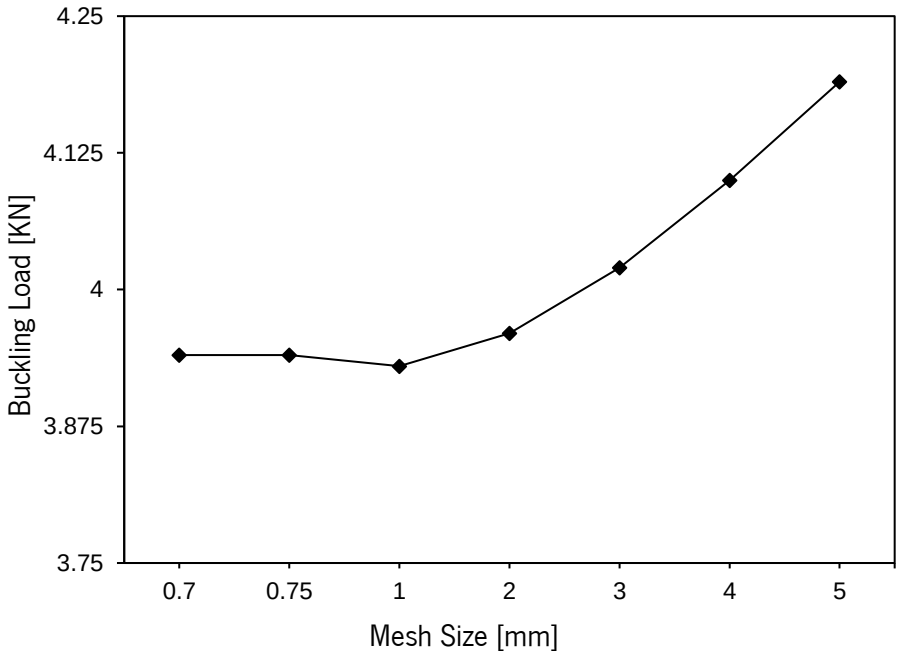

Figure 4.1 : Mesh size–buckling load relationship plot for compression wrinkling failure.

4.1.2. Impact of mesh size on wrinkling pattern for compression failure numerical analysis

On compression wrinkling failure test to see the impact of mesh size on the wrinkling pattern and wavelength evolution during buckling, we conducted a numerical simulation similar with the above discussion on buckling load effect. For this scenario, we used seven different mesh sizes, ranging from a minimum of 0.7 mm to a maximum of 5 mm, including 0.75 mm, 1 mm, 2 mm, 3 mm, 4 mm, and 5mm. We employed, C3D8R element type, which is an 8-node linear brick with reduced integration and hourglass control, for the isotropic foam and wood material. We utilized conventional shell elements for the laminates and deployed the R3D4 element type, a 4-node 3D bilinear quadrilateral, for the support load conditions at the center and ends. In this analysis, a structured hexagonal element form was employed for the foam, wood substance, laminates, and support load circumstances.

The smallest mesh size of 0.7 mm had a measured full wavelength of 12.73 mm, while the maximum mesh size of 5 mm had a measured full wavelength of 20 mm, as depicted in Figure 4.2. The intermediate mesh sizes obtained wavelengths of 12.76 mm (0.75 mm mesh), 13 mm (1 mm mesh), 14 mm (2 mm mesh), 15.06 mm (3 mm mesh), and 16 mm (4 mm mesh). The graph demonstrates a consistent and

proportional rise in the full wavelength measurement as the mesh size increases. Significantly, there is a convergence in the full wavelength for mesh sizes ranging from 1 mm to the smallest size of 0.7 mm. This suggests that after the mesh size is down to 1 mm, the values of the full wavelength stay consistent even if the mesh size is further reduced. The convergence indicates that utilizing the smallest mesh size is appropriate when compared with experimental wavelength values.

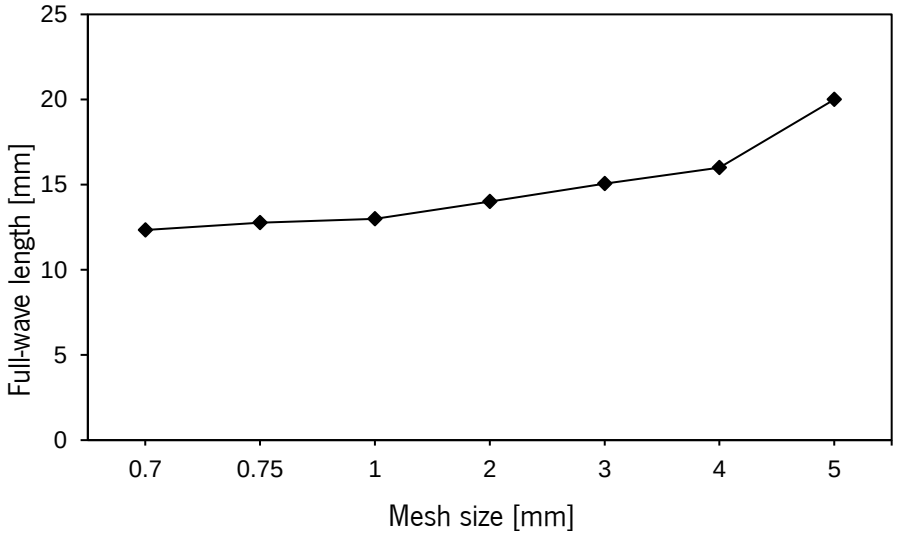

Figure 4.2 : Mesh size – full-wavelength relationship plot for shear wrinkling failure.

Figure 4.3 to Figure 4.9 depict the outcomes of the numerical simulation study, particularly the shape of the wrinkles. These figures demonstrate how the wrinkling pattern changes as the mesh sizes vary. The location of wrinkling occurs on the bottom compression face of the sandwich panel.

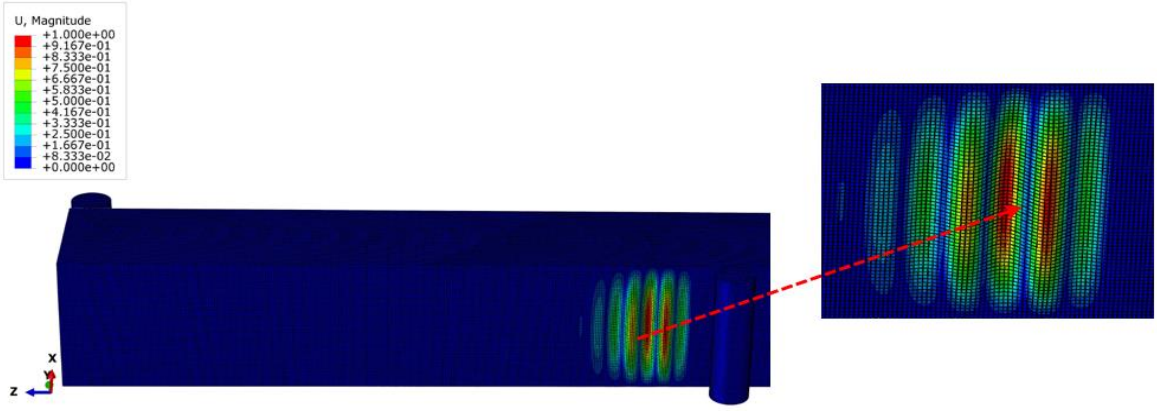

Figure 4.3 : Wrinkling pattern for mesh size 0.70mm.

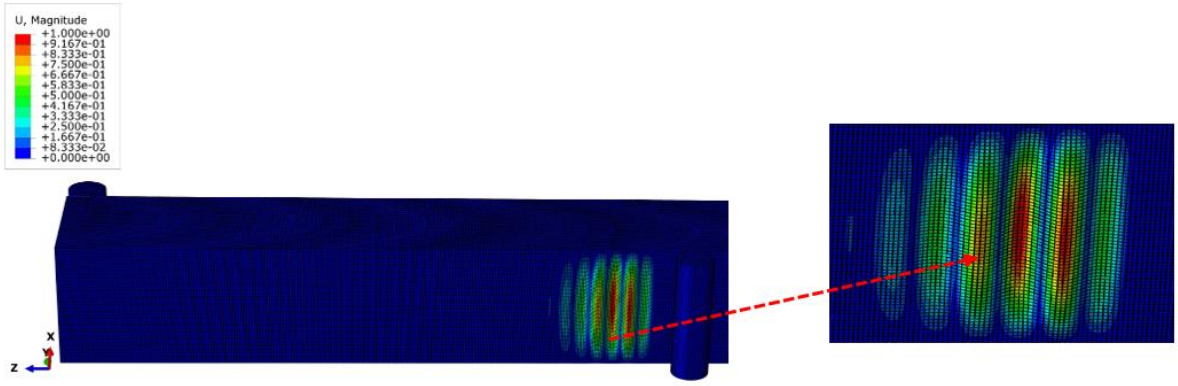

Figure 4.4 : Wrinkling pattern for mesh size 0.75mm.

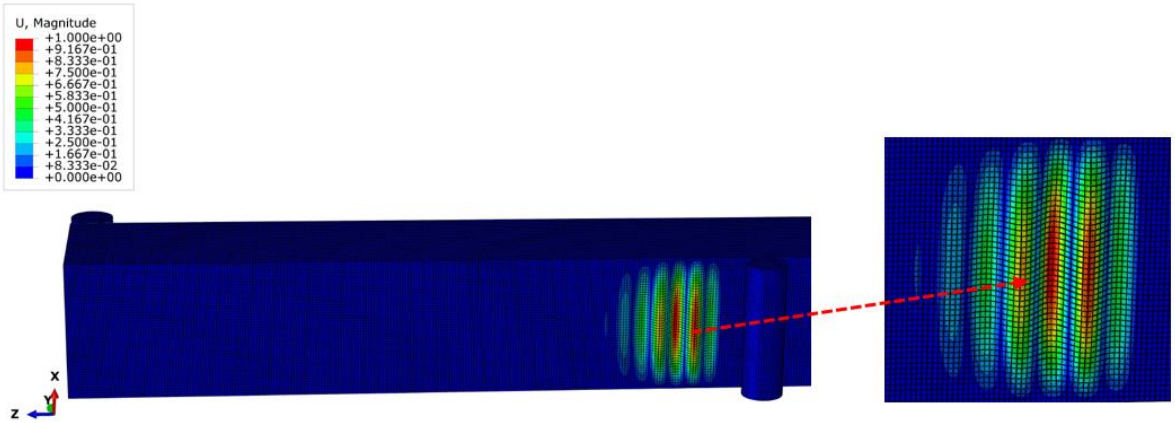

Figure 4.5 : Wrinkling pattern for mesh size 1.0mm.

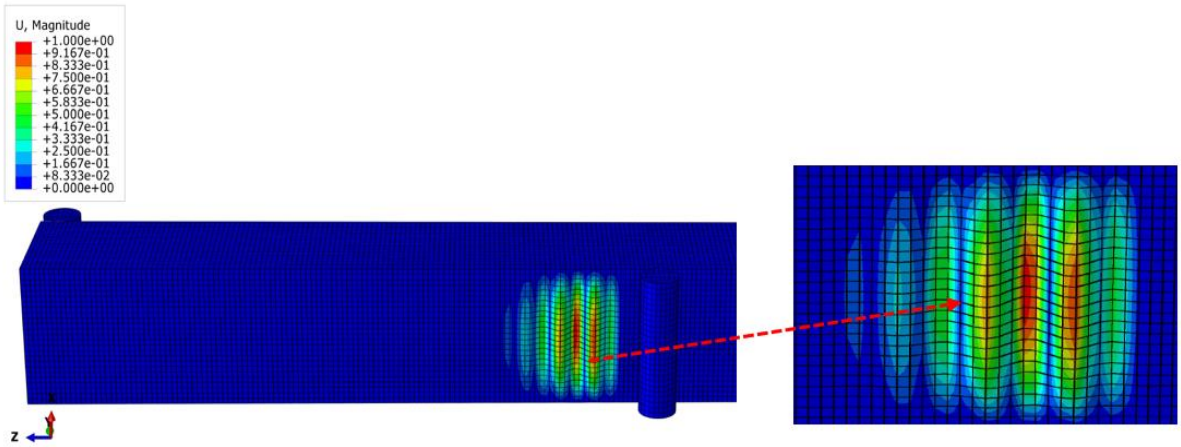

Figure 4.6 : Wrinkling pattern for mesh size 2.0mm.

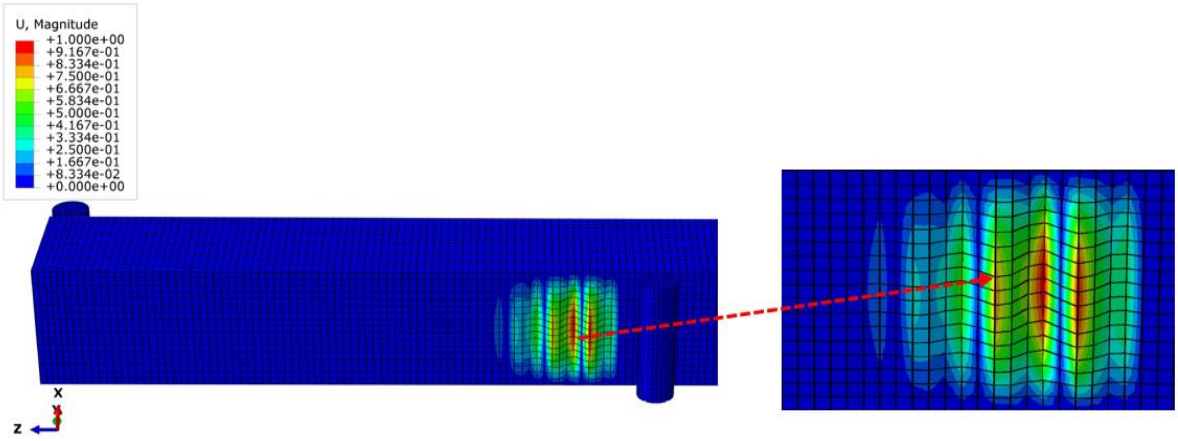

Figure 4.7 : Wrinkling pattern for mesh size 3.0mm.

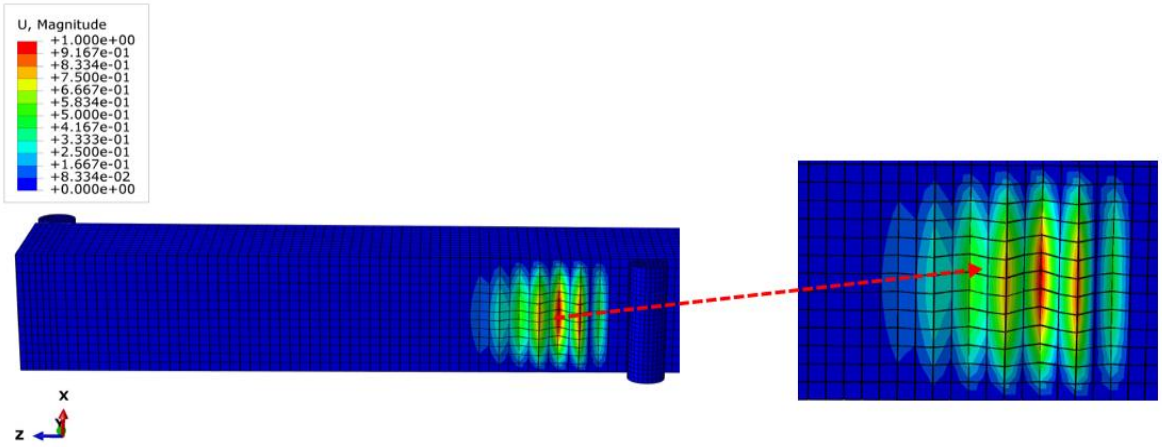

Figure 4.8 : Wrinkling pattern for mesh size 4.0mm.

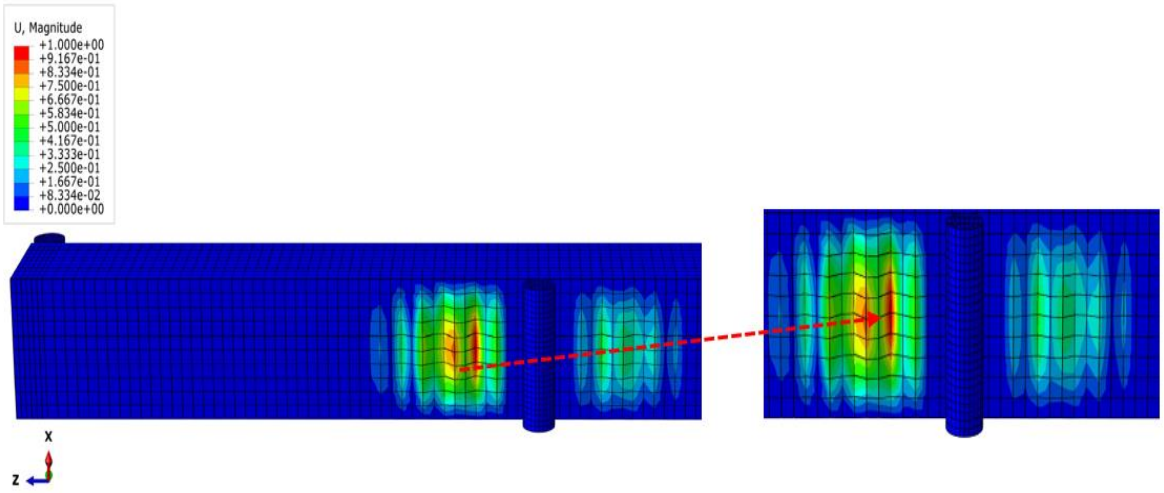

Figure 4.9 : Wrinkling pattern for mesh size 5.0mm.

4.1.3. Impact of mesh size on buckling load for shear failure numerical analysis

For the shear wrinkling failure test, we conducted a numerical simulation to examine the impact of mesh size on the eigenvalue of the buckling load. In this analysis, we employed seven different mesh sizes, ranging from a minimum of 0.7 mm to a maximum of 5 mm, including 0.75 mm, 1 mm, 2 mm, 3 mm, and 4 mm. We utilized the C3D8R element type, which is an 8-node linear brick with reduced integration and hourglass control, for the isotropic foam and wood material. We applied conventional shell elements for the laminates and deployed the R3D4 element type, a 4-node 3D bilinear quadrilateral, for the support load conditions at the center and ends. In this analysis, a structured hexagonal element form was employed for the foam, wood material, laminates, and support load circumstances.

The eigenvalue of the buckling load in the shear numerical simulation was determined 8.38 KN for the smallest mesh size of 0.7 mm and 15.78 KN for the largest mesh size of 5 mm, as illustrated in Figure 4.10. By examining the figure, it is evident that there is a steady and proportional rise in the buckling load with the increase in mesh size. It is worth mentioning that there is a convergence in the buckling load values when the mesh sizes range from 1 mm to the smallest size of 0.7 mm. This suggests that once the mesh size is reduced to 1 mm, the buckling load values remain constant, regardless of any additional reduction in mesh size. The convergence of buckling load values indicates that utilizing the lowest mesh size is appropriate when comparing with experimental load values. This method provides an accurate and reliable representation of the buckling behavior, avoiding the need for extremely small mesh sizes.

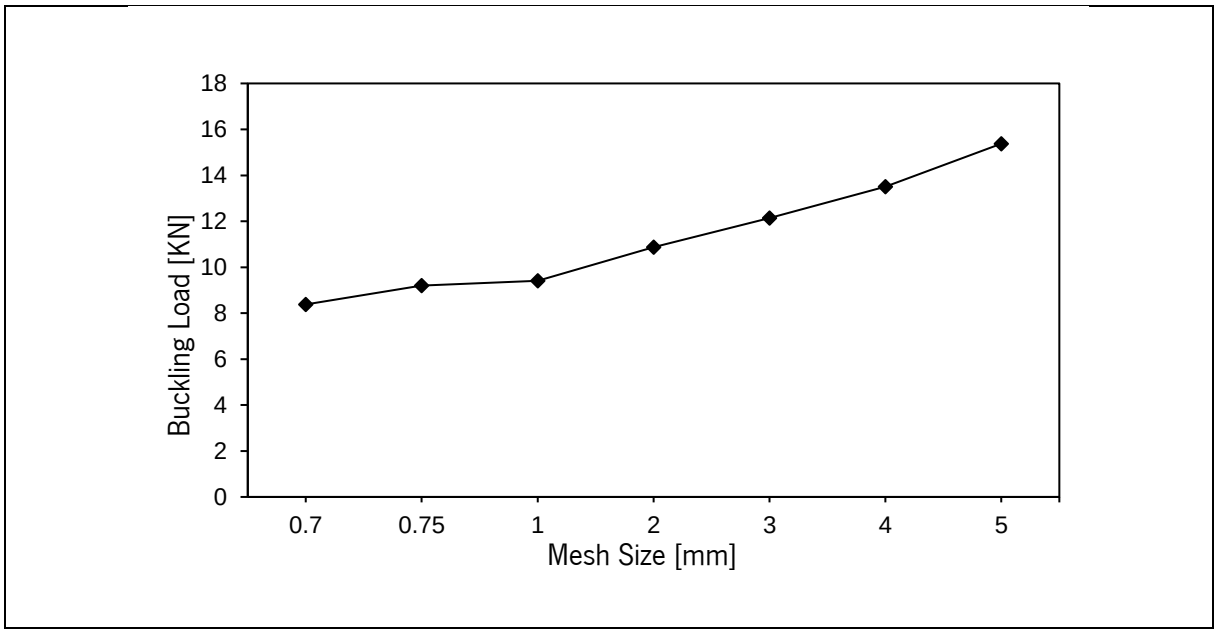

Figure 4.10 : Mesh size – buckling load relationship plot for shear wrinkling failure.

4.1.4. Impact of mesh size on wrinkling pattern for shear failure numerical analysis

We performed a numerical simulation to investigate the impact of mesh size on the wrinkling pattern and wavelength evolution during buckling in a shear wrinkling failure test. This simulation was similar with the previous discussion on the effect of buckling load. For this scenario, we used seven different mesh sizes, ranging from a minimum of 0.7 mm to a maximum of 5 mm, including 0.75 mm, 1 mm, 2 mm, 3 mm, 4 mm, and 5 mm. We employed, C3D8R element type, which is an 8-node linear brick with reduced integration and hourglass control, for the isotropic foam and wood material. We utilized conventional shell elements for the laminates and deployed the R3D4 element type, a 4-node 3D bilinear quadrilateral, for the support load conditions at the center and ends. In this analysis, a structured hexagonal element form was employed for the foam, wood substance, laminates, and support load circumstances.

The smallest mesh size of 0.7 mm had a measured full wavelength of 3.97 mm, while the maximum mesh size of 5 mm had a measured full wavelength of 11.2 mm, as depicted in Figure 4.11. The intermediate mesh sizes obtained wavelengths of 4.2 mm (0.75 mm mesh), 4.45 mm (1 mm mesh), 5.66 mm (2 mm mesh), 8.42 mm (3 mm mesh), and 8.88 mm (4 mm mesh). The graph demonstrates a consistent and proportional rise in the full wavelength measurement as the mesh size increases. Significantly, there is a convergence in the complete range of wavelengths for mesh sizes ranging from 1 mm to the smallest size of 0.7 mm. This suggests that after the mesh size is down to 1 mm, the values of the full wavelength stay consistent even if the mesh size is further reduced. The convergence indicates that utilizing the smallest mesh size is appropriate when compared with experimental wavelength values.

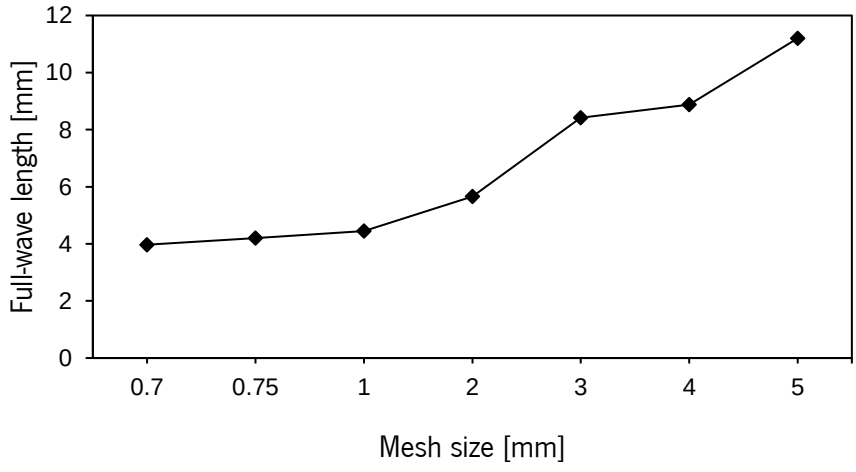

Figure 4.11 : Mesh size – full-wavelength relationship plot for shear wrinkling failure.

Figure 4.12 depicts a diagram of the sandwich specimen's face parts, specifically highlighting the notation of shear side for the occurrence of shear wrinkling during the simulation of a three-point bending test.

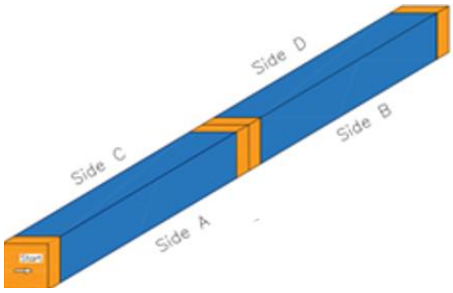

Figure 4.12 : Schematic representation on sandwich shear face specimen.

Table 4.1 provides a summary of the first eigenmode value buckling load and the corresponding location of wrinkling failure on the shear face of the specimen, based on different mesh sizes.

Table 4.1 : Summary of wrinkling load, wavelength, and location of wrinkling failure.

Mesh size [mm]	Wrinkling Load [KN]	Full wave length [mm]	Location of wrinkling failure
0.7	8.386	3.97	Side D
0.75	9.247	4.2	Side A
1	9.41	4.45	Side B
2	10.83	5.66	Side B
3	11.71	8.42	Side B
4	13.48	8.88	Side B
5	15.34	11.2	Side B

Figure 4.13 to Figure 4.18 illustrate the results of the numerical simulation study on shear wrinkling, specifically focusing on the shape of the wrinkles. These figures illustrate the alteration of the wrinkling pattern as the mesh sizes vary.

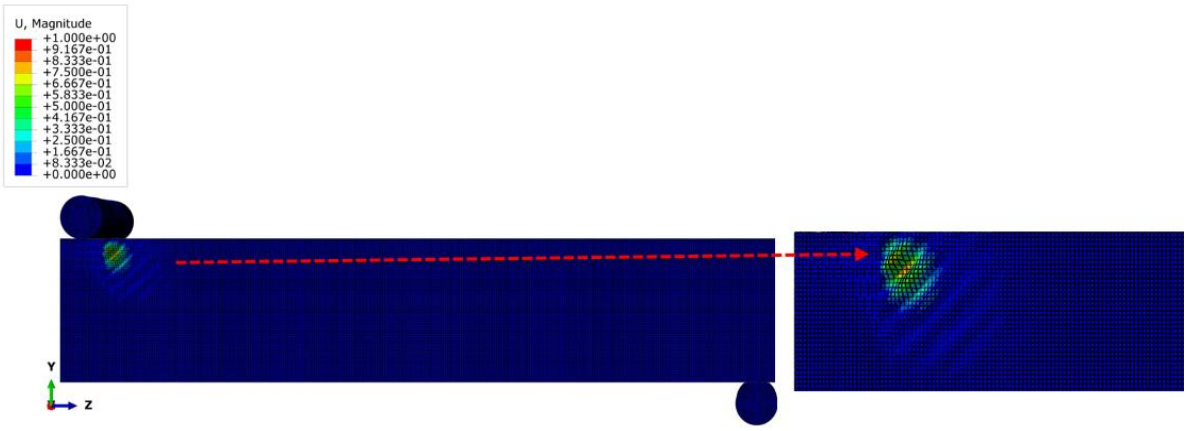

Figure 4.13 : Wrinkling pattern for shear failure mesh size 0.70mm.

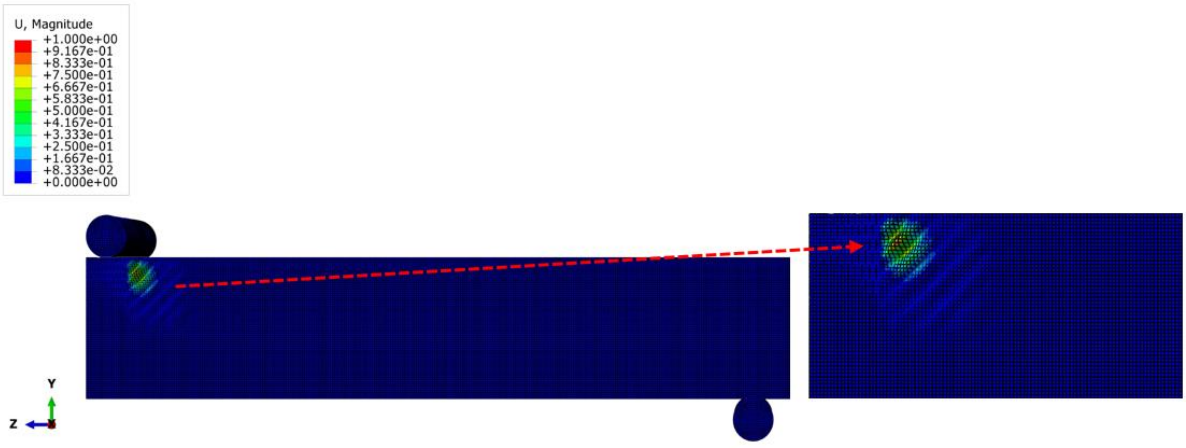

Figure 4.14 : Wrinkling pattern for shear failure mesh size 0.75mm.

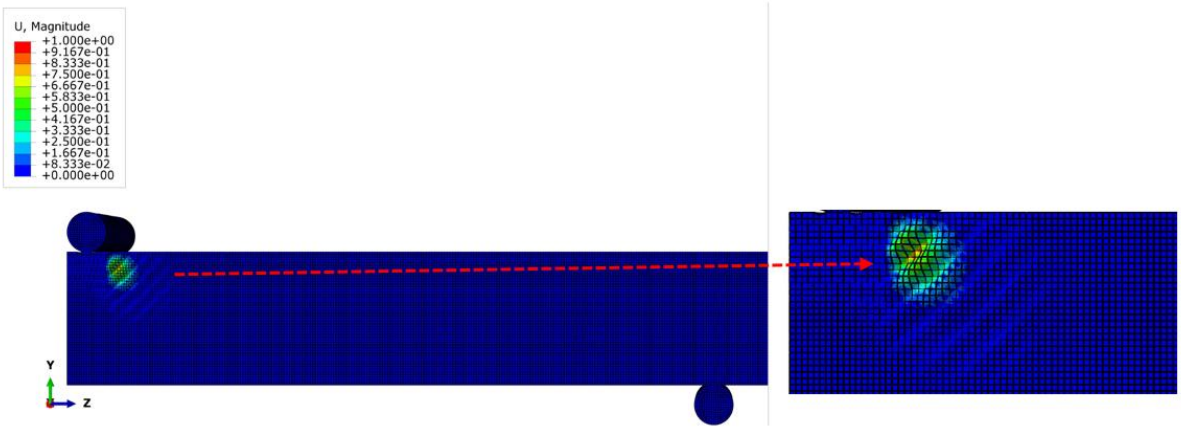

Figure 4.15 : Wrinkling pattern for shear failure mesh size 1.0mm.

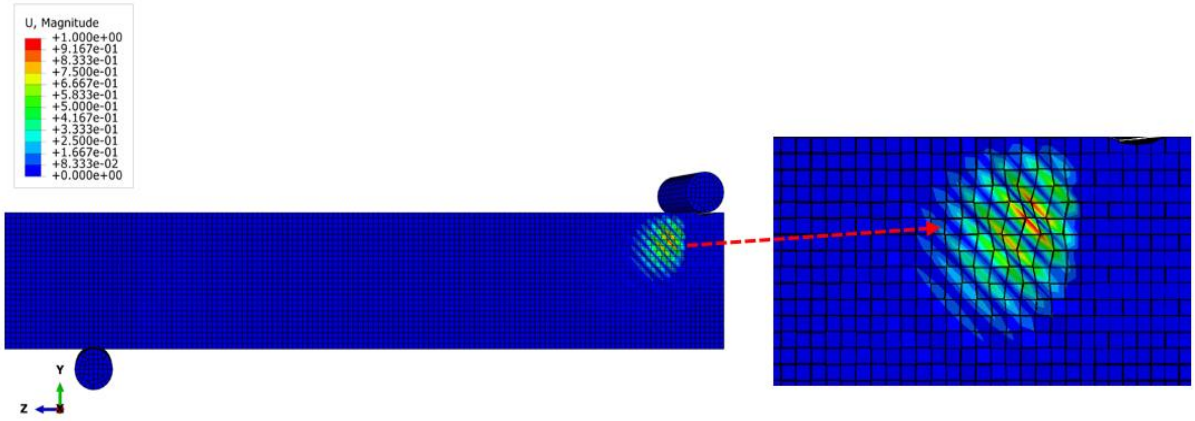

Figure 4.16 : Wrinkling pattern for shear failure mesh size 2.0mm.

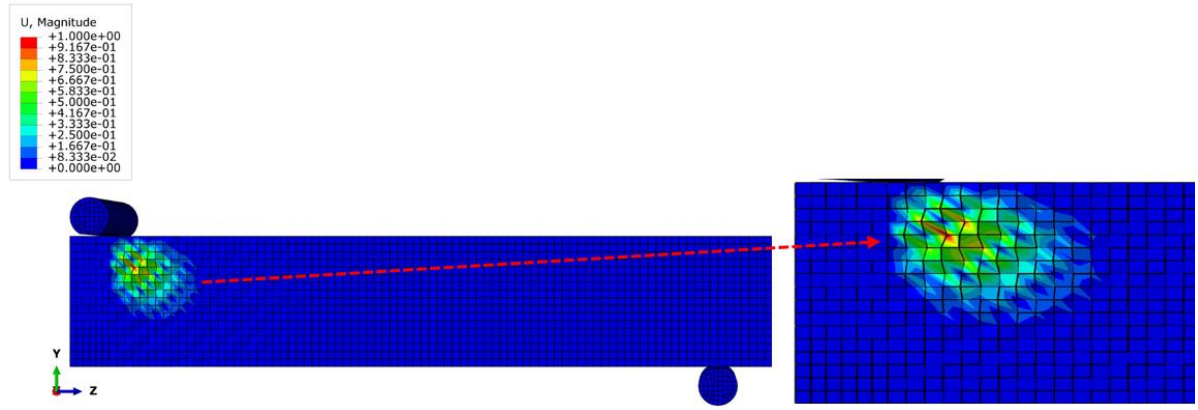

Figure 4.17 : Wrinkling pattern for shear failure mesh size 3.0mm.

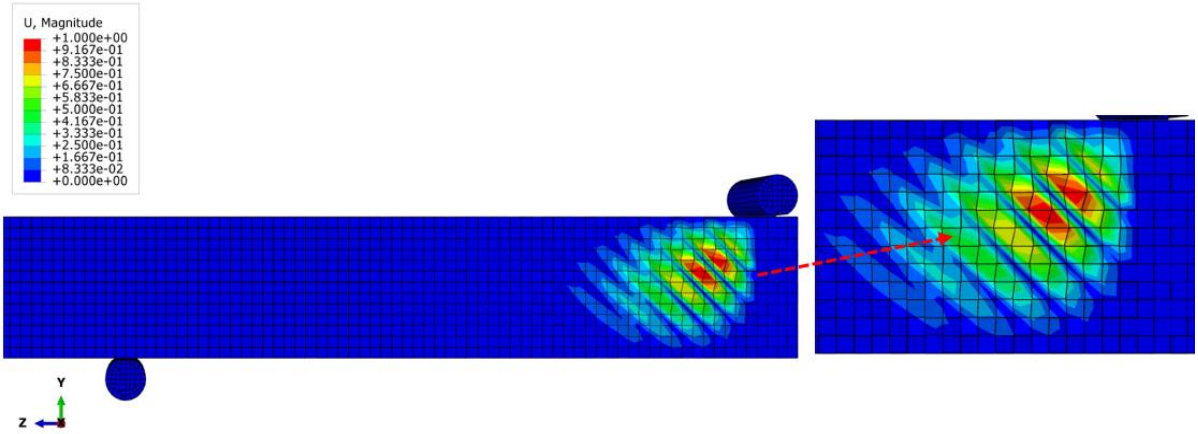

Figure 4.18 : Wrinkling pattern for shear failure mesh size 4.0mm.

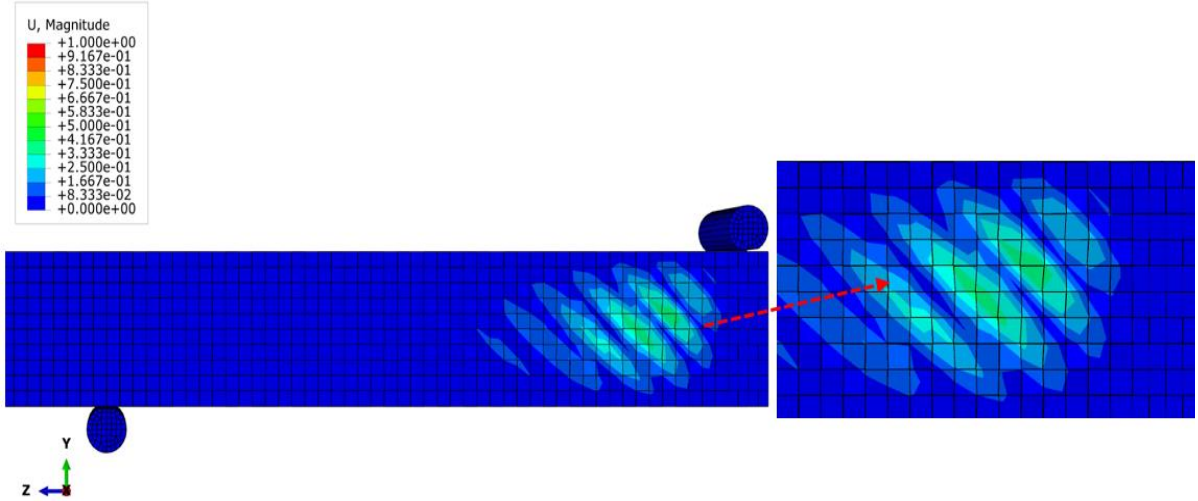

Figure 4.19 : Wrinkling pattern for shear failure mesh size 5.0mm.

4.2. Numerical analysis of compression failure tests

4.2.1. Overview of experimental results of compression failure test

The first phase entailed for compression tests were calibration of instruments, a crucial and time-intensive procedure that has a substantial impact on the quality of the outcomes. Focused efforts on optimizing the VIC system and cameras by adjusting elements such as diaphragm aperture, exposure time, distance, orientation, and focus. These adjustments were made based on the calibration sheet provided by the VIC program. The lighting was arranged appropriately to accommodate a wide measuring area and depth, and then the VIC SNAP acquisition system was calibrated using a target. To make the process more efficient, all tests were conducted on a single day. Following Digital Image Correlation (DIC) calibration, the sandwich specimen was positioned on the three-point bending machine and lightly secured. Force was incrementally exerted manually until wrinkles formed, assuring a uniform application to uphold precision.

The Digital Image Correlation (DIC) cameras were employed to record the initial condition of the speckle-patterned surfaces of the sandwich specimens before the application of any external force. The objective of this analysis is to determine whether the presence of a flatness fault is the cause of the formation of a curve. The acquired images were subsequently analyzed using the VIC-3D program. 2D processed pictures were acquired, coupled with XZ-plane plots shown in Figure 4.20, which depicted the distribution of colors in the Z-direction. This enabled the analysis of the initial fluctuation in the position of the object in relation to the plane, as well as the identification of potential imperfections. In this study, we noticed an average initial dispersion of 0.1mm for the six specimens, which can be considered negligible. This observation can be explained by the fact that these specimens were manually fabricated, in separate batches and molds. No significant imperfections were found: none of the six specimens exhibited wrinkling caused by any obvious imperfections.

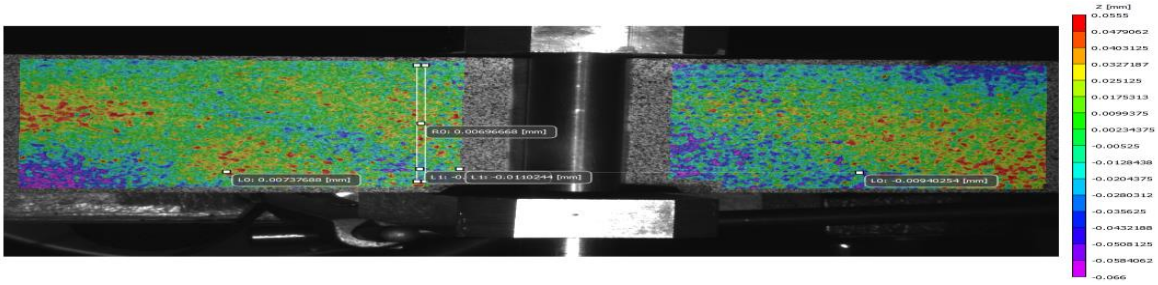

Figure 4.20 : Flatness Controlling for the initial-out of plane position.

Upon gathering all the data, the force was plotted as a function of displacement for the six compression test specimens. Initially, it is evident that there is a displacement occurring as the specimens are observed to be "moving away" from the cameras. Additionally, it is crucial to note that all specimens exhibit identical linear properties at the onset of the loading procedure, as illustrated in Figure 4.21. This suggests that they have the same stiffness. There is a noticeable difference in behavior among these tests. Specifically, four of the specimens showed the first wrinkling phenomena when subjected to high loading conditions (Test 2: 3.91 KN, Test 4: 3.91 KN, Test 5: 3.95 KN, Test 6: 3.56 KN). On the other hand, two specimens, Test 1 and Test 3, failed at lower loading ranges (1.46 KN and 1.79 KN, respectively).

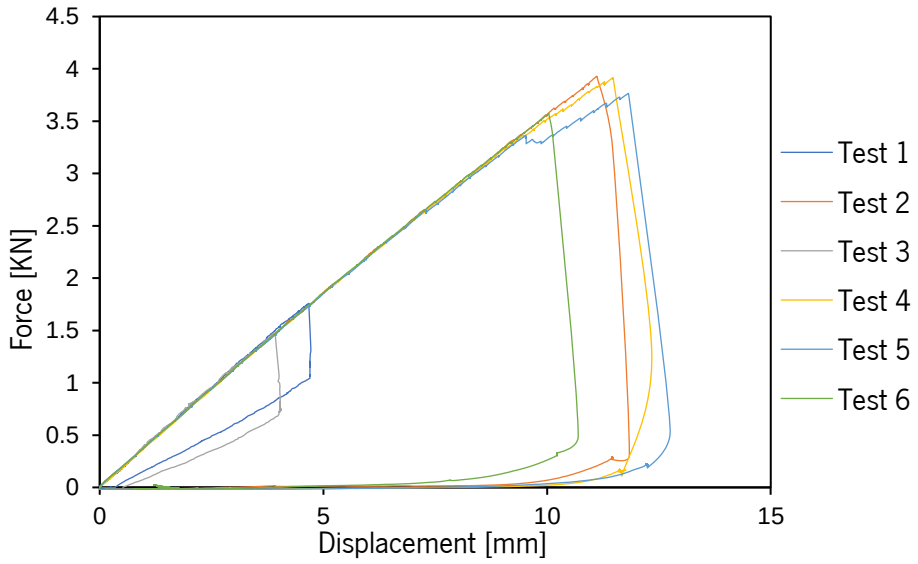

Figure 4.21 : Force [KN] as a function of relative displacement [mm].

When studying wavelengths of those two tests which are failed at a lower load, it could not clearly identify the appearance of wrinkling (bump or hollow) just before the rupture, unlike other specimens. This information and their early rupture led us not to consider these two tests, as we are not sure they broke because of wrinkling. Further study would have been necessary to determine the cause of their early rupture.

As illustrated on Figure 4.21, we determined the appearance force of wrinkling following our post-processing protocol. Once again, this force has a similar magnitude for four of the specimens (2, 4, 5 & 6). Upon the specimen's fracture, two potential shapes emerged. Initially, the fiber experienced compressive force, resulting in its fracture and the formation of a hollow. Subsequently, the outer layer of the specimen detached, creating a small bump, as shown in Figure 4.22.

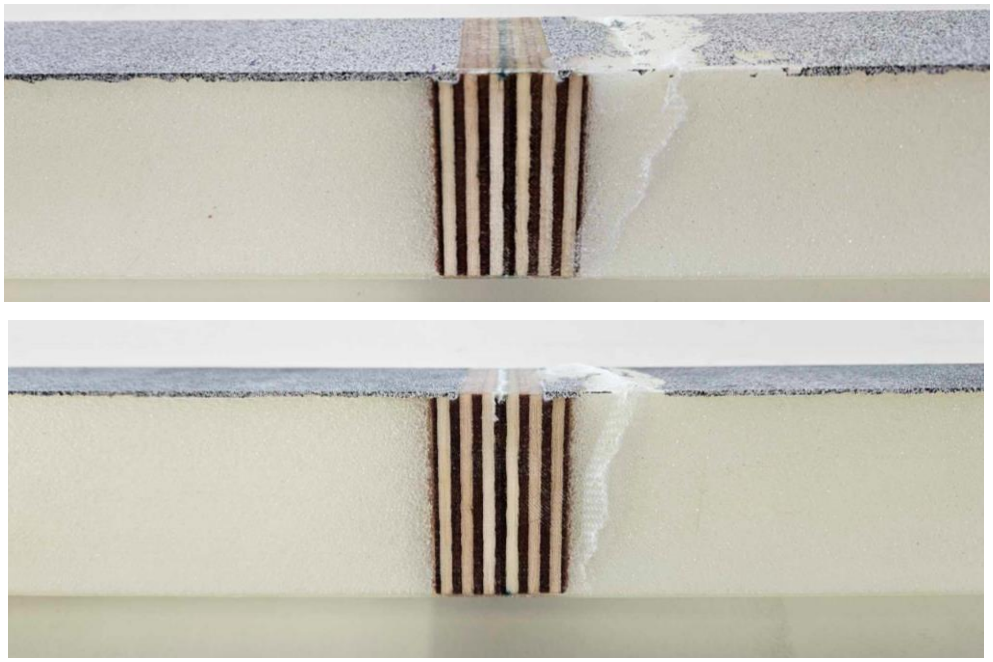

Figure 4.22 : Rupture causing a hollow [top image] or a bump [bottom image].

4.2.2. Classical analytical wrinkling stress analysis for compression failure test

The wrinkling stresses in this instance were calculated using the equations provided in Table 2.1 of the theoretical models, taking into account the mechanical properties of the materials as described in Table 3.1 and Table 3.2. It should be noted that the equations are primarily constructed to describe wrinkling failure caused by axial compressive stress. For this case, our loading condition for the compression failure test is three point bending test. To align with this condition, the properties of the materials were adjusted at a 45^0 angle for the computations. Since the fabrics were put at a 45^0 angle and the core is isotropic, it is appropriate to use the mechanical properties as they are without any additional adjustments.

The material parameters for bidirectional fiber fabrics and the foam core provided in Table 3.1 and Table 3.2 are as follows:

$E_l = E_t$ = 23000 MPa; G_{lt} = 2900 MPa; V_{lt} = 0.098; t_s = 016 mm. E_c = 75 MPa.

G_c = 24 MPa; t_{core} = 50 mm

Hoff and Mautner drive the wrinkling stress as illustrated on equation (2-10) and (2-11)

$$\sigma_{wr} = 0.910 * \sqrt[3]{E_f E_c G_c} \quad \text{(without Knockdown factor)}$$

$$\sigma_{wr} = 0.50 * \sqrt[3]{E_f E_c G_c} \quad \text{(with Knockdown factor)}$$

By this formulation, we can calculate the wrinkling stress:

$\sigma_{wr} = 0.910 * \sqrt[3]{23000 * 75 * 24}$ = 314.81 MPa; without Knockdown factor

$$\sigma_{wr} = 0.50 * \sqrt[3]{23000 * 75 * 24} \quad = 173.0 \text{ MPa; with Knockdown factor}$$

The results of different theoretical models presented in Table 2.1 have been calculated and emphasized in Table 4.2 below.

Table 4.2 : Wrinkling stress value from classical analytical formulation

Reference [Classical]	C	Wrinkling Stress σ_{wr} [MPa]	Full wavelength [mm]
Hoff and Mautner (NK)	0.961	332.45	4.30
Hoff and Mautner (WK)	0.5	172.97	-
Plantema	0.85	294.05	4.96
Gouge, Elam and Debruyne	0.794	274.68	-
Yusuf	0.96	332.10	3.41
Allen	-	286.95	4.51

NK = No Knockdown factor, WK = with Knockdown factor

4.2.3. Comparison of Numerical results with experimental results and analytical results

The compression test results, as indicated by the load-displacement graph on Figure 4.23, exhibit a good correlation with the initial stiffness of the material properties. The numerical analysis predicts that the first eigenvalue buckling load for the lowest mesh is 3.94 KN. The first wrinkling loads in the experimental test results are as follows: 1.75 KN for Test 1, 3.91 KN for Test 2, 1.46 KN for Test 3, 3.91 KN for Test 4, 3.76 KN for Test 5, and 3.56 KN for Test 6. The results exhibit a strong correlation between the numerical analysis and the experimental tests.

Furthermore, the position of the wrinkling observed in the expermental testing, as shown in Figure 4.22, matches the shape and location of the numerical wrinkling illustrated in Figure 4.24. This consistent pattern further validates the accuracy of the numerical analysis in predicting the wrinkling behavior of the material.

In the numerical analysis, we performed a geometrical non-linear analysis by using general static, after obtaining the buckling load from the linear buckling analysis. For this scenario, we applied an additional 25% load beyond the first buckling eigenvalue load during the geometrical non-linear analysis. This approach was used to accurately capture the wrinkling shape in the final step of the analysis, as illustrated in the Figure 4.24.

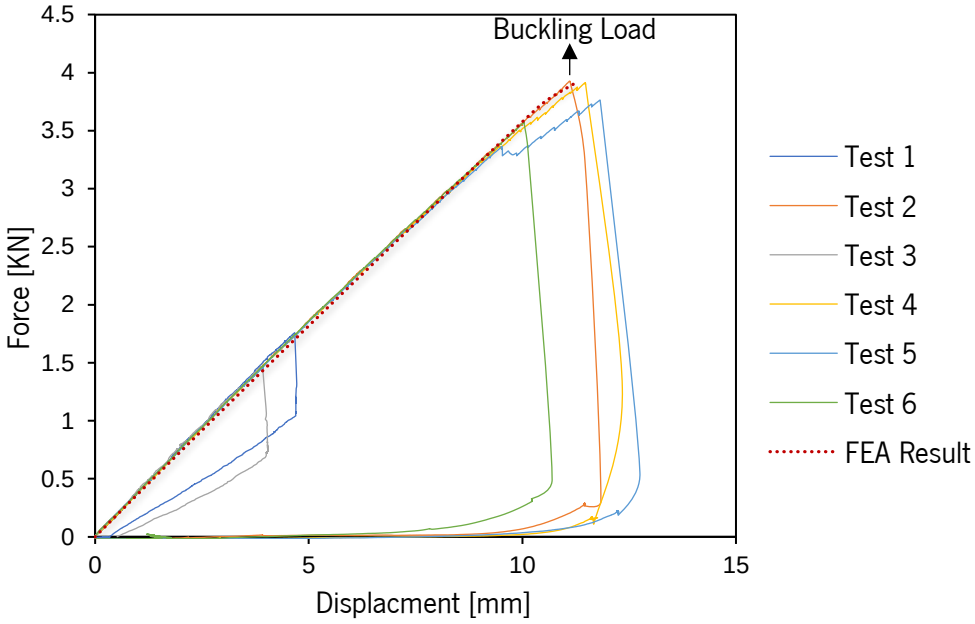

Figure 4.23 : Load–displacment relationship graph for expermental and numerical results.

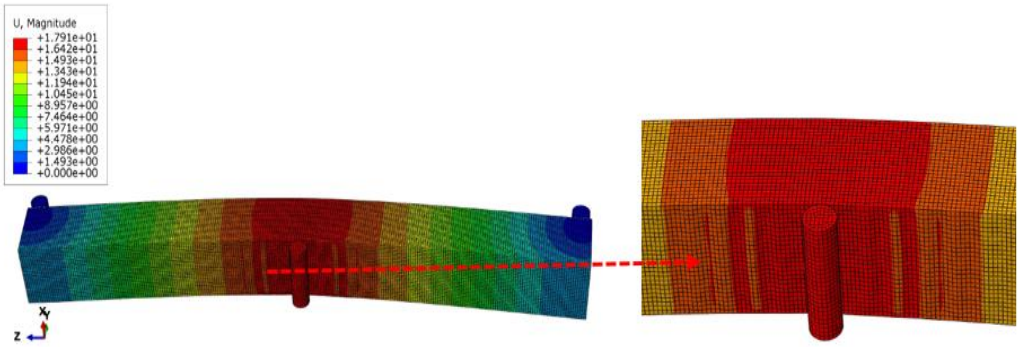

Figure 4.24 : Wrinkling pattern shape for geometrical non-linear analysis.

Table 4.3 summarizes the comparison of analytical, experimental, and numerical test stress results. For the numerical test analysis, we performed simulations both with and without side lamina (shear effect lamina) to compare the compression results with the classical analytical analysis as illustrated on Figure 4.25. It is important to note that the analytical equations are primarily derived for wrinkling failure due to axial compressive stress.

In the numerical analysis with the side shear effect laminate, the results were almost identical to those without the side lamina. This indicates that the side shear effect has minimal influence on the overall results. The numerical analysis stress values show good correlation with the analytical stress results, particularly with the reference formulations of Hoff and Mautner, and Yusuff's equations.

However, the experimental stress values are lower when compared to both the numerical and analytical results. Regarding the full wavelength, the analytical results are lower when compared to the experimental and numerical results.

Table 4.3 : Summary of analysis results for Analytical, FEA and Experimental analysis.

Analysis	References	C	Wrinkling Stress σ_{wr} [MPa]	Full wavelength [mm]
Analytical	Hoff and Mautner (NK)	0.961	332. 45	4.30
	Hoff and Mautner (WK)	0.5	172.97	-
	Plantema	0.85	294.05	4.96
	Gouge, Elam and Debruyne	0.794	274.68	-
	Yusuff	0.96	332.10	3.41
	Allen	-	286.95	4.51
FEA	With shear face lamina	-	343.74	12.75
	Without shear face lamina	-	342.64	
Experimental	Test 1	-	-	-
	Test 2	-	313	18
	Test 3	-	-	-
	Test 4	-	264	9.8
	Test 5	-	254	10.2
	Test 6	-	270	18

(a) (b)

Figure 4.25 : Finite element wrinkling pattern (a) without shear face lamina (b) with shear face lamina

4.3. Numerical analysis of shear failure tests

4.3.1. Overview of experimental shear failure test

The experimental shear test was performed by Alawode A [16], first phase entailed for this shear tests were calibration of instruments. Focused efforts on optimizing the VIC system and cameras by adjusting elements such as diaphragm aperture, exposure time, distance, orientation, and focus. These

adjustments were made based on the calibration sheet provided by the VIC program. The sandwich specimen was positioned on the base of the manually operated three-point bending machine and secured with free clamps to avoid any pre-loading in the form of tension or compression on the specimen. As shown in Figure 3.2, the two outer arms functioned as supports, while the central arm served as the location where the load was applied. A 25mm LVDT displacement sensor was mounted on the middle arm to measure the vertical displacement during loading. In addition, a 2mVN HBM S9M/10kN force sensor was attached to the middle arm to accurately measure the force being exerted. The LVDT displacement sensor and the force sensor were linked to an acquisition system for the purpose of storing data [16].

The Digital Image Correlation (DIC) cameras and laser displacement sensors (LDS) were employed to record the initial condition of the speckle-patterned surfaces of the sandwich specimens before the application of any external force. The objective of this analysis is to determine whether the presence of a flatness fault is the cause of the formation of a curve. The acquired images were subsequently analyzed using the VIC-3D program. As shown in Figure 4.26 for the test specimen A1, which depicted the distribution of colors in the Z-direction. This enabled the analysis of the initial fluctuation in the position of the object in relation to the plane, as well as the identification of potential imperfection. In this study, the level of imperfection for the shape and size differs among various specimens. This variability can be attributed to the production method utilized, specifically manual lay-up. The specimens were found to have resin-rich spatial areas in comparison to other sections. The locations with a high concentration of resin cause humps on the surface of the facesheet, as result of these six specimens exhibited initial out of plane imperfection with a different magnitude [16].

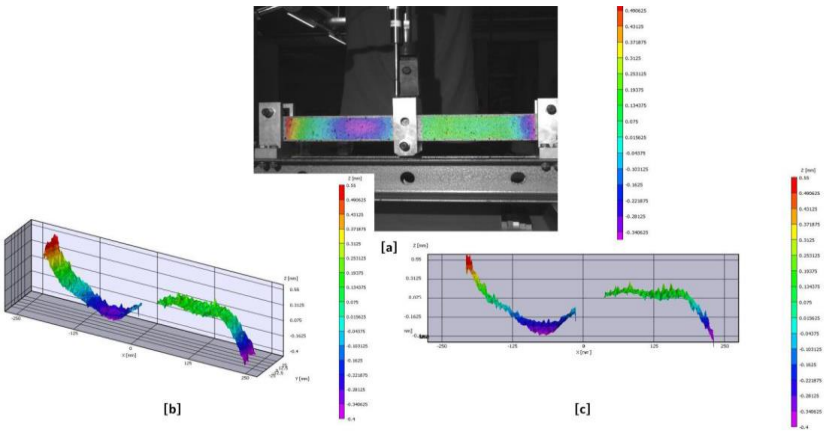

Figure 4.26 : Test sample A1 DIC initial imperfection displacement result in [a] 2D-plot; [b] 3D-plot; and [c] XZ-plane plot [16].

Upon gathering all the data, the force was plotted as a function of displacement for the six compression test specimens. Initially, it is evident that there is a displacement occurring as the specimens are observed to be "moving away" from the cameras. Additionally, it is crucial to note that all specimens exhibit identical linear properties at the onset of the loading procedure, as illustrated on Figure 4.27. This suggests that they have the same stiffness. There is a noticeable difference in behavior among these tests. Specifically, three of the specimens showed the first wrinkling phenomena when subjected to high wrinkling loading conditions (Test A1: 3.25 KN, Test A2: 2.65 KN, Test A6: 4.39 KN). On the other hand, three specimens, Test A3, Test A4 and Test A5, have a wrinkling loading at lower ranges (1.438 KN, 1.486 KN, and 1.487 respectively).

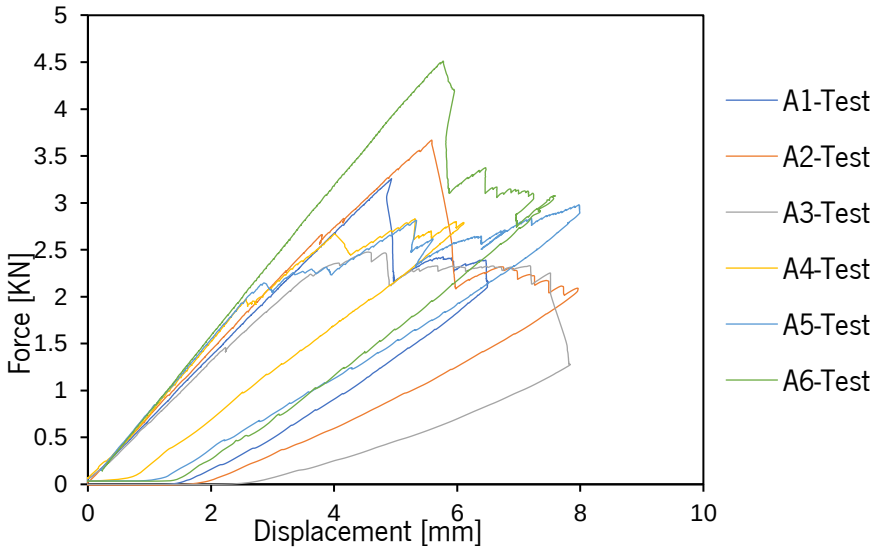

Figure 4.27 : Force [KN] as a function of relative displacement [mm] for shear experimental test.

4.3.2. Comparison of Numerical shear test results with experimental shear test results

The shear test results, as demonstrated by the load-displacement graph on Figure 4.28, exhibit a significant correlation with the initial stiffness of the material properties. The numerical analysis predicts that the first eigenvalue buckling load is 8.386 KN. Nevertheless, the initial wrinkling loads observed in the shear test findings, as previously noted, are lower than the calculated buckling load. This suggests that the wrinkling load was overestimated in the finite element study.

The numerical analysis, depicted in Figure 4.13 indicates that wrinkling forms around the corners of the sample material. Conversely, the experimental results suggest that the creation of wrinkles takes place in the vicinity of the foam's center as shown on Figure 4.29 . The disparity between the numerical and

experimental outcomes can be ascribed to initial out-of-plane imperfections in the samples. The presence of these imperfections can have a substantial impact on the wrinkling behavior and load-bearing capacity, resulting in discrepancies between the predicted and observed outcomes.

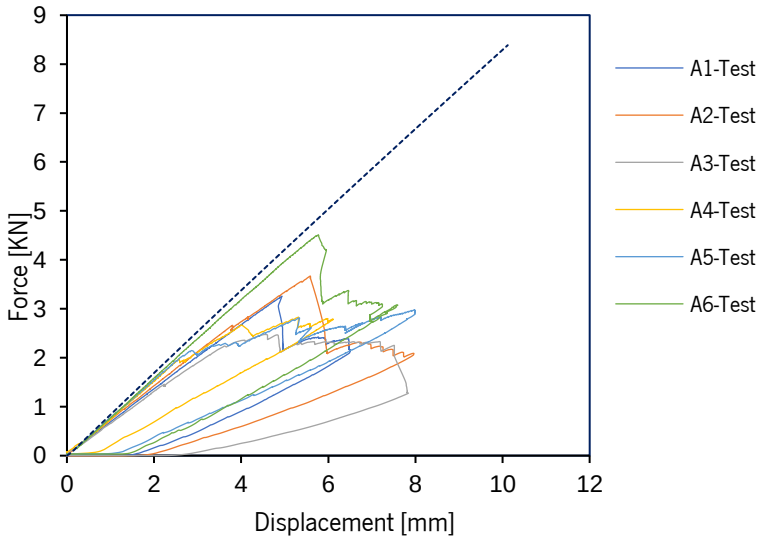

Figure 4.28 : Load–displacement relationship graph for expermental and numerical shear results.

Figure 4.29 : Location of expermental shear failure samples.

4.4. Study of geometrical imperfection analysis for shear failure test

4.4.1. Overview of geometrical imperfection

Initial geometric imperfection is crucial element that must be considered during the initial phase of design, particularly for sandwich composite materials. To effectively simulate the real buckling behavior of the stiffened panel, it is necessary to incorporate various defects into the Finite Element (FE) model. These imperfections include initial deflection, distortion, weld-induced residual stress, and others. Imperfections in sandwich composite materials might originate from the core material, face sheets, or the bonding process. Typically, these early flaws arise from the shipping, fabrication, and manufacturing procedures [51].

It is essential to include these imperfections in the finite element model to appropriately forecast the performance and failure mechanisms of sandwich composite materials. These materials are highly susceptible to imperfections because of their layered composition and the possibility of errors occurring at the interfaces. The presence of initial defects can have a substantial impact on the wrinkling behavior and load-bearing capability, resulting in discrepancies between expected and observed outcomes. Hence, it is imperative to consider these elements while designing and analysing sandwich composite structures to ensure reliability.

Several investigations have found specific types of initial deflection forms that have a substantial impact on structural integrity. The shapes include the Hungry Horse mode, Mountain mode, Spoon mode, Sinusoidal mode, and Buckling mode. Each mode corresponds to a unique configuration of deformation that might impact the overall strength of structural components such as a sandwich composite structures, stiffened panels, and plate elements. It is essential to acknowledge and consider this initial imperfection since they create uncertainties that can impact the overall safety and performance of the structure [51]. The aim of this research is to replicate the initial out-of-plane imperfection that was identified in the experimental shear testing conducted by Alawode A [16]. We chose a sinusoidal wave defect on the shear surface of side B, as shown in the Figure 4.30. This methodology guarantees a close alignment between our computational model and the actual imperfection identified in real-world experiments.

4.4.2. Approach for Initial Out-of-Plane Imperfection

To replicate the original out-of-plane defect, we utilized a Python script in combination with an INP file obtained from a Finite Element Analysis (FEA). The procedure entails the subsequent stages:

a. Extracting of nodes from shear side B of sandwich structure:
   - ✓ We extract all the nodes located on the foam shear side B from the FEA. Subsequently, we modify the INP file to incorporate the newly identified nodes along with their respective coordinates.

b. Python Implementation:
   - ✓ Reading the INP File: The script interprets the INP file and extracts the node coordinates specifically for the shear face on side B.
   - ✓ Applying Sinusoidal Transformation: The X-coordinates undergo a sinusoidal modification to introduce the intended wave pattern by using sine wave formulation.

- ✓ Modifying the INP File: The python subsequently modifies the INP file by incorporating the converted coordinates, thereby ensuring that the Finite Element Analysis (FEA) appropriately reflects the original defect.

Due to problems with convergence, we amended the element type for this analysis. For the modeling of foam and wood materials, we employed C3D10, which is a type of meshing that utilizes 10-node quadratic tetrahedrons. In the case of laminates, we utilized standard shell elements. Due to convergence and numerical singularity issues, we eliminated the support loading condition from this analysis. Additionally, we incorporated amplitude (bump and hollow) sizes of 0.1mm, 0.2mm, and 0.3mm on side B of the shear face to simulate surface imperfections and apply a sinusoidal transformation.

Figure 4.30 depicts the sinusoidal wave pattern being applied to side B of the shear face, and shows the top view, and the initial out-of-plane deformation as modeled in the Finite Element Analysis (FEA). This methodology enables us to effectively examine the influence of initial geometric imperfection on shear wrinkling stress. By utilizing this sinusoidal wave defect, we can accurately replicate the physical conditions of experimental tests, thus improving the precision and dependability of our simulations. This rigorous approach guarantees that our Finite Element Analysis (FEA) includes accurate imperfection, offering vital insights into the structural response to shear loads.

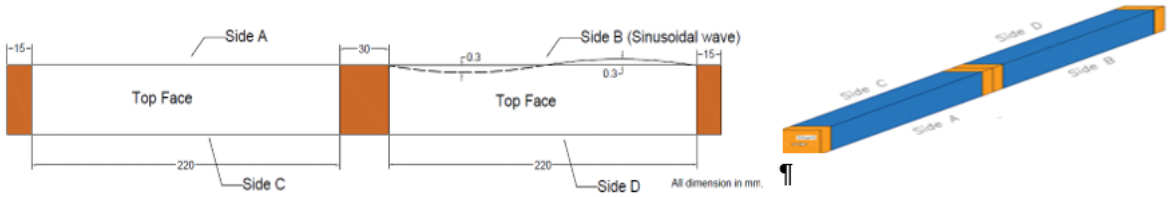

Figure 4.30 : Sinusoidal wave applying for shear face side B for sandwich structure.

4.4.3. Shear failure results after applying initial out-of-plane imperfection

After applying a sinusoidal wave on shear side B of the sandwich structure, we conducted a finite element analysis using geometric linear perturbation buckling analysis. This involved varying the mesh size and the amplitude of the sinusoidal imperfection to observe the effect of initial imperfections on the buckling load and wrinkling pattern. As shown in Table 4.4, the buckling load value remained unaffected by the initial imperfections when comparing models without imperfections to those with varying amplitudes of imperfections.

The full wavelength obtained from experimental shear tests conducted by Alawode A [16] were 9 mm for A1, 18 mm for A2, and 11 mm for A3 to A6 test specimens. In contrast, the numerical results for the full

wavelength with the smallest mesh size yielded a value of 4.5 mm, which is less than half the experimental values. Concerning the location of wrinkling failure as shown on Figure 4.31, for mesh sizes of 0.7 mm, 1 mm, and 3 mm, wrinkling appeared on side B, while for mesh size of 2 mm, it appeared on side C. Compared to experimental results, where wrinkling failure occurred in the central part of the foam, the numerical analysis showed the wrinkling pattern at the corners of the specimen.

Table 4.4 : Numerical analysis results for different mesh sizes and different initial imperfection sizes

Mesh size	Initial imperfection size on side B	Wrinkling Load [KN]	Relative Error (%)	Full wave length [mm]	Location of wrinkling failure
Mesh size 0.7mm (tetrahedron meshing)	Without initial imperfection	6.773		4.5	Side B
Mesh size 1 mm (tetrahedron meshing)	Without initial imperfection	6.774	0.0148	5	Side B
	Initial Imperfection (0.10mm)	6.77		5	Side B
Mesh size 2 mm (tetrahedron meshing)	Without initial imperfection	7.014	3.4217	7.21	Side C
	Initial Imperfection (0.10mm)	7.0137		7.21	Side C
	Initial Imperfection (0.20mm)	7.0137		7.21	Side C
	Initial Imperfection (0.3mm)	7.0136		7.21	Side C
Mesh size 3 mm (tetrahedron meshing)	Without initial imperfection	7.699	8.8973	8.42	Side B
	Initial Imperfection (0.10mm)	7.664		8.42	Side B
	Initial Imperfection (0.20mm)	7.627		8.42	Side B
	Initial Imperfection (0.3mm)	7.591		8.42	Side B

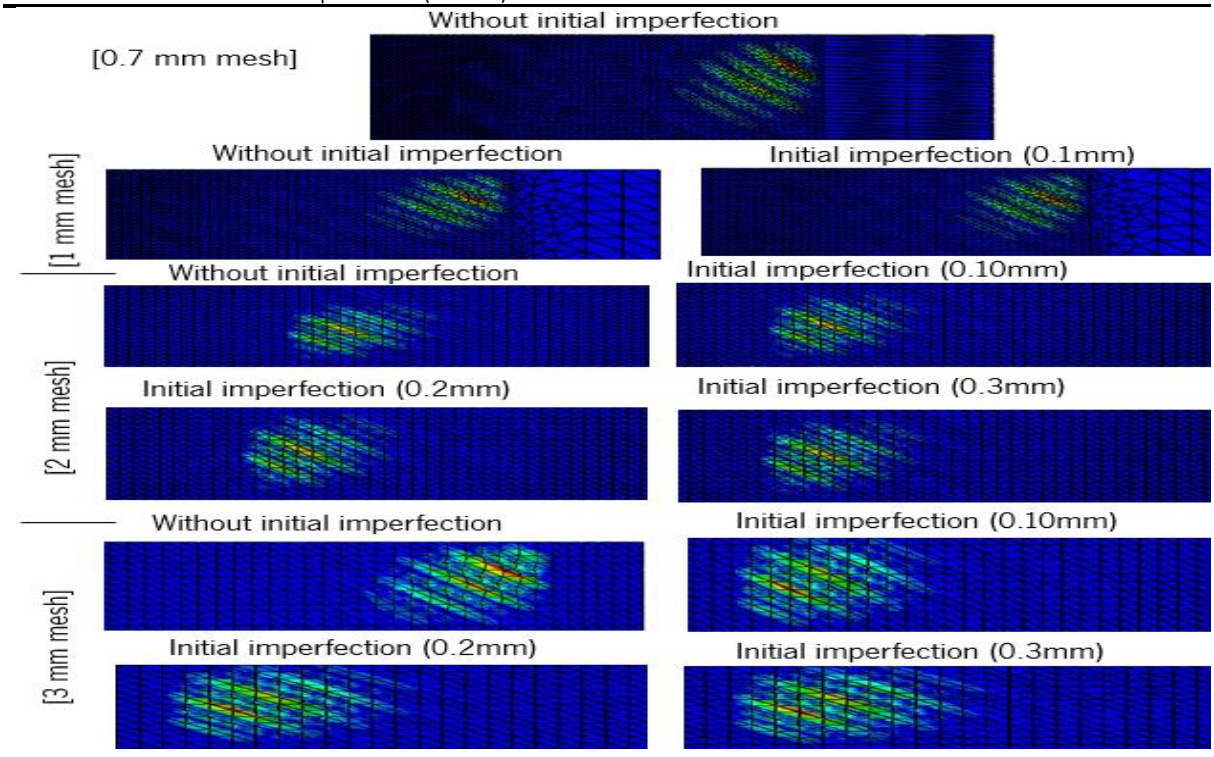

Figure 4.31 : Wrinkling pattern failure for different mesh sizes with different initial imperfection sizes.

Following the linear geometric buckling analysis, we performed a non-linear geometric analysis using the first eigenvalue of the buckling load as shown on Figure 4.33. This was done to fit the curve with experimental values and assess the stiffness of the material. Figure 4.32 illustrates that the buckling load predicted by numerical analysis, which includes initial geometric imperfections, is overestimated compared to the experimental wrinkling load. This suggests that the initial out-of-plane imperfection analysis has insignificant impact on the shear analysis. However, there is a good correlation between the initial stiffness of the material and the experimental results up to the point of buckling.

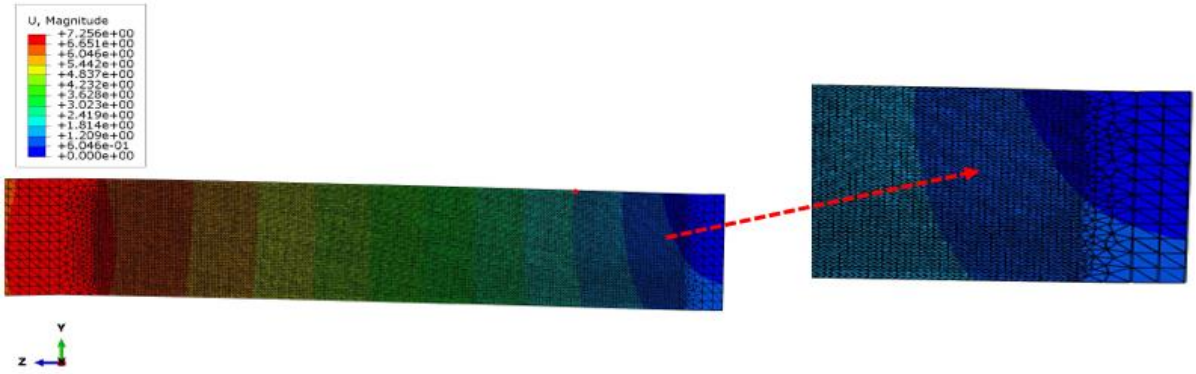

Figure 4.32: Wrinkling pattern failure for geometrical non-linear analysis.

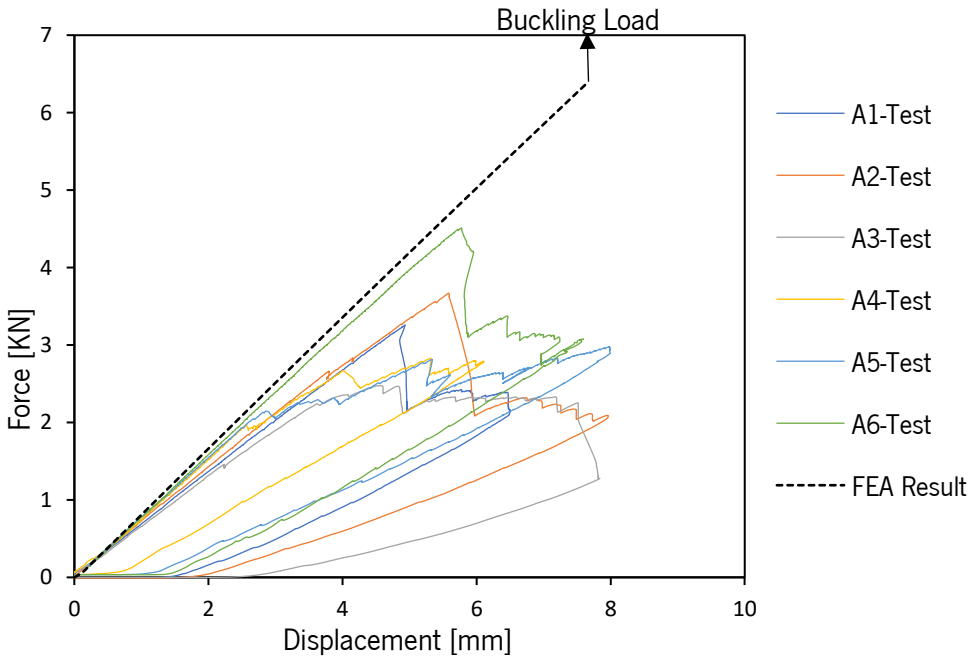

Figure 4.33 : Load–displacement relationship graph for expermental test and numerical shear results.

THIS PAGE WAS INTENTINALY LEFT BLANK

5. CHAPTER 5. CONCLUSION AND FURTHER DEVELOPMENT

5.1. Conclusion

The approach used in this research provides an important baseline for future investigations into wrinkling in sandwich structures for both shear and compression failure tests. The numerical analysis demonstrated that the mesh size has a significant impact on both the wrinkling load and the shape of the wrinkling pattern on wavelength in sandwich composite structures. For compression failure, the numerical results correlate well with both experimental data and analytical predictions, indicating the reliability of the finite element models in these scenarios. However, for shear failure tests, the numerical analysis tends to overestimate the wrinkling load when compared to experimental results, suggesting a need for refinement in modeling techniques for these cases.

Additionally, the presence of initial geometric imperfections in shear failure tests was found to have a minimal effect on stress distribution and failure modes, indicating that these imperfections do not significantly alter the structural response under shear loading conditions. This comprehensive study understanding and underscores the importance of considering mesh size and the nature of imperfections in accurately predicting the behavior of sandwich composite materials.

5.2. Further Development

a. Develop more sophisticated computational models that incorporate non-linearities, damage progression, and failure criteria (including foam, skin, and debonding) to enhance the accuracy and predictive capability for sandwich structures for shear failure senario. Regrettably, the limited timeframe of this study restricted the investigation of this concept.
b. Study the long-term effects of sustained loads, environmental conditions, and aging on the wrinkling behavior and overall durability of sandwich structures to better understand and mitigate potential failure mechanisms over time.
c. Develop comprehensive four-point bending experimental tests and corresponding numerical modelling techniques specifically for analysing compression wrinkling failure in sandwich structures, to provide a more detailed and reliable assessment of their performance under various loading conditions.

REFERENCE

[1] A. Petras and M. P. F. Sutcliffe, "Failure mode maps for honeycomb COMPOSITE STRUCTURES sandwich panels," 1999.

[2] R. P. Ley, W. Lin, and U. Mbanefo, "Facesheet Wrinkling in Sandwich Structures," 1999. [Online]. Available: http://www.sti.nasa.gov

[3] I. M. Daniel, E. E. Gdoutos, I. M. Daniel, R. R. Mccormick, and E. E. Gdoutos, "Failure Modes of Composite Sandwich Beams."

[4] M. Ginot, O. Polit, C. Bouvet, and B. Castanié, "Benchmark of wrinkling formulae and methods for pre-sizing of aircraft lightweight sandwich structures," 2021.

[5] J. P. Nunes and J. F. Silva, "Sandwiched composites in aerospace engineering," in *Advanced Composite Materials for Aerospace Engineering*, Elsevier, 2016, pp. 129–174. doi: 10.1016/b978-0-08-100037-3.00005-5.

[6] N. J. HOFF and S. E. MAUTNER, "The Buckling of Sandwich-Type Panels," *Journal of the Aeronautical Sciences*, vol. 12, no. 3, pp. 285–297, Jul. 1945, doi: 10.2514/8.11246.

[7] Q. Ma, M. R. M. Rejab, J. P. Siregar, and Z. Guan, "A review of the recent trends on core structures and impact response of sandwich panels," Aug. 01, 2021, *SAGE Publications Ltd*. doi: 10.1177/0021998321990734.

[8] A. Manalo, T. Aravinthan, and M. Asce, "Behavior of Full-Scale Railway Turnout Sleepers from Glue-Laminated Fiber Composite Sandwich Structures," 2012, doi: 10.1061/(ASCE)CC.1943-5614.

[9] A. Krzyzak, M. Mazur, M. Gajewski, K. Drozd, A. Komorek, and P. Przybyłek, "Sandwich Structured Composites for Aeronautics: Methods of Manufacturing Affecting Some Mechanical Properties," *International Journal of Aerospace Engineering*, vol. 2016, 2016, doi: 10.1155/2016/7816912.

[10] J. P. Vitale, G. Francucci, J. Xiong, and A. Stocchi, "Failure mode maps of natural and synthetic fiber reinforced composite sandwich panels," *Compos Part A Appl Sci Manuf*, vol. 94, pp. 217–225, Mar. 2017, doi: 10.1016/j.compositesa.2016.12.021.

[11] S. Laustsen, E. Lund, L. Kühlmeier, and O. T. Thomsen, "Failure behaviour of grid-scored foam cored composite sandwich panels for wind turbine blades subjected to realistic multiaxial loading conditions," *Journal of Sandwich Structures and Materials*, vol. 16, no. 5, pp. 481–510, Sep. 2014, doi: 10.1177/1099636214541367.

[12] I. M. Daniel, E. E. Gdoutos, K. A. Wang, and J. L. Abot, "Failure modes of composite sandwich beams," *International Journal of Damage Mechanics*, vol. 11, no. 4, pp. 309–334, 2002, doi: 10.1106/105678902027247.

[13] E. E. Gdoutos, I. M. Daniel, K.-A. Wang, and R. R. Mccormick, "Compression facing wrinkling of composite sandwich structures." [Online]. Available: www.elsevier.com/locate/mechmat

[14] L. Léotoing, S. Drapier, and A. Vautrin, "First applications of a novel unified model for global and local buckling of sandwich columns," 2002.

[15] D. J. Wadsworth, D. P. W. Horrigan, G. Moltschaniwskyj, and I. Collins, "Facesheet wrinkling of damaged honeycomb sandwich structures," *Journal of Sandwich Structures and Materials*, vol. 11, no. 2–3, pp. 105–131, Mar. 2009, doi: 10.1177/1099636209103555.

[16] A. Abiodun ALAWODE, "Abdulmaliq Abiodun ALAWODE Experimental Analysis of Wrinkling of Sandwich Structures Year of Conclusion: 2023 Master Course in Advanced Structural Analysis and Design using Composite Materials THE ENTIRE REPRODUCTION OF THIS THESIS IS AUTHORIZED ONLY FOR," 2023. Accessed: Aug. 19, 2024. [Online]. Available: https://msc-frp.org/wp-content/uploads/2023/10/MSc-Thesis_2022-23_UT3-INSA_AAlawode.pdf

[17] B. Harris, "ENGINEERING COMPOSITE MATERIALS."

[18] K. Mohan, Y. T. Hon, S. Idapalapati, and H. P. Seow, "Failure of sandwich beams consisting of alumina face sheet and aluminum foam core in bending," *Materials Science and Engineering: A*, vol. 409, no. 1–2, pp. 292–301, Nov. 2005, doi: 10.1016/j.msea.2005.06.070.

[19] U. Icardi and F. Sola, "Indentation of sandwiches using a plate model with variable kinematics and fixed degrees of freedom," *Thin-Walled Structures*, vol. 86, pp. 24–34, 2015, doi: 10.1016/j.tws.2014.10.002.

[20] A. C. Manalo, "Behaviour of fibre composite sandwich structures under short and asymmetrical beam shear tests," *Compos Struct*, vol. 99, pp. 339–349, May 2013, doi: 10.1016/j.compstruct.2012.12.010.

[21] J. Sena-Cruz, "FRP++4: Design of Structures with FRP Materials Lesson 3: Sandwich Structures-Part II FRP++ 4: Design of Structures with FRP Materials," 2024.

[22] G. S. Gough, C. F. Elam, G. H. Tipper, and N. A. De Bruyne, "The Stabilisation of a Thin Sheet by a Continuous Supporting Medium," *The Journal of the Royal Aeronautical Society*, vol. 44, no. 349, pp. 12–43, Jan. 1940, doi: 10.1017/s036839310010495x.

[23] S. Yusuff, "Theory of Wrinkling in Sandwich Construction," *The Journal of the Royal Aeronautical Society*, vol. 59, no. 529, pp. 30–36, Jan. 1955, doi: 10.1017/s0368393100131761.

[24] W. Su and S. Liu, "A couple-stress model to predict the wrinkling stress of sandwich panels with foam cores," *Compos Struct*, vol. 268, Jul. 2021, doi: 10.1016/j.compstruct.2021.113978.

[25] V. Birman and C. W. Bert, "Wrinkling of composite-facing sandwich panels under biaxial loading," *Journal of Sandwich Structures and Materials*, vol. 6, no. 3, pp. 217–237, May 2004, doi: 10.1177/1099636204033643.

[26] L. Fagerberg and D. Zenkert, "Effects of anisotropy and multiaxial loading on the wrinkling of sandwich panels," *Journal of Sandwich Structures and Materials*, vol. 7, no. 3, pp. 177–194, May 2005, doi: 10.1177/109963205048525.

[27] Q. Zhang *et al.*, "Bioinspired engineering of honeycomb structure - Using nature to inspire human innovation," Jul. 16, 2015, *Elsevier Ltd*. doi: 10.1016/j.pmatsci.2015.05.001.

[28] M. R. and S. M, "Flexural Behavior of Functionally Graded Sandwich Composite," in *Finite Element Analysis - Applications in Mechanical Engineering*, InTech, 2012. doi: 10.5772/51134.

[29] B. CASTANIE, C. BOUVET, and M. Ginot, "Review of composite sandwich structure in aeronautic applications," Aug. 01, 2020, *Elsevier B.V.* doi: 10.1016/j.jcomc.2020.100004.

[30] Z. Kamble, "Advanced structural and multi-functional sandwich composites with prismatic and foam cores: A review," 2023, *John Wiley and Sons Inc*. doi: 10.1002/pc.27849.

[31] B. Tah, "MANUFACTURING AND STRUCTURAL ANALYSIS OF A LIGHTWEIGHT SANDWICH COMPOSITE UAV WING A THESIS SUBMITTED TO THE GRADUATE SCHOOL OF NATURAL AND APPLIED SCIENCES OF MIDDLE EAST TECHNICAL UNIVERSITY," 2007.

[32] G. Di Bella, L. Calabrese, and C. Borsellino, "Mechanical characterisation of a glass/polyester sandwich structure for marine applications," *Mater Des*, vol. 42, pp. 486–494, Dec. 2012, doi: 10.1016/j.matdes.2012.06.023.

[33] S. E. Mouring, "Buckling and postbuckling of composite ship panels stiffened with preform frames," 1999.

[34] C. Borsellino, L. Calabrese, and G. Di Bella, "Effect of bonder at skin/core interface on the mechanical performances of sandwich structures used in Marine industry," *Applied Composite Materials*, vol. 14, no. 5–6, pp. 307–323, Nov. 2007, doi: 10.1007/s10443-007-9048-9.

[35] T. Okada, K. Suzuki, and Y. Kawamura, "Lecture Notes in Civil Engineering Practical Design of Ships and Other Floating Structures." [Online]. Available: http://www.springer.com/series/15087

[36] A. Manalo, T. Aravinthan, A. Fam, and B. Benmokrane, "State-of-the-Art Review on FRP Sandwich Systems for Lightweight Civil Infrastructure," *Journal of Composites for Construction*, vol. 21, no. 1, Feb. 2017, doi: 10.1061/(asce)cc.1943-5614.0000729.

[37] T. Keller, E. Schaumann, and T. Vallée, "Flexural behavior of a hybrid FRP and lightweight concrete sandwich bridge deck," *Compos Part A Appl Sci Manuf*, vol. 38, no. 3, pp. 879–889, Mar. 2007, doi: 10.1016/j.compositesa.2006.07.007.

[38] P. Jagadeesh *et al.*, "A comprehensive review on polymer composites in railway applications," Mar. 01, 2022, *John Wiley and Sons Inc*. doi: 10.1002/pc.26478.

[39] H. G. ALLEN, "WRINKLING AND OTHER FORMS OF LOCAL INSTABILITY," in *Analysis and Design of Structural Sandwich Panels*, Elsevier, 1969, pp. 156–189. doi: 10.1016/b978-0-08-012870-2.50012-2.

[40] K. Niu and R. Talreja, "MODELING OF WRINKLING IN SANDWICH PANELS UNDER COMPRESSION."

[41] L. Fagerberg and D. Zenkert, "Imperfection-induced wrinkling material failure in sandwich panels," *Journal of Sandwich Structures and Materials*, vol. 7, no. 3, pp. 195–219, May 2005, doi: 10.1177/1099636205048526.

[42] B. Hayman, C. Berggreen, and N. G. Tsouvalis, "A review of the causes of production defects in marine composite structures and their influence on performance," 2007. [Online]. Available: https://www.researchgate.net/publication/289192519

[43] M. Ginot, M. D'Ottavio, O. Polit, C. Bouvet, and B. Castanié, "Benchmark of wrinkling formulae and methods for pre-sizing of aircraft lightweight sandwich structures," *Compos Struct*, vol. 273, Oct. 2021, doi: 10.1016/j.compstruct.2021.114387.

[44] V. Vadakke and L. A. Carlsson, "Experimental investigation of compression failure mechanisms of composite faced foam core sandwich specimens," *Journal of Sandwich Structures and Materials*, vol. 6, no. 4, pp. 327–342, Jul. 2004, doi: 10.1177/1099636204036041.

[45] B. D. Manshadi, A. P. Vassilopoulos, J. De Castro, and T. Keller, "Shear Wrinkling of GFRP Webs in Cell-Core Sandwiches."

[46] J. Susainathan, F. Eyma, E. DE Luycker, A. Cantarel, and B. Castanie, "Numerical modeling of impact on wood-based sandwich structures," *Mechanics of Advanced Materials and Structures*, vol. 27, no. 18, pp. 1583–1598, Sep. 2020, doi: 10.1080/15376494.2018.1519619.

[47] N. Pokharel, "Behaviour and Design of Sandwich Panels Subject to Local Buckling and Flexural Wrinkling Effects."

[48] H. D. Hibbitt, “A GENERAL PURPOSE FINITE ELEMENT CODE WITH EMPHASIS ON NONLINEAR APPLICATIONS,” 1984.

[49] U. S. Dixit, S. N. Joshi, and J. P. Davim, “Incorporation of material behavior in modeling of metal forming and machining processes: A review,” Aug. 2011. doi: 10.1016/j.matdes.2011.03.049.

[50] R. De Borst, L. J. Sluys, H.-B. Muhlhaus, and J. Pamin, “Feature & Review ARTICLES FUNDAMENTAL ISSUES IN FINITE ELEMENT ANALYSES OF LOCALIZATION OF DEFORMATION*,” 1993.

[51] D. K. Kim, H. L. Lim, and S. Y. Yu, “A technical review on ultimate strength prediction of stiffened panels in axial compression,” Dec. 15, 2018, *Elsevier Ltd*. doi: 10.1016/j.oceaneng.2018.10.022.

ANNEX I

1. **Hoff and Mautner** [6] **analytical formulation for wrinkling stress for sandwich struture for thick core.**

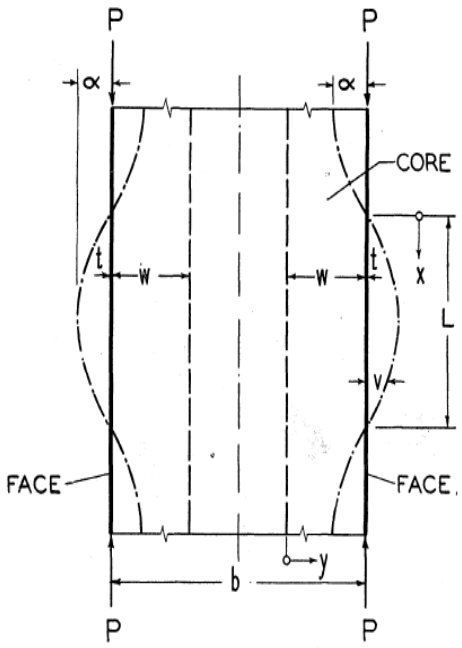

Basic assumptions:

Strain energy calculation of the symmetric ripples.

The vertical displecment U at buckling is assumed to be negligible small.

The Horizontal displacement V of the point originally at x,y in the right side of the picture.

By using sinusoidal function:

$$V = \alpha \frac{y}{W} \sin[\frac{\pi x}{L}]$$

Where α amplitude of the wave; {y – horizontal position, and w – width of marginal zone}, where shearing is significant.

$\frac{\pi x}{L}$ – Angular frequency of the wave; sine wave completes one full cycle, 0 → 2π, as x → 0 to L

The buckling load can calculate by/from the requirement that the work done by compressive force during the vertical displacement of its point of attack caused by the bending of the face layer be equal to the strain energy of bending stored in the face material plus the strain energy of the extension and shear stored in the core.

✓ Normal strain energy in the core - the derivative of deflection

$$e = \frac{dw}{dy} = \frac{\alpha}{W} \sin[\frac{\pi x}{L}]$$ - shows how it changes linearly with distance from face.

✓ Extensional strain energy within one half of wavelength → Extensional strain energy arises from (compression or tensile) in the material.

Ue = $\frac{1}{2}\sigma e = \frac{1}{2}Ee^2$

Ue = $\frac{E_c}{2}\int_0^L \int_0^W e^2$ dy dx

Ue = $\frac{E_c}{2}\int_0^L \int_0^W [\frac{\alpha}{W}\sin[\frac{\pi x}{L}]]^2$ dy dx

Integrate over Y

$\int_0^w \frac{\alpha^2}{W^2}$ dy = $\frac{\alpha^2}{W}$

Integrate over X

$\int_0^L \sin[\frac{\pi X}{L}]^2$ – for half wavelength (L) – the integral property of $\sin^2(\frac{\pi X}{L})$ = ½ = $\frac{L}{2}$

Ue = $\frac{E_c}{2}\frac{\alpha^2}{W}\frac{L}{2} = \left[\frac{\alpha^2}{2}\right]\left[\frac{E_c}{2}\right]\left[\frac{L}{W}\right]$

✓ The shear strain in the core is given by:

U_γ = ½ τ γ – where τ – shear stress, and γ – shear strain

U_γ = ½ $G_c\gamma^2$

$\gamma = \frac{dw}{dx} = \frac{\alpha y}{W}\ \frac{\pi}{L}\cos\left[\frac{\pi x}{L}\right]$ - Differentiating of displacement w with respect to X

$U_\gamma = \left[\frac{Gc}{2}\right]\int_0^L \int_0^W \gamma^2$ dydx

$= \left[\frac{Gc}{2}\right]\int_0^L \int_0^W \alpha^2 \frac{y^2}{W^2}\frac{\pi^2}{L^2}\left[\cos\frac{\pi X}{L}\right]^2$ dy dx

Integrate over Y

$\int_0^W \alpha^2 \frac{y^2}{w^2}$ dy = $\alpha^2\frac{W}{3}$

Integrate over X

$\int_0^L \alpha^2 \frac{w}{3}\frac{\pi^2}{L^2}\frac{L}{2} = \left[\frac{G_c}{2}\right]\left[\alpha^2\frac{W}{6}\frac{\pi^2}{L}\right] = G_c\left[\frac{\alpha^2}{2}\right]\left[\frac{W}{6}\right]\left[\frac{\pi^2}{L}\right] - G_c$ = shear modulus of the core.

✓ The strain energy stored in one face

$U_f = \left[E_f\frac{I_f}{2}\right]\int_0^L \left[\frac{d^2v_w}{dx^2}\right]^2$ dx -- v_w = horizontal displecment at y=w

V = $\alpha\frac{\cancel{W}}{\cancel{W}}\sin[\frac{\pi x}{L}]$ - since y=w

$\frac{d^2v_w}{dx^2}$, first derivative, $\frac{dv_w}{dx} = \frac{\pi}{L}\cos\left[\frac{\pi x}{L}\right]$

$\frac{d^2v_w}{dx} = \left[\frac{\pi^2}{L^2}\alpha - \sin\left[\frac{\pi x}{L}\right]\right]^2$

$= \frac{\pi^4}{L^4}\alpha^2 \sin\left[\frac{\pi x}{L}\right]^2$ ..... I = $\frac{t^3}{12}$ .....Moment of inertia

$U_f = E_f \frac{t^3}{12}\int_0^L \frac{\pi^4}{L^4}\alpha^4 \sin\left[\frac{\pi x}{L}\right]^3 dx$

$U_f = \left[\frac{\alpha^2}{2}\right]\left[\frac{\pi^4}{24}\right] E_f \left[\frac{t}{L}\right]^3$ ..... The energy stored in one face – The energy stored for displecment w,

✓ With y=w assumption the shortening △ L of the distance b/n points that were originally at x=0 and X=L

$\triangle L = \frac{1}{2}\int_0^L \left[\frac{d_w}{d_x}\right]^2 dx$ ..... $w = \alpha\left[\frac{y}{w}\right]\sin\left[\frac{\pi x}{L}\right]$

$\frac{d_w}{d_x} = \alpha\left[\frac{y}{w}\right]\cos\left[\frac{\pi x}{L}\right]$

$= \frac{1}{2}\int_0^L \left[\alpha\left[\frac{y}{w}\right]\cos\left[\frac{\pi x}{L}\right]\right]^2 dx$

$\triangle L = \frac{\pi^2}{4}\frac{\alpha^2}{2}$

✓ The work done by the constant force, P = $\sigma_{cr} t$

W = P △L

$W = \sigma_{cr} t \frac{\pi^2}{4}\frac{\alpha^2}{2} = \sigma_{cr}\left[\frac{\alpha^2}{2}\right]\left[\frac{\pi^2}{2}\right]\left[\frac{t}{2}\right]$

$W = U_e + U_s + U_f$

$\sigma_{cr}\left[\frac{\alpha^2}{2}\right]\left[\frac{\pi^2}{2}\right]\left[\frac{t}{2}\right] = \left[\frac{\alpha^2}{2}\right]\left[\frac{E_c}{2}\right]\left[\frac{L}{W}\right] + G_c\left[\frac{\alpha^2}{2}\right]\left[\frac{W}{6}\right]\left[\frac{\pi^2}{L}\right] + \left[\frac{\alpha^2}{2}\right]\left[\frac{\pi^4}{24}\right] E_f \left[\frac{t}{L}\right]^3$

$\sigma_{cr} = \frac{1}{\pi^2} E_c \frac{L^2}{tw} + \frac{1}{3} G_c \frac{w}{t} + \frac{\pi^2}{12} E_f \frac{t^2}{L^2}$ (1)

The critical stress in this equation depends upon the parameters w and L — The actual values of W and L is at which the critical stress will be minimum.

Therefore, $\frac{d\sigma_{cr}}{dw}$ and $\frac{d\sigma_{cr}}{dL}$, must vanish

$\frac{d\sigma_{cr}}{dw} = -\frac{1}{\pi^2} E_f \frac{L^2}{tw^2} + \frac{1}{3} G_c \frac{w^2}{t} = 0$ (2)

$\frac{d\sigma_{cr}}{dL} = \frac{2}{\pi^2} E_c \frac{L^2}{tw} - \frac{\pi^2}{6} E_c \frac{t^2}{L^3} = 0$ (3)

From equation (2)

$\frac{1}{\pi^2} E_f \frac{L^2}{tw^2} = \frac{1}{3} G_c \frac{w^2}{t}$

$w = \frac{L}{\pi}\left[\frac{3E_f}{G_c}\right]^{\frac{1}{2}}$ (4)

From equation (3)

$$\frac{2}{\pi^2} E_c \frac{L^2}{tw} = \frac{\pi^2}{6} E_c \frac{t^2}{L^3}$$

$$L^4 = \frac{\pi^4 E_f t^3 w}{12 E_c} \quad (5)$$

Substitute equation 4 on 5

$$L^4 = \frac{\pi^4 E_f t^3 \frac{L}{\pi}\left[\frac{3E_c}{G_c}\right]^{\frac{1}{2}}}{12 E_c}$$

$$L = \frac{\pi t E_f^{\frac{1}{3}} 3^{\frac{1}{6}} E_c^{\frac{1}{6}}}{12^{\frac{1}{3}} G_c^{\frac{1}{6}} E_c^{\frac{1}{3}}}$$

$$\frac{L}{t} = 1.65 \left[\frac{E_f^2}{E_c G_c}\right]^{\frac{1}{6}} \quad (6)$$

Substitute equation 6 on equation 4

$$W = \frac{1.65t}{\pi} \left[\frac{E_f^2}{E_c G_c}\right]^{\frac{1}{6}} \left[\frac{3E_c}{G_c}\right]^{\frac{1}{6}}$$

$$\frac{w}{t} = 0.91 \left[\frac{E_f E_c}{G_c^2}\right]^{\frac{1}{3}} \quad (7)$$

Then after this we substitute from equation 4 to 7 on equation 1:

$$\sigma_{cr} = \underbrace{\frac{1}{\pi^2} E_c \frac{L^2}{tw}}_{a} + \underbrace{\frac{1}{3} G_c \frac{w}{t}}_{b} + \underbrace{\frac{\pi^2}{12} E_f \frac{t^2}{L^2}}_{c}$$

$$a = \frac{1}{\pi^2} E_c \frac{L}{t} \frac{L}{w}$$

$$a = \frac{1}{\pi^2} E_c \left[\frac{E_c E_f^{\frac{1}{3}}}{E_c^{\frac{1}{6}} G_c^{\frac{1}{3}}}\right] \left[\frac{1.65 G_c^{\frac{1}{3}}}{E_c^{\frac{1}{2}} 0.91 G_c^{\frac{1}{6}}}\right] \quad \text{simplify to}$$

$$a = \frac{1}{\pi^2} \frac{1.65 * 1.65}{0.91} \left[E_c^{\frac{1}{3}} E_f^{\frac{1}{3}} G_c^{\frac{1}{3}}\right]$$

$$a = 0.3031 \left[E_c E_f G_c\right]^{\frac{1}{3}} \quad (8)$$

$$b = \frac{1}{3} G_c \frac{w}{t}$$

$$b = \frac{1}{3} G_c 0.91 \left[\frac{E_f E_c}{G_c^2}\right]^{\frac{1}{3}}$$

b = $0.3031\left[E_c E_f G_c\right]^{\frac{1}{3}}$

c = $\frac{\pi^2}{12} E_f \frac{t^2}{L^2}$ substitute equation (6)

c = $\frac{\pi^2}{12} E_f \left[\frac{E_c^{\frac{2}{6}} G_c^{\frac{2}{6}}}{1.65^2 E_f^{\frac{1}{3}}}\right]$

c = $0.3032\left[E_c E_f G_c\right]^{\frac{1}{3}}$

Then, sum a,b, and c to get the critical wrinkling stress formulated by Hoff and Mautiner:

$\sigma_{cr} = 0.3031\left[E_c E_f G_c\right]^{\frac{1}{3}} + 0.3031\left[E_c E_f G_c\right]^{\frac{1}{3}} + 0.3032\left[E_c E_f G_c\right]^{\frac{1}{3}}$

$\boldsymbol{\sigma_{cr} = 0.91\left[E_c E_f G_c\right]^{\frac{1}{3}}}$

2. Syed Yusuff [23] analytical formulation for wrinkling of sandwich structure:

2.1 Face separated by core of finite thickness:

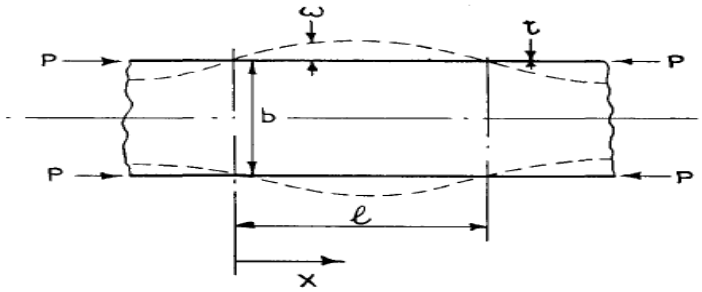

For this case the core is sufficiently thin.

The modulus of the foundation corresponding one half of the core,

K = $\frac{2E_c}{b}$, where E_c – young modulus of the core, and b – the thickness of the core.

The differential equation of the the buckling of the beam, which is elastically supported and subjected to the axial force P.

As a type of buckling, wrinkles can be explained using the differential of the fourth order bending theory, which is elastically supported and subjected to the axial force p.

$$\frac{d^4w}{dx^4} - \frac{P}{EI}\frac{d^2w}{dx^2} + \frac{k}{EI}w = 0 \qquad (9)$$

w is the deflection of the beam, since this analysis is a periodic solution of equations, the beam (skin) may be assumed to buckle in a sine wave of deflection, which is dependent on the amplitude of the wave

(A) and angular frequency of the wave which is described by half wavelength across in the X-direction as follows:

$$w = A * sin\left(\frac{\pi x}{L}\right)$$

Second order derivative:

$$\frac{d^2w}{dx^2} = \frac{\pi^2}{L^2}\mathrm{A} - \sin\left[\frac{\pi x}{L}\right]$$

The fourth order derivatives

$$\frac{d^4w}{dx^4} = \frac{\pi^4}{L^4}\mathrm{Asin}\left[\frac{\pi x}{L}\right]$$

Substitute on equation 9:

$$\frac{\pi^4}{L^4}\mathrm{Asin}\left[\frac{\pi x}{L}\right] - \frac{P}{EI}\frac{\pi^2}{L^2}\mathrm{A} - \sin\left[\frac{\pi x}{L}\right] + \frac{k}{EI}A * sin\left(\frac{\pi x}{L}\right) = 0$$

$$P_{min} = E_f I\frac{\pi^2}{L^2} + \frac{kL^2}{\pi^2} \quad (10)$$

The minimum value of P can be obtained by differentiating with respect to L = $\frac{dp}{dL} = 0$

$$\frac{dp}{dL} = -2E_f I\frac{\pi^2}{L^3} + \frac{2kL}{\pi^2} = 0$$

The critical L (Lcr)

$$2E_f I\frac{\pi^2}{L^3} = \frac{2kL}{\pi^2}$$

$$L_{cr} = \pi\left[\frac{E_f I}{k}\right]^{\frac{1}{4}} \quad (11)$$

Substitute equation 11 on equation 10

$$P_{min} = E_f I\frac{\pi^2}{\pi\left[\frac{E_f I}{k}\right]^{\frac{1}{4}^2}} + \frac{k\pi\left[\frac{E_f I}{k}\right]^{\frac{1}{4}^2}}{\pi^2}$$

$$P_{min} = 2\left[E_f Ik\right]^{\frac{1}{2}} \quad (12)$$

For skin of thickness t and of unit width, the moment of inertia is; $I = \frac{t^3}{12}$

$$L_{cr} = \pi\left[\frac{E_f\frac{t^3}{12}}{\frac{2E_c}{b}}\right]^{\frac{1}{4}}$$

$\lambda = 2L_{cr} = 2\pi t\left[\frac{2}{3}\frac{E_f}{E_c}\frac{b}{t}\right]$ The critical wavelength of wrinkling in sandwich structure.

The critical load is:

$$P_{min} = 2\left[E_f Ik\right]^{\frac{1}{2}}$$

$$P_{min} = 2\left[E_f \frac{t^3}{12}\frac{2E_c}{b}\right]^{\frac{1}{2}}$$

$$P_{min} = 2t\left[E_f E_c \frac{t}{b}\frac{2}{12}\right]^{\frac{1}{2}}$$

$$P_{min} = t\left[\frac{2}{3}E_f E_c \frac{t}{b}\right]^{\frac{1}{2}}$$

$$\boldsymbol{\sigma_{cr} = t\left[\frac{2}{3}E_f E_c \frac{t}{b}\right]^{\frac{1}{2}}}$$

Where E_f is Young's modulus of the face, E_c is Young's modulus of the core, t is the thickness of the core, and b is the thickness of the core.

2.2 Face supported by sufficiently thick core:

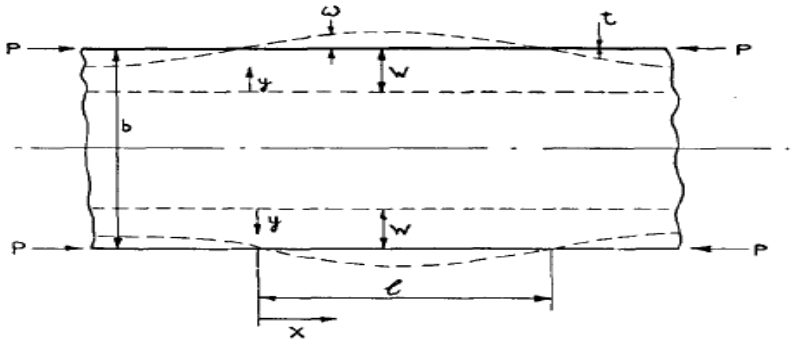

The transverse displacement (y-direction) of the core, we use sinusoidal wave:

$$w = A\frac{y}{W}sin\left(\frac{\pi x}{L}\right)$$

Where $\frac{\pi x}{L}$ is angular frequency of the wave – sinewave completes one full cycle 0 to 2π as x ⟶ 0 to L, y- vertical position, W is width of marginal zone, where the shearing is significant.

According to Yusuf, The strain energy stored in the springs must be equal to the sum of the extensional (tension or compression) and shear strain energy in the core. [basic assumption].

✓ The normal strain in the core is:

$$e_y = \frac{dw}{dy} = \mathrm{A}\frac{\mathrm{y}}{W}\sin[\frac{\pi x}{L}]$$

$$= \frac{\mathrm{A}}{W}\sin[\frac{\pi x}{L}]$$

The extensional strain energy within one-half of the length:

$$\mathrm{Ue} = \frac{1}{2}\sigma e_y = \frac{1}{2}E{e_y}^2$$

Ue = $\frac{E_c}{2}\int_0^L\int_0^W {e_y}^2$ dy dx

Ue = $\frac{E_c}{2}\int_0^L\int_0^W \left[\frac{\mathrm{A}}{W}\sin[\frac{\pi x}{L}]\ \right]^2$ dy dx

Integrate over Y

$\int_0^w \frac{\mathrm{A}^2}{W^2}$ dy = $\frac{\mathrm{A}^2}{W}$

Integrate over X

$\int_0^L \sin[\frac{\pi X}{L}]^2$ – for half wavelength (L) – the integral property of $\sin^2\frac{\pi X}{L}$ = ½ = $\frac{L}{2}$

U_e = $\frac{E_c}{2}\frac{A^2}{W}\frac{L}{2}$ = $\left[\frac{A^2}{4}\right]\left[E_c\right]\left[\frac{L}{W}\right]$, where Ec –young modulus of the core, Normal to the surface y.

✓ The shear strain energy in the core is:

U_γ = ½ τ γ – where τ – shear stress, and γ – shear strain

U_γ = ½ $G_c\gamma^2$

$\gamma = \frac{dw}{dx} = \frac{\mathrm{Ay}}{W}\ \frac{\pi}{L}\cos\left[\frac{\pi x}{L}\right]$ - Differentiating of displacement w with respect to X

U_γ = $\left[\frac{Gc}{2}\right]\int_0^L\int_0^W \gamma^2$ dydx

U_γ = $\left[\frac{Gc}{2}\right]\int_0^L\int_0^W A^2\frac{y^2}{W^2}\frac{\pi^2}{L^2}\left[\cos\frac{\pi X}{L}\right]^2$ dy dx

Integrate over Y

$\int_0^W A^2\frac{y^2}{w^2}$ dy = $\alpha^2\frac{W}{3}$

Integrate over X

$\int_0^L A^2\frac{w}{3}\frac{\pi^2}{L^2}\frac{L}{2}$ =U_γ= $\left[\frac{G_c}{2}\right]\left[A^2\frac{W}{6}\frac{\pi^2}{L}\right]$ = $G_c\left[\frac{A^2}{12}\right][w]\left[\frac{\pi^2}{L}\right] - G_c$ = shear modulus of the core corresponding to the longitudinal and transverse direction (x, y)

✓ The stored energy by the core, If the core is replaced by an equivalent spring of constant K at y=w, the energy stored for the displecment w,

U_s = $\frac{1}{2}\int_0^L Kw^2$dx, where w= $\mathrm{A}*\sin\frac{\pi x}{L}$

U_s = $\frac{1}{2}\int_0^L K\left[\mathrm{A}*\sin\frac{\pi x}{L}\right]^2$ dx

U_s = $\frac{A^2}{4}KL$

The strain energy stored in the springs must be equal to the sum of extensional and shear strain energy stored in the core,

$U_s = U_e + U_\gamma$

$\frac{A^2}{4}KL = \left[\frac{A^2}{4}\right][E_c]\left[\frac{L}{W}\right] + G_c\left[\frac{A^2}{12}\right][w]\left[\frac{\pi^2}{L}\right]$, Solve for K

$K = \frac{E_c}{w} + \frac{\pi^2}{3}G_c\frac{w}{L^2}$

To find the actual value of w, which is that makes k will be minimum: $\frac{d_k}{d_w}$

$\frac{d_k}{d_w} = -\frac{E_c}{w^2} + \frac{\pi^2}{3}G_c\frac{w}{L^2} = 0$, Rearrange it.

$\left[\frac{L}{w}\right]^2 = \frac{\pi^2 G_c}{3E_c}$, substitute this equation to K

$K = \frac{E_c}{w} + \frac{\pi^2}{3}G_c\left[\frac{3E_c}{\pi^2 G_c}\right]\frac{1}{w}$

$K = \frac{2E_c}{w}$, where $E_c = \frac{\pi^2}{3}\frac{G_c}{L^2}w^2$, $K = \frac{2}{3}\pi^2 G_c\frac{w}{L^2}$

We have obtained the modulus of foundation, and we have a critical load and wavelength from Part 1(Face separated by core of finite thickness):

We had the following equations, $K = \frac{2E_c}{b}$, $= \frac{2}{3}\pi^2 G_c\frac{w}{L^2}$

$\left[\frac{L}{w}\right]^2 = \frac{\pi^2 G_c}{3E_c}$, $P_{min} = 2\left[E_f I k\right]^{\frac{1}{2}}$, $L_{cr} = \pi\left[\frac{E_f I}{k}\right]^{\frac{1}{4}}$

$K = \frac{2}{3}\pi^2 G_c\frac{w}{L^2}$, substitute L_{cr} into L

$$K = \frac{2}{3}\pi^2 G_c \frac{w}{\pi\left[\frac{E_f\frac{t^3}{12}}{\frac{2E_c}{w}}\right]^{\frac{1}{4}2}}, \quad \text{since } w = \frac{2E_c}{k}$$

$$K = \frac{2G_c 24^{\frac{1}{2}}E_c^{\frac{1}{2}}[2E_c]^{\frac{1}{2}}}{E_f^{\frac{1}{2}}t^{\frac{3}{2}}k^{\frac{1}{2}}}, \quad KK^{\frac{1}{2}}t^{\frac{2}{3}} = \frac{2*24^{\frac{1}{2}}*2^{\frac{1}{2}}G_c E_c^{\frac{1}{2}}E_c^{\frac{1}{2}}}{E_f^{\frac{1}{2}}}$$

$$Kt = 2.773\left[\frac{[G_c E_c]^2}{E_f}\right]^{\frac{1}{3}} \tag{13}$$

$\left[\frac{L}{w}\right]^2 = \frac{\pi^2 G_c}{3E_c}$, $= \frac{w}{L} = \left[\frac{3E_c}{\pi^2 G_c}\right]^{\frac{1}{2}}$, $L_{cr} = \pi\left[\frac{E_f I}{k}\right]^{\frac{1}{4}}$, $K = \frac{2E_c}{w}$, $I = \frac{t^3}{12}$, by using equation Solve for $\frac{w}{t}$

$$\frac{w}{t} = 0.721\left[\frac{E_f E_c}{G_c^2}\right]^{\frac{1}{2}} \tag{14}$$

$L_{cr} = \pi \left[\frac{E_f I}{k}\right]^{\frac{1}{4}}$, $L_{cr} = \pi \left[\frac{E_f \frac{t^3}{12}}{k}\right]^{\frac{1}{4}}$, by using this solve for $\frac{L_{cr}}{w}$

$$\frac{L_{cr}}{t} = 1.3078 \left[\frac{E_f^2}{G_c E_c}\right]^{\frac{1}{6}}, \quad \frac{\lambda}{t} = \frac{2L_{cr}}{t} = 2.615 \left[\frac{E_f^2}{G_c E_c}\right]^{\frac{1}{6}} \tag{15}$$

$P_{min} = 2\left[E_f I k\right]^{\frac{1}{2}}$, $P_{min} = 2\left[E_f \frac{t^3}{12} \frac{2.773}{t} \left[\frac{[G_c E_c]^2}{E_f}\right]^{\frac{1}{3}}\right]^{\frac{1}{2}}$

$P_{min} = 2t \left(\frac{2.773}{12}\right)^{\frac{1}{2}} \left[E_f^{\frac{2}{3}} E_c^{\frac{2}{3}} G_c^{\frac{2}{3}}\right]^{\frac{1}{2}}$

$P_{min} = 0.9614 \left[E_c E_f G_c\right]^{\frac{1}{3}} t$

The critical stress, $\boldsymbol{\sigma_{cr} = \frac{P_{min}}{A}}$, The area will be with a unit width with t thickness,

$$\boldsymbol{\sigma_{cr} = 0.9614 \left[E_c E_f G_c\right]^{\frac{1}{3}}} \tag{16}$$

Seid Yesuff's wrinkling stress formulation for thick core sandwich structure.